



UvA-DARE (Digital Academic Repository)

Unitary matrix integrals, long-range random walks, and spectral statistics

Vleeshouwers, W.L.

Publication date

2023

Document Version

Final published version

[Link to publication](#)

Citation for published version (APA):

Vleeshouwers, W. L. (2023). *Unitary matrix integrals, long-range random walks, and spectral statistics*. [Thesis, fully internal, Universiteit van Amsterdam].

General rights

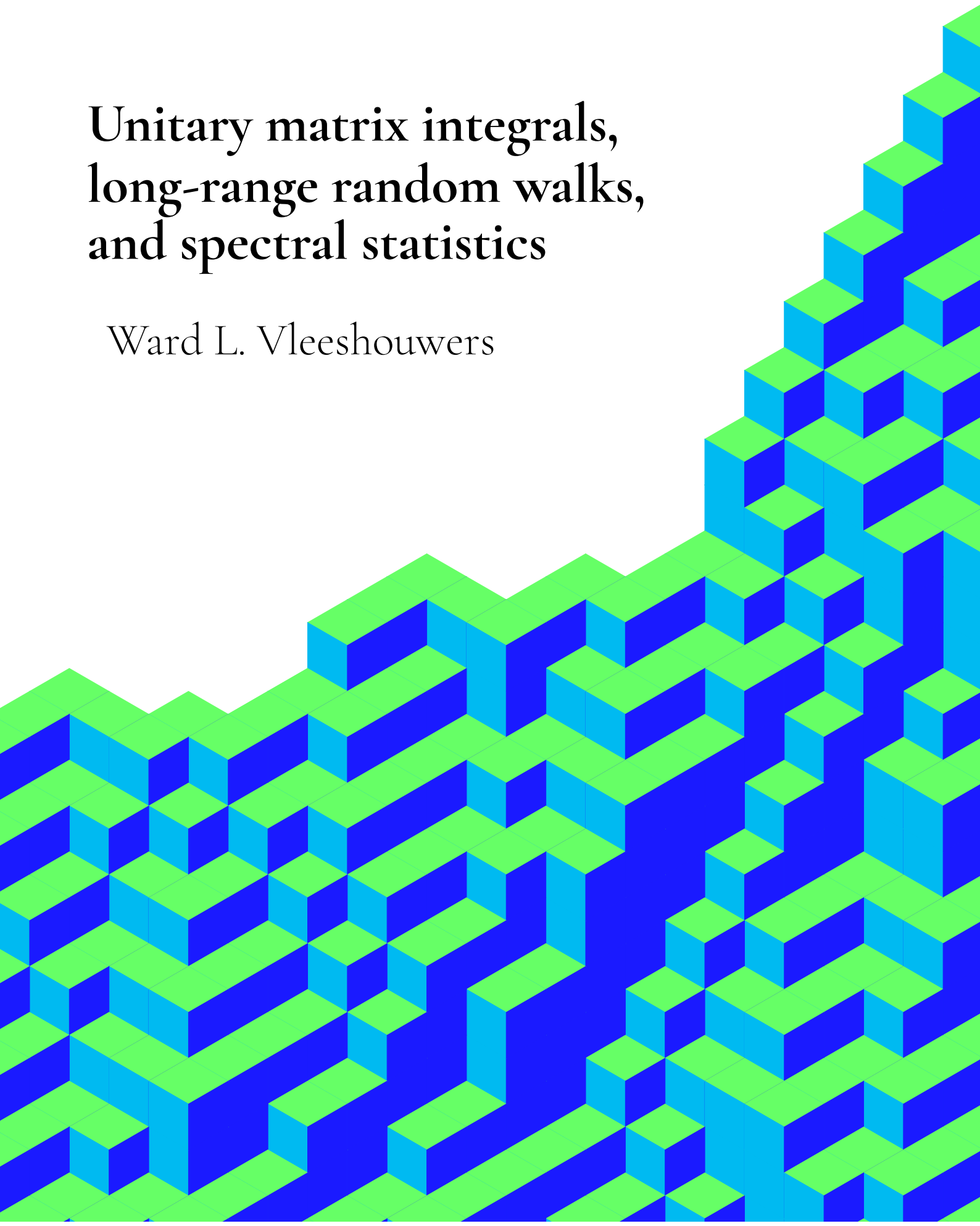
It is not permitted to download or to forward/distribute the text or part of it without the consent of the author(s) and/or copyright holder(s), other than for strictly personal, individual use, unless the work is under an open content license (like Creative Commons).

Disclaimer/Complaints regulations

If you believe that digital publication of certain material infringes any of your rights or (privacy) interests, please let the Library know, stating your reasons. In case of a legitimate complaint, the Library will make the material inaccessible and/or remove it from the website. Please Ask the Library: <https://uba.uva.nl/en/contact>, or a letter to: Library of the University of Amsterdam, Secretariat, Singel 425, 1012 WP Amsterdam, The Netherlands. You will be contacted as soon as possible.

Unitary matrix integrals, long-range random walks, and spectral statistics

Ward L. Vleeshouwers



Unitary matrix integrals, long-range random walks, and spectral statistics

ACADEMISCH PROEFSCHRIFT

ter verkrijging van de graad van doctor
aan de Universiteit van Amsterdam
op gezag van de Rector Magnificus
prof. dr. ir. P.P.C.C. Verbeek
ten overstaan van een door het College voor Promoties ingestelde commissie,
in het openbaar te verdedigen in de Aula der Universiteit
op vrijdag 20 oktober 2023, te 11.00 uur

door Ward Vleeshouwers
geboren te Nijmegen

Promotiecommissie

<i>Promotores:</i>	prof. dr. C. Morais Smith dr. V. Gritsev	Universiteit Utrecht Universiteit van Amsterdam
<i>Copromotores:</i>	prof. dr. C.J.M. Schoutens	Universiteit van Amsterdam
<i>Overige leden:</i>	prof. dr. J.S. Caux prof. dr. N. Reshetikhin prof. dr. G.A. Mussardo dr. M.L. Vonk prof. dr. J.V. Stokman dr. A. Safavi Naini prof. dr. E.A. Demler	Universiteit van Amsterdam University of Berkeley SISSA Universiteit van Amsterdam Universiteit van Amsterdam Universiteit van Amsterdam ETH Zurich

Faculteit der Natuurwetenschappen, Wiskunde en Informatica

Aan Lukas, die graag mijn blokkentorens afbouwt

*You can hide a lot in a large- N
matrix.*

Stephen Shenker

*Each problem that I solved
became a rule which served
afterwards to solve other
problems.*

René Descartes

*These days I spend more time
babysitting and less time writing
books. You never know which
job will turn out to be most
important!*

Freeman Dyson

Contents

List of abbreviations	vii
List of publications	ix
Introduction	1
1 Background material	6
1.1 Symmetric functions	6
1.2 Matrix integrals and Toeplitz minors	25
1.2.1 Finite matrix size	32
1.3 Long-range random walkers	33
1.4 Random matrices and spectral statistics	40
1.4.1 Random matrix theory and quantum chaos	41
1.4.2 Intermediate statistics	47
1.4.3 Level density and spectral form factor	50
1.5 Chern–Simons theory	53
1.5.1 Knot operator formalism	53
1.5.2 Chern–Simons matrix model	59

2	Unitary matrix integrals	69
2.1	Power sums and hook-shaped diagrams	69
2.1.1	Applying Wick's theorem	72
2.2	Integrating over generalized power sums	76
2.3	Schur polynomials and border strips	78
2.3.1	Expansion in Schur polynomials	78
2.3.2	Expansion in power sum polynomials	87
 3	 Long-range random walks	 96
3.1	Correlation functions	96
3.2	Row and column diagrams	99
3.3	Quasi-local particle-hole duality	104
3.4	Power sums and border strips	106
3.5	Time evolution	113
3.6	Fermionic models	115
3.7	Schur function expansion	120
3.8	Power sum expansion	123
3.9	Experimental benchmarking	125
 4	 Spectral statistics	 127
4.1	Spectral form factors and universality	127
4.2	General matrix size	129
4.3	Appearance of the linear ramp	131
4.4	Saturation at plateau	136
4.5	Taking the 't Hooft-limit	141
4.6	Non-commutativity of limits	153
 Concluding remarks		 156
 Bibliography		 160

Contents

Dankwoord	172
Lekensamenvatting	175
Lay summary	182
Curriculum vitæ	188

List of abbreviations

This work contains the following abbreviations, in order of appearance.

- RMT: Random matrix theory
- CSMM: Chern–Simons matrix model
- LRRW: Long-range random walk
- CUE: Circular unitary ensemble
- WD: Wigner–Dyson
- SFF: Spectral form factor
- HOMFLY: Hoste–Ocneanu–Millett–Freyd–Lickorish–Yetter
- JT: Jackiw–Teitelboim
- SYK: Sachdev–Ye–Kitaev
- RME: Random matrix ensemble
- GOE: Gaussian orthogonal ensemble
- GUE: Gaussian unitary ensemble
- GSE: Gaussian symplectic ensemble

List of abbreviations

- COE: Circular orthogonal ensemble
- CSE: Circular symplectic ensemble
- BGS: Bohigas–Giannoni–Schmit
- BT: Berry–Tabor
- WZNW: Wess–Zumino–Novikov–Witten
- QLPH: Quasi-local particle-hole (duality)

List of publications

This thesis is based on the following publications:

Chapters 2 and 3 are based on

[1] W.L. Vleeshouwers and V. Gritsev. Unitary matrix integrals, symmetric polynomials, and long-range random walks. *Journal of Physics A: Mathematical and Theoretical*, 56(18):185002, 2023.

The first section of chapter 4 is based on

[2] W.L. Vleeshouwers and V. Gritsev. Topological field theory approach to intermediate statistics. *SciPost Phys.*, 10:146, 2021.

The remaining sections of chapter 4 are based on

[3] W.L. Vleeshouwers and V. Gritsev. The spectral form factor in the ‘t Hooft limit – Intermediacy versus universality. *SciPost Phys. Core*, 5:051, 2022.

List of publications

Publications that I am involved in which are not featured in this work are:

- D. Lüst and W.L. Vleeshouwers. Black hole information and thermodynamics. SpringerBriefs in Physics. *Springer*. 2019.
- D. Liška, V. Gritsev, W.L. Vleeshouwers, J. Minář. Holographic Quantum Scars. *SciPost Phys.*, 15:106, 2023.
- C. Chao, W.L. Vleeshouwers, S. Heatley, V. Gritsev, C. Morais Smith. Quantum geometry of non-Hermitian topological systems. *arXiv: 2305.17675*, 2023.
- W. Buijsman, W.L. Vleeshouwers, V. Gritsev. The spectral statistics of the Chern–Simons matrix model. *In preparation*.

Introduction

We provide here a brief overview of both the research process and the resulting thesis. This serves only to guide the reader. We will therefore introduce terms whose further explanation and contextualization is postponed to the following chapter.

The main focus of this thesis is the study of unitary integrals over symmetric functions, weighted by some weight function. Our original motivation for studying these objects is their application to random matrix theory (RMT) and spectral statistics. While RMT has mainly been applied to the study of chaotic quantum systems, a unitary ensemble was introduced in 1993 by Muttalib and co-authors [4], which was found to display the ‘intermediate’ statistics of quantum systems somewhere in between chaotic and integrable, such as disordered electrons at the mobility edge of Anderson localization. This same matrix model was later found [5] to describe $U(N)$ Chern–Simons theory on a three-sphere, for which reason we refer to it as the Chern–Simons matrix model (CSMM). Chern–Simons theory is a topological theory; our aim was to use topological methods to better understand the chaotic-to-integrable transition. Indeed, this transition lacks a local order parameter, which lead to the suspicion by my supervisor, Vladimir Gritsev, that it is in fact a topological transition, borrowing intuition from topological condensed matter physics. However, despite a large collection of previous publications on intermediate statistics in the CSMM (see e.g. [6], [7], [8], [9], [10], [11], [12], [13]), our calculations did not reveal

any intermediate statistics in this model. Due to the usage of different techniques, our results are difficult to reconcile (or even compare) with the previous literature. With Wouter Buijsman, we are currently pursuing the question of intermediacy in the CSMM through a numerical approach.

Although, contrary to our expectations, we did not find intermediacy in the CSMM, our efforts described above eventually resulted in various results on unitary matrix integrals over symmetric polynomials, including certain recursive expansions. These allow one to break down a complicated problem into a set of simpler ones, resulting in an expansion in terms of objects which are well understood. It soon became apparent that our results could be naturally applied to the study of (what we refer to as) long-range random walkers (LRRW), essentially given by long-range generalizations of the XY-spin chain. These are given by non-intersecting (hard-core bosonic) random walkers which can hop over greater distances than a single site, subject to mild fall-off conditions on the hopping parameters. These models have gained increasing attention in the last 15 years due in part to their experimental realizability in trapped ion systems [14], see e.g. [15] for a review. They have also been increasingly applied to various physical questions, such as localization on low-dimensional long-range models by addition of diagonal disorder [16], [17] and systems with random hopping parameters [18], [19], see e.g. [20], [21], [22] for other examples. It was shown by Bogoliubov for the nearest-neighbor case, given by the XY-model at zero magnetic field, that correlation functions of random walkers are given by unitary integrals over symmetric polynomials [23], see also [24], [25]. This was later generalized to the long-range case by Pérez-García and Tierz [26]. Applying our results on unitary matrix integrals, as well as standard identities from the theory of symmetric functions, we find various surprising relations and dualities between various LRRW correlation functions, as well as convenient ways to compute them. In passing, we demonstrate various results on long-range fermionic models as well, and suggest mathematical and experimental applications.

This shift of focus, from RMT and spectral statistics, to unitary integrals as such and their application to LRRW models, is reflected in the structure of the thesis. In chapter 1, we will treat the relevant background material, starting from symmetric functions and partitions, and applying them to the evaluation of unitary integrals over symmetric polynomials. The remainder of chapter 1 presents various areas in which these objects may be applied, starting from long-range random walkers before continuing with RMT and spectral statistics, with particular attention given to the CSMM and its previous application to the study of intermediate statistics.

Chapter 2 presents our mathematical results and is based mainly on [1]. Building on the main result of [2], given in equation (2.8), we compute the average over generalized power sum polynomials. Our expression, given in equation (2.30), generalizes a long-standing result due to Diaconis and Shahshahani, who considered the same object in the CUE [27], [28]. We then apply our expression to bilinears of Schur polynomials, leading to recursive expansions in terms of Schur polynomials and generalized power sum polynomials. These are given in equation (2.46) and (2.62), respectively.

In chapter 3, which is also based mainly on [1], we apply our results on unitary integrals to long-range random walkers. Before doing so, we first consider standard identities from the theory of symmetric functions. This leads to various results, including equations (3.16), (3.17), (3.23), (3.24), (3.25). Most striking of these results is quasi-local particle-hole duality, written in equation (3.33), which arises from the involution between elementary and complete homogeneous symmetric polynomials corresponding to the transposition of Young diagrams. We then note a relation between the multiplication properties of power sum polynomials of degree n and fermionic particles hopping by n sites. This allows us to interpret various results in terms of an auxiliary fermionic (rather than hard-core bosonic) system. This reasoning can be applied to the computation of the irreducible characters of the

symmetric group, as we explain just above section 3.5. Further, combined with identities we found in [2], the relation between power sums and fermions leads immediately to expressions for certain correlation functions such as (3.52). In section 3.5, we use the relation between border strips and particle hopping to characterize the action of the hamiltonian in terms of Young diagrams. In section 3.6, we use the aforementioned relation between power sums and fermions to derive two results on long-range fermionic models. First of all, if we take a fermionic configuration (on a one-dimensional lattice) and consecutively move fermions to the right by various step sizes, the outcome depends only on the distribution of the step sizes and not the order in which they are taken. Naturally, this statement also holds if we move fermions to the left instead of the right. Secondly, we find that going from any fermionic configuration A to another configuration B by consecutively moving fermions by n lattice sites involves hopping over *either* an even *or* an odd number of particles, depending only on the choice of A, B, and n . Sections 3.7 and 3.8 consider the application of the recursive expansions derived in chapter 2 to long-range correlation functions. Here, the expansion in generalized power sums is particularly useful, as it gives an expansion in terms of powers of the time parameter, where the expansion coefficients have simple expressions in terms of the relevant hopping parameters. In section 3.9, we suggest particular correlation functions which could be used for the benchmarking of experimental setups, such as the aforementioned trapped ion systems.

Chapter 4 considers the application of unitary matrix integrals to RMT and spectral statistics, focusing in particular on the calculation of the spectral form factor (SFF) in the CSMM. First, a special case of the main result in [2] demonstrates that the SFF of a broad class of matrix models is of standard Wigner-Dyson type, consisting of a linear ramp which saturates at a plateau. We then consider the CSMM for general matrix size before taking the 't Hooft limit, which should correspond to the maximal disorder limit. Nonetheless, after unfolding, we recover WD-universality in

the cases we consider, as was mentioned above. Interestingly, however, taking the ‘t Hooft limit turns the SFF into a sequence of polynomials with surprising properties which do not appear to have been described in the literature thus far, see section 4.5. Further, the calculations in chapter 4 have applications in Chern–Simons theory and knot theory as well, as the SFF is proportional to the HOMFLY invariant of a $(2n, 2)$ -torus link with components in the fundamental and antifundamental representations. These, to the best of our knowledge, have not been calculated before.

Chapter 1

Background material

1.1 Symmetric functions

We review here some aspects of symmetric functions and Young diagrams that will be useful to us later. Symmetric functions have been studied for centuries due to the fact that they arise naturally in the study of polynomial roots, as expressed in Viète's formulas. Symmetric functions have an intimate relationship with certain combinatorial objects known as Young diagrams. Symmetric functions and Young diagrams play an important role in a wide variety of mathematical fields, including Galois theory [29], representation theory [30], enumerative combinatorics [31], and geometry [32]. Throughout the remainder of this thesis, we will be applying the properties of symmetric polynomials to the evaluation of unitary matrix integrals.

We first consider certain basic types of symmetric functions. Take a set of variables $x = (x_1, x_2, \dots)$. The *elementary symmetric polynomials* are then defined as

$$e_k(x) = \sum_{i_1 < \dots < i_k} x_{i_1} \dots x_{i_k} . \quad (1.1)$$

Some examples include

$$\begin{aligned} e_0 &= 1 , \\ e_1(x_1) &= x_1 , \\ e_1(x_1, x_2) &= x_1 + x_2 , \\ e_2(x_1, x_2) &= x_1 x_2 . \end{aligned} \tag{1.2}$$

Closely related are the *complete homogeneous symmetric polynomials*, defined as

$$h_k(x) = \sum_{i_1 \leq \dots \leq i_k} x_{i_1} \dots x_{i_k}, \tag{1.3}$$

which contain all monomials of degree k . Note the difference in the summation bounds between (1.1) and (1.3). Some examples of h_k include

$$\begin{aligned} h_0 &= 1 , \\ h_1(x_1) &= x_1 , \\ h_1(x_1, x_2) &= x_1 + x_2 , \\ h_2(x_1, x_2) &= x_1 x_2 + x_1^2 + x_2^2 . \end{aligned} \tag{1.4}$$

Another type of symmetric polynomial is the *power-sum polynomial*,

$$p_k(x) = \sum_j x_j^k = x_1^k + x_2^k + \dots \tag{1.5}$$

The generating functions of e_k and h_k and their relation with power sums are as

follows [see e.g [33]],

$$\begin{aligned} E(x; z) &= \sum_{k=0}^{\infty} e_k(x)z^k = \prod_{k=1}^{\infty} (1 + x_k z) = \exp \left[\sum_{k=1}^{\infty} \frac{(-1)^{k+1}}{k} p_k(x) z^k \right], \\ H(x; z) &= \sum_{k=0}^{\infty} h_k(x)z^k = \prod_{k=1}^{\infty} \frac{1}{1 - x_k z} = \exp \left[\sum_{k=1}^{\infty} \frac{1}{k} p_k(x) z^k \right]. \end{aligned} \quad (1.6)$$

From the above expressions, it is clear that $H(x; z)E(x; -z) = 1$. Checking every order of z then gives, for all $n \geq 1$ and any choice of x [e.g. (2.6') from [33]],

$$\sum_{r=0}^n (-1)^r h_{n-r}(x) e_r(x) = 0. \quad (1.7)$$

Partitions play an important role in the study of symmetric polynomials. A partition of $n \in \mathbb{Z}^+$ is a sequence of non-negative integers $\lambda = (\lambda_1, \lambda_2, \dots, \lambda_{\ell(\lambda)})$, which we will order these as $\lambda_1 \geq \lambda_2 \geq \dots$, satisfying $\sum_j \lambda_j = n$. The *size* (or *weight*) of a partition is given by the sum of its terms $|\lambda| = \sum_j \lambda_j$ and its *length* $\ell(\lambda)$ is the largest value of j such that $\lambda_j \neq 0$. Closely related to partitions of n are *compositions* of n , consisting also of a sequence of positive integers which sum to n , but where a different ordering in these integers defines a different composition. A *weak composition* of n is a composition which may include zeroes as its entries, that is, a set of non-negative integers which sum up to n . A partition of n corresponds to a Young (or Ferrers) diagram containing n cells, or ‘boxes’. We will use these terms interchangeably. As an example, the diagram corresponding to a partition of 12 given by $\lambda = (6, 4, 2, 1)$ is given below, where λ_j equals the number of cells in the

j^{th} row.



$$(1.8)$$

For future use, we define $n(\lambda) = \sum_j (j-1)\lambda_j$. Further, for elements of λ , $x = (j, k) \in \lambda$ with j, k positive integers, $c(x) = k - j$ is the *content* of x , and $h(x) = \lambda_j + \lambda_k^t - j - k + 1$ is its *hook-length*. The latter equals one plus the number of boxes to the right and below x .

We will denote a diagram consisting of b rows of a cells by (a^b) . For a partition λ , we will write

$$e_\lambda = \prod_{j \geq 1} e_{\lambda_j}, \quad h_\lambda = \prod_{j \geq 1} h_{\lambda_j}, \quad p_\lambda = \prod_{j \geq 1} p_{\lambda_j}. \quad (1.9)$$

Further, we write

$$z_\lambda = \prod_{j \geq 1} j^{m_j} m_j!, \quad m_j(\lambda) = \text{Card}\{k : \lambda_k = j\}, \quad (1.10)$$

i.e. $m_j(\lambda)$ is the number of rows in λ of length j . We also write $\varepsilon_\lambda = (-1)^{|\lambda| - \ell(\lambda)}$. Newton's identities then read

$$\begin{aligned} h_n &= \sum_{|\lambda|=n} z_\lambda^{-1} p_\lambda, \\ e_n &= \sum_{|\lambda|=n} \varepsilon_\lambda z_\lambda^{-1} p_\lambda. \end{aligned} \quad (1.11)$$

In terms of the complete exponential Bell polynomial B_n ¹, we have

$$\begin{aligned} h_n &= \frac{1}{n!} B_n(p_1, p_2, 2!p_3, \dots, (n-1)!p_n) , \\ e_n &= \frac{(-1)^n}{n!} B_n(-p_1, -p_2, -2!p_3, \dots, -(n-1)!p_n) . \end{aligned} \quad (1.12)$$

Another type of symmetric polynomial is the *Schur polynomial*. Schur polynomials play an important role as characters of irreducible representations, often referred to as irreps, of general linear groups and subgroups thereof. Schur polynomials are associated to a partition λ and a set of variables $x = (x_1, x_2, \dots)$ in the following way. For a choice of λ , a *semistandard Young tableau* (SSYT) is given by positive integers $T_{i,j}$ satisfying $1 \leq i \leq \ell(\lambda)$ and $1 \leq j \leq \lambda_i$. These integers are required to increase weakly along every row and increase strongly along every column, i.e. $T_{i,j} \geq T_{i,j+1}$ and $T_{i,j} > T_{i+1,j}$ for all i, j . Label by α_i the number of times that the number i appears in the SSYT. We then define

$$x^T = x_1^{\alpha_1} x_2^{\alpha_2} \dots . \quad (1.13)$$

The *Schur polynomial* $s_\lambda(x)$ is given by [31].

$$s_\lambda(x) = \sum_T x^T , \quad (1.14)$$

where the sum runs over all SSYT's corresponding to λ i.e. all possible ways to inscribe the diagram corresponding to λ with positive integers that increase weakly along rows and strictly along columns. If $\lambda_j = 0$ for all j , then λ is the empty partition, which we denote by $\lambda = \emptyset$. The Schur polynomial of the empty partition

¹Complete Bell polynomials $B_n(x_1 \dots x_n)$ can be defined by their generating function, $\sum_{n=0}^{\infty} B_n(x_1 \dots x_n) t^n / n! = \exp(\sum_{j=1}^{\infty} x_j t^j / j!)$

is set to unity, i.e.

$$s_{\emptyset}(x) = 1 , \quad (1.15)$$

which is independent of the choice of variables x . Schur polynomials with N variables equal to 1 and all other variables equal to zero give the hook-length formula for the dimension of the representation, that is

$$s_{\lambda}(1^N) = \prod_{x \in \lambda} \frac{N + c(x)}{h(x)} =: \dim(\lambda) , \quad (1.16)$$

We give an example of an SSYT corresponding to a Young diagram $\lambda = (3, 2)$ and with non-zero variables x_1, x_2, x_3 .

$$\begin{array}{|c|c|c|} \hline 1 & 1 & 3 \\ \hline 2 & 3 & \\ \hline \end{array} \quad (1.17)$$

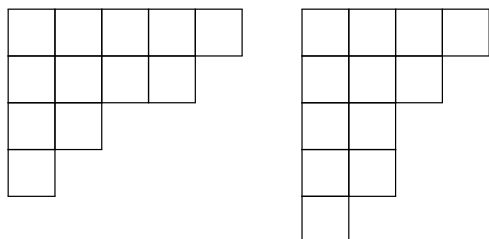
From (1.26) one can see that the contribution of this SSYT is given by $x_1^2 x_2 x_3^2$. Summing over all monomials corresponding to all SSYT's then gives the Schur polynomial $s_{(3,2)}(x_1, x_2, x_3)$. We emphasize that the result is generally a symmetric polynomial, as this may not be obvious from the definition. Consider the Schur polynomials corresponding to a row or a column of n cells, shown below for $n = 4$.

$$\begin{array}{|c|c|c|c|} \hline & & & \\ \hline & & & \\ \hline & & & \\ \hline & & & \\ \hline \end{array} \quad \begin{array}{|c|} \hline \\ \hline \\ \hline \\ \hline \\ \hline \end{array} \quad (1.18)$$

One can see that

$$s_{(1^n)} = e_n , \quad s_{(n)} = h_n , \quad (1.19)$$

for any choice of x . That is, the Schur polynomial of a column or row of n cells is given by the degree n elementary or complete homogeneous symmetric polynomial, respectively. Equation (1.19) simply follows from the requirement for SSYT's that integers increase weakly along rows and strongly along columns, compare with (1.1) and (1.3). It follows that we can exchange between e_n and h_n by transposing diagrams, that is, by reflecting across the main diagonal of the diagram, as this exchanges rows and columns. For a diagram λ , its transpose is denoted as λ^t . Since transposition is a reflection, it is an involution, i.e. $(\lambda^t)^t = \lambda$. It is clear that $(n)^t = (1^n)$ i.e. this involution maps rows to columns and vice versa. As a somewhat less trivial example, take $\lambda = (5, 4, 2, 1)$, shown below on the left, and $\lambda^t = (4, 3, 2^2, 1)$, shown on the right.



$$(1.20)$$

Power sum polynomials can also be expressed in terms of Schur polynomials, in this case in the form of a sum,

$$p_n = \sum_{r=0}^{n-1} (-1)^r s_{(n-r, 1^r)}. \quad (1.21)$$

Here, $(a, 1^b)$ is a hook-shaped diagram consisting of a row with a cells followed by b rows with a single cell. For example, $\lambda = (5, 1^3)$ is given by the following diagram.

$$\begin{array}{cccccc}
 \square & \square & \square & \square & \square & \\
 \square & & & & & \\
 \square & & & & & \\
 \square & & & & &
 \end{array} \tag{1.22}$$

Although equation (1.21) may not be immediately obvious, it can easily be seen to arise in simple examples. If $x = (x_1, x_2)$ and $n = 1$, we have the following SSYT's.

$$\boxed{1} + \boxed{2} \tag{1.23}$$

Which gives $p_1(x) = s_{(1)}(x_1, x_2) = x_1 + x_2$. For $n = 2$, the following SSYT's contribute,

$$\boxed{1 \mid 1} + \boxed{1 \mid 2} + \boxed{2 \mid 2} - \begin{array}{c} \boxed{1} \\ \boxed{2} \end{array} \tag{1.24}$$

Note that the rightmost SSYT corresponding to (1^2) contributes with a minus sign, which results in $p_2(x) = s_{(2)}(x_1, x_2) - s_{(1^2)}(x_1, x_2) = x_1^2 + x_2^2$. One may convince oneself that this generalizes to higher n and general choice of x .

Schur polynomials have a natural generalization to so-called *skew Schur polynomials*, which are associated to skew diagrams. Skew diagrams are constructed from two non-skew diagrams λ and μ such that $\mu \subseteq \lambda$, which means that $\mu_i \leq \lambda_i, \forall i$. The skew diagram denoted by λ/μ is then the complement of μ in the diagram corresponding to λ . For $\lambda = (4, 3, 2)$ and $\mu = (2, 1)$, the skew diagram λ/μ is given by the following, where we indicate in black those cells which are removed from λ .

$$(1.25)$$

The skew diagram on the right hand side is a *border strip*, which is a connected skew diagram not containing a 2 by 2 subdiagram. This is an important class of skew diagrams which we will encounter again later. For a general skew diagram, define a skew semistandard Young tableau corresponding to λ/μ as above, namely, as an array of positive integers T_{ij} satisfying $1 \leq i \leq \ell(\lambda)$ and $\mu_i \leq j \leq \lambda_i$ which increase weakly along rows and strictly along columns. We then define the *skew Schur polynomial* corresponding to λ/μ as

$$s_{\lambda/\mu} = \sum_T x^T, \quad (1.26)$$

where the sum again runs over all SSYT's corresponding to λ/μ . Note that if $\mu = \emptyset$, we have $s_{\lambda/\mu} = s_\lambda$, and if $\mu = \lambda$, $s_{\lambda/\lambda} = s_\emptyset = 1$. Let us consider $\lambda = (3, 2)$ and $\mu = (1)$. Below, we give a skew SSYT corresponding to the skew partition λ/μ , which would contribute $x_1^2 x_2 x_3$ to the skew Schur polynomial.

$$(1.27)$$

From the strong increase of integers along the rows of a (skew) SSYT, it follows that,

$$s_{\lambda/\mu}(x_1, \dots, x_n) = 0 \text{ unless } 0 \leq \lambda_i^t - \mu_i^t \leq n \text{ for all } i \geq 1. \quad (1.28)$$

Note that an example of (1.28) is given by the fact that $e_k(x_1, \dots, x_N) = 0$ for $k > N$.

We have the following expressions for skew Schur polynomials,

$$s_{\lambda/\mu} = \sum_{\nu} c_{\mu\nu}^{\lambda} s_{\nu} , \quad (1.29)$$

and products of non-skew Schur polynomials,

$$s_{\lambda} s_{\mu} = \sum_{\nu} c_{\lambda\mu}^{\nu} s_{\nu} . \quad (1.30)$$

The expansion coefficients $c_{\mu\nu}^{\lambda}$ are known as *Littlewood-Richardson coefficients*, which are given by the number of Littlewood-Richardson tableaux of shape ν/λ and weight μ . A Littlewood-Richardson tableau is an SSYT such that, when we read its entries from right to left and top to bottom, any positive integer j appears at least as many times as $j+1$. Note from (1.30) that $c_{\mu\nu}^{\lambda} = c_{\nu\mu}^{\lambda}$. For example, of the SSYT's pictured below, the one on the left is a Littlewood-Richardson tableau while the one on the right is not.

$$\begin{array}{c}
 \begin{array}{|c|c|c|}
 \hline
 & 1 & 1 \\
 \hline
 & 2 & 2 \\
 \hline
 1 & 3 & \\
 \hline
 \end{array}
 \qquad
 \begin{array}{|c|c|c|}
 \hline
 & 1 & 2 \\
 \hline
 & 2 & 2 \\
 \hline
 1 & 3 & \\
 \hline
 \end{array}
 \end{array}
 \quad (1.31)$$

The Littlewood-Richardson coefficients also appear in the following expression [equation (5.10) in [33]]

$$s_{\lambda/\mu}(x, y) = \sum_{\nu} s_{\lambda/\nu}(x) s_{\nu/\mu}(y) , \quad (1.32)$$

where the sum is over all ν satisfying $\mu \subseteq \nu \subseteq \lambda$. We apply the Littlewood-Richardson rule to the special case where one of the diagrams consists of a single

row. The result is known as the Pieri formula [33],

$$s_\lambda h_n = \sum_{\nu} s_\nu, \quad (1.33)$$

where the sum is over all ν such that ν/λ is a horizontal strip, i.e. a skew diagram with at most one cell in each column. Applying the involution which transposes all diagrams, and therefore exchanges $h_n = s_{(n)}$ with $e_n = s_{(1^n)}$, we have

$$s_\lambda e_n = \sum_{\nu} s_\nu, \quad (1.34)$$

where the sum is now over all ν such that ν/λ is a vertical strip, i.e. a skew diagram with at most one cell in each row. The Pieri formula states that $c_{\lambda\mu}^\nu$ for $\mu = (n)$ is equal to 1 when ν/λ is a horizontal strip, and zero otherwise. Applying this to $s_{\lambda/(n)}$, we have

$$s_{\lambda/(n)} = \sum_{\nu} s_\nu, \quad (1.35)$$

where the sum is now over all ν such that λ/ν is a horizontal strip. From (1.34), we also have

$$s_{\lambda/(1^n)} = \sum_{\nu} s_\nu, \quad (1.36)$$

where λ/ν is a vertical strip. The Pieri formula in (1.35) is illustrated below for $\lambda = (2, 1)$ and $n = 2$, with the cells that are added onto λ are indicated in gray. It is clear that ν/λ is a horizontal strip for all diagrams ν on the right hand side, as there are no two gray cells in any column. For equation (1.34), one should simply transpose the diagrams.

$$\begin{array}{|c|c|} \hline \square & \square \\ \hline \square & \square \\ \hline \end{array} \begin{array}{|c|c|c|} \hline \square & \square & \square \\ \hline \end{array} = \begin{array}{|c|c|c|c|} \hline \square & \square & \blacksquare & \blacksquare \\ \hline \square & & & \\ \hline \end{array} + \begin{array}{|c|c|c|} \hline \square & \square & \blacksquare \\ \hline \square & \blacksquare & \\ \hline \end{array} + \begin{array}{|c|c|c|} \hline \square & \square & \blacksquare \\ \hline \square & & \\ \hline \blacksquare & & \\ \hline \end{array} + \begin{array}{|c|c|} \hline \square & \square \\ \hline \square & \blacksquare \\ \hline \blacksquare & \\ \hline \end{array} \quad (1.37)$$

We can use the Pieri rule to demonstrate $\sum_{r=0}^n (-1)^r h_{n-r} e_r = 0$, equation (1.7). In particular, for $a, b \geq 1$, we have

$$h_a e_b = s_{(a,1^b)} + s_{(a+1,1^{b-1})}. \quad (1.38)$$

The example for $a = 4$ and $b = 3$ gives the following:

$$\begin{array}{|c|c|c|c|} \hline \square & \square & \square & \square \\ \hline \end{array} \begin{array}{|c|} \hline \square \\ \hline \square \\ \hline \square \\ \hline \end{array} = \begin{array}{|c|c|c|c|} \hline \square & \square & \square & \square \\ \hline \blacksquare & & & \\ \hline \blacksquare & & & \\ \hline \blacksquare & & & \\ \hline \end{array} + \begin{array}{|c|c|c|c|} \hline \square & \square & \square & \blacksquare \\ \hline \blacksquare & & & \\ \hline \blacksquare & & & \\ \hline \blacksquare & & & \\ \hline \end{array} \quad (1.39)$$

Plugging this in gives

$$\sum_{r=0}^n (-1)^r h_{n-r} e_r = h_n + (-1)^n e_n + \sum_{r=1}^{n-1} (-1)^r (s_{(n-r,1^r)} + s_{(n-r+1,1^{r-1})}) = 0. \quad (1.40)$$

For $1 \leq r \leq n-1$, the summand on the left for any r is cancelled with terms coming from $r-1$ and $r+1$. For $r=0$ and $r=n$, we get the contributions h_n and $(-1)^n e_n$ which cancel with term from $r=1$ and $r=n-1$, respectively. For example, for $n=3$, applying the Pieri formula gives the diagrams below.

$$\begin{aligned}
 \sum_{r=0}^3 (-1)^r h_{3-r} e_r &= \begin{array}{|c|c|c|} \hline \square & \square & \square \\ \hline \end{array} - \begin{array}{|c|c|c|} \hline \square & \square & \square \\ \hline \end{array} + \begin{array}{|c|} \hline \square \\ \hline \square \\ \hline \end{array} \begin{array}{|c|} \hline \square \\ \hline \end{array} - \begin{array}{|c|} \hline \square \\ \hline \square \\ \hline \square \\ \hline \end{array} \\
 &= \begin{array}{|c|c|c|} \hline \square & \square & \square \\ \hline \end{array} - \begin{array}{|c|c|c|} \hline \square & \square & \square \\ \hline \end{array} - \begin{array}{|c|} \hline \square \\ \hline \square \\ \hline \end{array} + \begin{array}{|c|} \hline \square \\ \hline \square \\ \hline \end{array} + \begin{array}{|c|} \hline \square \\ \hline \square \\ \hline \square \\ \hline \end{array} - \begin{array}{|c|} \hline \square \\ \hline \square \\ \hline \square \\ \hline \end{array} = 0. \tag{1.41}
 \end{aligned}$$

Further, we have [e.g. theorem 7.17.1, [31]]

$$s_{\lambda} p_n = \sum_{\nu} (-1)^{\text{ht}(\nu/\lambda)} s_{\nu}, \tag{1.42}$$

where ν/λ is a border strip of size n , i.e. a containing n cells. The height $\text{ht}(\nu/\lambda)$ equals the numbers of rows that the border strip occupies minus one. We will also denote these border strips by (e.g.) η with $|\eta| = n$ and write $\nu \setminus \eta$ for the partition obtained from ν after removing the border strip η . For $\lambda = (3, 2)$ and $n = 3$, equation (1.42) is as follows:

$$\begin{array}{|c|c|c|c|c|} \hline \square & \square & \square & \blacksquare & \blacksquare & \blacksquare \\ \hline \square & \square & & & & \end{array} - \begin{array}{|c|c|c|c|} \hline \square & \square & \square & \blacksquare \\ \hline \square & \square & \blacksquare & \blacksquare \\ \hline \end{array} - \begin{array}{|c|c|c|} \hline \square & \square & \square \\ \hline \square & \square & \square \\ \hline \blacksquare & \blacksquare & \blacksquare \\ \hline \blacksquare & & \blacksquare \\ \hline \end{array} + \begin{array}{|c|c|c|} \hline \square & \square & \square \\ \hline \square & \square & \square \\ \hline \blacksquare & & \blacksquare \\ \hline \blacksquare & & \blacksquare \\ \hline \blacksquare & & \blacksquare \\ \hline \end{array} \tag{1.43}$$

Similar to the Pieri formula, equation (1.42) can be inverted to give the following expression for skew Schur polynomials,

$$\sum_{r=0}^{n-1} (-1)^r s_{\lambda/(n-r, 1^r)} = \sum_{\nu} (-1)^{\text{ht}(\lambda/\nu)} s_{\nu}, \tag{1.44}$$

where the sum is now over all ν such that λ/ν is a border strip of size n .

Schur polynomials can be expressed in determinantal form. First of all, the (anti-symmetric) Vandermonde determinant can be expressed as

$$\det \left(x_j^{(N-k)} \right)_{j,k=1}^N = \prod_{1 \leq j < k \leq N} (x_j - x_k) . \quad (1.45)$$

We then have

$$s_\lambda(x_j) = \frac{\det \left(x_j^{N-k+\lambda_k} \right)_{j,k=1}^N}{\det \left(x_j^{N-k} \right)_{j,k=1}^N} . \quad (1.46)$$

(Skew) Schur polynomials can be expressed in terms of elementary symmetric polynomials or complete homogeneous symmetric polynomials via the following determinantal expressions, known as the Jacobi-Trudi identities,

$$\begin{aligned} s_{(\mu/\lambda)} &= \det(h_{\mu_j - \lambda_k - j + k})_{j,k=1}^{\ell(\mu)} = \det(e_{\mu_j^t - \lambda_k^t - j + k})_{j,k=1}^{\mu_1} , \\ s_{(\mu/\lambda)^t} &= \det(e_{\mu_j - \lambda_k - j + k})_{j,k=1}^{\ell(\mu)} = \det(h_{\mu_j^t - \lambda_k^t - j + k})_{j,k=1}^{\mu_1} . \end{aligned} \quad (1.47)$$

Again, we see that the expressions in terms of h_j and e_j are related by transposition of the skew diagram, $(\mu/\lambda) \rightarrow (\mu/\lambda)^t$.

Schur polynomials can also be expanded in terms of power sum polynomials,

$$s_\lambda = \sum_{\alpha} \frac{\chi_{\alpha}^{\lambda}}{z_{\alpha}} p_{\alpha} , \quad (1.48)$$

where the sum is over all partitions α , z_{α} is defined in (1.10), and where χ_{α}^{λ} is the character of the symmetric group S_n with $n = |\lambda|$ of an irrep λ associated to a permutation of cycle type α , see e.g. [33], [31]. In fact, α can generally be a weak

composition, and χ_α^λ does not depend on the order of the entries of α . However, in (1.48), we only sum over a single α corresponding to each cycle type, which is equivalent to summing over partitions. Equation (1.48) generalizes to the case of a skew partition λ/μ instead of λ . The inverse of (1.48) is given by

$$p_\alpha = \sum_{\lambda} \chi_\alpha^\lambda s_\lambda. \quad (1.49)$$

It is clear that p_α does not depend on the order of the entries of α , it then follows from the above expression that the same is true for χ_α^λ . To construct the latter objects, we first define a *border-strip tableau* (BST) of shape λ and type α as follows. We take a diagram λ and inscribe it with positive integers such that

1. The integers are weakly increasing along both rows and columns
2. The cells of λ that are inscribed by j form a border strip of size α_j

The resulting object is called a *border strip tableau*, which we denote as $T \in \text{BST}(\lambda, \alpha)$. We show an example below for $\lambda = (7, 5^2, 3, 1)$ and $\alpha = (4^2, 5, 3, 5)$ (remember that α is a composition and its entries are not generally in non-decreasing order) where cells belonging to a single border strip share the same color.

1	1	1	2	2	2	2
1	3	3	3	5		
	3	3	5	5	5	
	4	4	5			
	4					

(1.50)

Denoting the border strips of length α_j that appear in T as B_j , the height of T is

defined as

$$\text{ht}(T) = \sum_{j=1}^{\ell(\alpha)} \text{ht}(B_j) . \quad (1.51)$$

For example, for the above BST for $\lambda = (7, 5^2, 3, 1)$ and $\alpha = (4^2, 5, 3, 5)$, we have

$$\text{ht}(T) = 1 + 0 + 1 + 1 + 2 = 5 . \quad (1.52)$$

We then have

$$\chi_{\alpha}^{\lambda} = \sum_{T \in \text{BST}(\lambda, \alpha)} (-1)^{\text{ht}(T)} . \quad (1.53)$$

This is known as the Murnaghan-Nakayama rule, see e.g. [33] or [31]. The Murnaghan-Nakayama rule generalizes to skew diagrams λ/μ .

Consider a simple example we have encountered before. From (1.49), we have

$$p_n = \sum_{\lambda} \chi_{(n)}^{\lambda} s_{\lambda} = \sum_{r=0}^{n-1} (-1)^r s_{(n-r, 1^r)} . \quad (1.54)$$

This arises simply from the fact that any Young diagram consisting of a single border strip is a hook shape, as this is the only type of non-skew diagram that has no two by two subdiagram. This gives a sum over all hook shapes containing n cells, $(n-r, 1^r)$, where the sign appears from the fact that $\text{ht}((n-r, 1^r)) = r$. We thus see how equation (1.21) arises as a special case of (1.49). To calculate χ_{α}^{λ} , one can use the following recursive formula [e.g. (2.4.4) [34]]

$$\chi_{\alpha}^{\lambda} = \sum_{\rho} (-1)^{\text{ht}(\rho)} \chi_{\alpha - \alpha_1}^{\lambda \rho} , \quad (1.55)$$

where the sum runs over all border strips ρ of λ containing α_1 cells, $\lambda \setminus \rho$ is the results of removing ρ from λ , and $\alpha - \alpha_j = (\alpha_1, \alpha_2, \dots, \alpha_{j-1}, \alpha_{j+1}, \dots)$. We emphasize again that χ^λ_α does not depend on the order of the entries of α . This implies that we can consecutively apply equation (1.55) by removing border strips of different sizes in different orders, and end up with the same result. This may at first sight be surprising, as removing border strips in different orders generally leads to a different set of diagrams. Let us consider a simple example, where we remove border strips of sizes 1 and 2 from $\lambda = (3, 2) = \begin{array}{|c|c|c|} \hline \square & \square & \square \\ \hline \square & \square & \square \\ \hline \end{array}$ in the two different orders. This is indicated in the figure below, where two diagrams connected by an arrow as

$$\lambda - p_j \rightarrow \mu \tag{1.56}$$

indicates that partitions λ and μ are related by the removal of a border strip of size j .

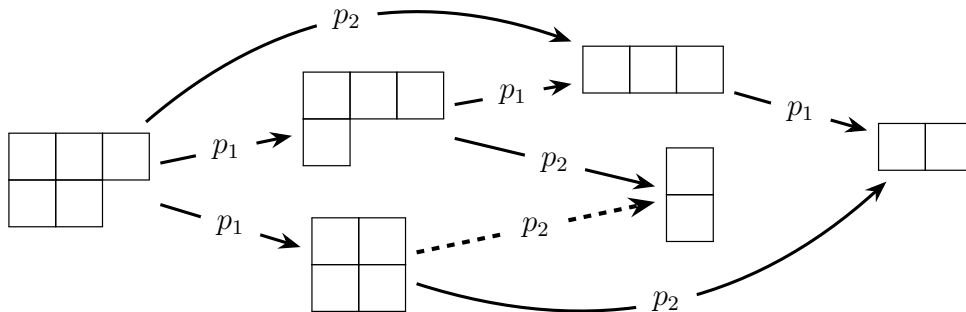




Figure 1.1: The Young diagram for $\lambda = (3, 2)$ and the removal of border strips of sizes 1 (single cell) and 2 (domino), indicated by p_1 and p_2 , respectively. The dashed line connecting $(2, 2)$ and $(1, 1)$ indicates the only case where a border strip of odd height is removed.

It is clear from figure 1.1 that going first along p_2 and then along p_1 only leads to the result $\begin{array}{|c|c|} \hline \square & \square \\ \hline \end{array}$, where going first along p_1 and then p_2 leads to $\begin{array}{|c|c|} \hline \square & \square \\ \hline \end{array}$ as well as $\begin{array}{|c|} \hline \square \\ \hline \end{array}$, the latter in two different ways. As indicated in the figure, the dashed line connecting

 and  involves the removal of a border strip of height equal to 1, whereas all other border strips that are removed in figure 1.1 have height equal to 0. Consider a composition α containing at least one row of length one and length two. Applying (1.55) then gives

$$\begin{aligned} \chi_{\alpha}^{(3,2)} &= \sum_{\mu, \rho} (-1)^{\text{ht}(\rho) + \text{ht}(\mu)} \chi_{\alpha - (2,1)}^{((3,2) \setminus \mu) \setminus \rho} = \chi_{\alpha - (2,1)}^{(2)} + (1 - 1) \chi_{\alpha - (2,1)}^{(1,1)} \\ &= \sum_{\mu, \rho} (-1)^{\text{ht}(\rho) + \text{ht}(\mu)} \chi_{\alpha - (2,1)}^{((3,2) \setminus \rho) \setminus \mu} = \chi_{\alpha - (2,1)}^{(2)} \end{aligned} \quad (1.57)$$

where μ and ρ are BS of sizes 1 and 2, respectively, and where $\alpha - (2, 1)$ indicates that we remove a row of length 1 and a row of length 2 from α . Note the different order of removal of μ and ρ in the top and bottom rows. We see that the sign given by $(-1)^{\text{ht}(\rho)}$ ensures that removing border strips of different sizes in different orders, as it leads to the cancellation between various ways to arrive at certain diagrams that are unattainable via a different order of removal. We will treat the removal of border strips from $\lambda = \begin{array}{|c|c|c|} \hline \square & \square & \square \\ \hline \square & & \end{array}$ more extensively in section 2.3, see figure 2.1.

Let us consider the object $(p_n)^k$. Using (1.49), we have

$$(p_n)^k = \sum_{\lambda} \chi_{(n^k)}^{\lambda} s_{\lambda}. \quad (1.58)$$

From (1.53) (or (1.42) with $\lambda = \emptyset$), the $\chi_{(n^k)}^{\lambda}$ appearing in (1.58) are of the following form

$$\chi_{(n^k)}^{\lambda} = \sum_{T \in \text{BST}(\lambda, (n^k))} (-1)^{\text{ht}(T)}, \quad (1.59)$$

where the sum is over all *border strip tableaux* of shape λ and type $\alpha = (n^k)$. For $\alpha = (n^k)$, it has been shown that the expansion in (1.59) is cancellation-free

[corollary 10, [35]]. That is, for any fixed choice of λ , all BST's appear with the same sign, so that

$$\chi_{(n^k)}^\lambda = \pm \sum_{T \in \text{BST}(\lambda, (n^k))} 1. \quad (1.60)$$

In fact, there is a more general result [theorem 2.7.27 in [34]], which states that

$$\chi_{(n^k)}^{\lambda/\alpha} = \pm \sum_{T \in \text{BST}(\lambda/\alpha, (n^k))} 1. \quad (1.61)$$

In the above expression, μ is the so-called n -core of λ , which is the diagram that remains after removing the maximum possible of border strips of size n . We denote by $w(\lambda)$ the n -weight of λ , which is the number of border strips of size n which one has to remove to obtain the n -core of λ . The number of partitions with n -core given by μ is then given by [theorem 2.7.17 in [34]]

$$b(w) = \sum_{\{w_j\}} \prod_{j=1}^n p(w_j), \quad (1.62)$$

where the sum is over all sets of n non-negative integers w_j satisfying $\sum_{j=1}^n w_j = w(\lambda)$, and where $p(w_j)$ is the number of partitions of w_j .

We illustrate (1.61) for λ with empty n -core (i.e. (1.60)), in particular, for $\lambda = (6, 5, 2^2, 1)$ and $\alpha = (n^k) = (4^4)$. This gives the following border strip tableaux, where border strips again share the same color.

We see that the heights of the tableaux are given, from left to right, by 4, 6, 4, 6, so that $(-1)^{\text{ht}(T)} = 1$. Note that the two leftmost BST's appear with multiplicity two, as one can remove the green and blue border strips in either order. This means that $\chi_{(4^4)}^{(6,5,2^2,1)} = 6$. We see, then, that all BST's contribute with the same sign as they are all of even height. Equation (1.60) states that the BST's *always* appear with the same sign for any choice of λ and (n^k) . One can see that this generalizes to skew partitions λ/ρ by considering λ and ρ for which $\text{BST}(\lambda, (n^k))$ and $\text{BST}(\rho, (n^k))$ are non-empty, and using the fact that $\text{ht}(T_{\lambda/\rho}) = \text{ht}(T_\lambda) - \text{ht}(T_\rho)$, where $T_{\lambda/\rho}$ is a border strip tableau of type (n^k) for some k .

1.2 Matrix integrals and Toeplitz minors

We review here the evaluation of weighted unitary integrals over Schur polynomials using their relation with minors of Toeplitz matrices. The study of the asymptotics of Toeplitz determinants dates back at least to Szegő, whose limit theorem proved the existence of a phase transition in the Ising model on a square 2D lattice with sides

identified (i.e. a square torus). One may consult e.g. [36] for further background and other important applications. Szegő's results were generalized by various authors including Gessel [37], who applied them to various important enumerative problems. The major work by Baik, Deift, and Johansson [38] on the asymptotics of longest increasing subsequences of random permutations follows a similar approach, see also e.g. [39]. These results were extended and related to unitary integrals by Bump and Diaconis [40]. The main expression of interest for us, which we give in this section, was derived by García-García and Tierz [41], [42], which draws mainly from the aforementioned work by Bump and Diaconis.

Take an absolutely integrable function on the unit circle in \mathbb{C} ,

$$f(e^{i\theta}) = \sum_{k \in \mathbb{Z}} d_k e^{ik\theta} . \quad (1.64)$$

We require that $f(e^{i\theta})$ satisfies the assumptions of Szegő's theorem. That is, we write $f(e^{i\theta})$ as

$$f(e^{i\theta}) = \exp \left(\sum_{k \in \mathbb{Z}} c_k e^{ik\theta} \right) , \quad (1.65)$$

and demand that

$$\sum_{k \in \mathbb{Z}} |c_k| < \infty , \quad \sum_{k \in \mathbb{Z}} |k| |c_k|^2 < \infty . \quad (1.66)$$

Writing

$$D_N(f) = \det(T_N(f)) = \det (d_{j-k})_{j,k=1}^N , \quad (1.67)$$

the strong Szegő limit theorem then states that [43],

$$\lim_{N \rightarrow \infty} \frac{D_N(f)}{e^{-Nc_0}} = \exp \left(\sum_{k=1}^{\infty} k c_k c_{-k} \right) . \quad (1.68)$$

The above determinant and various generalization thereof can be related to integrals over the group of N by N unitary matrices with some weight function f with the insertion of Schur polynomials. We denote by $T_N(f)$ the N by N principal submatrix of $T(f)$, i.e. the matrix obtained from $T(f)$ by taking its first N rows and columns and neglecting the remainder. That is,

$$T_N^{\lambda, \mu}(f) = (d_{j-\lambda_j-k+\mu_k})_{j,k=1}^N . \quad (1.69)$$

We will see that various matrix integrals with weight function f can be expressed as minors of $T_N(f)$, that is, as determinants of matrices obtained from $T_N(f)$ by removing a (necessarily equal) number of rows and columns. For a unitary matrix U with eigenvalues $e^{i\theta_1}, e^{i\theta_2}, \dots$, we write,

$$\tilde{f}(U) = \det f(U) = \prod_{k=1}^N f(e^{i\theta_k}) . \quad (1.70)$$

We employ Weyl's integral formula [44] to express the integral of $\tilde{f}(U)$ over $U(N)$ with respect to the de Haar measure as

$$\int \tilde{f}(U) dU = \frac{1}{N!} \int_0^{2\pi} \prod_{j < k} |e^{i\theta_j} - e^{i\theta_k}|^2 \prod_{k=1}^N f(e^{i\theta_k}) \frac{d\theta_k}{2\pi} , \quad (1.71)$$

where the angles satisfy $0 \leq \theta_k < 2\pi$. The expression for the Vandermonde determinant in (1.45) allows us to use an identity due to Andreiéf, sometimes referred to as Heine or Gram identity [45]. Take g_j and h_j , $j \in \{1, 2, \dots, N\}$, to be two sequences

of integrable functions on some measure space with measure μ , then

$$\frac{1}{N!} \int \det(g_j(x_k))_{j,k=1}^N \det(h_j(x_k))_{j,k=1}^N \prod_{k=1}^N d\mu(x_k) = \det \left(\int g_j(x) h_j(x) d\mu(x) \right)_{j,k=1}^N \quad (1.72)$$

Choosing $g_j(e^{-i\theta}) = e^{i(N-j)\theta} = h_j(e^{i\theta})$ and $d\mu(e^{i\theta}) = f(e^{i\theta}) \frac{d\theta}{2\pi}$, we find

$$\int \tilde{f}(U) dU = \det(d_{j-k})_{j,k=1}^N, \quad (1.73)$$

where d_k are again the Fourier coefficients of f ,

$$d_k = \frac{1}{2\pi} \int_0^{2\pi} f(e^{i\theta}) e^{ik\theta} d\theta. \quad (1.74)$$

As before, let $\lambda = (\lambda_1, \dots, \lambda_m)$ and $\mu = (\mu_1, \dots, \mu_n)$ be partitions of $|\lambda| = \sum_i^{\ell(\lambda)} \lambda_i$ and $|\mu| = \sum_j^{\ell(\mu)} \mu_j$, respectively. One then obtains a *Toeplitz minor* $T_N^{\lambda, \mu}(f)$ via the following procedure:

- Take $T_{N+\kappa}(f)$, where $\kappa = \max\{\lambda_1, \mu_1\}$
- If $\lambda_1 - \mu_1 > 0$, remove the first $\lambda_1 - \mu_1$ columns from $T_{N+\kappa}(f)$, otherwise remove $\mu_1 - \lambda_1$ rows.
- Then, keep the first row and remove the next $\lambda_1 - \lambda_2$ rows, then keep the following row and remove the next $\lambda_2 - \lambda_3$ rows, and so on and so forth.
- Repeat the third step, replacing λ_j by μ_j and removing columns instead of rows

Note that the second step ensures that the resulting matrix $T_N^{\lambda, \mu}(f)$ is of order N . We write $s_\lambda(U) = s_\lambda(e^{i\theta_1}, e^{i\theta_2}, \dots)$. The determinant of $T_N^{\lambda, \mu}(f)$ can then be expressed

as [40],

$$\begin{aligned}
D_N^{\lambda,\mu}(f) &:= \det T_N^{\lambda,\mu}(f) = \int_{U(N)} s_\lambda(U^{-1}) s_\mu(U) \tilde{f}(U) dU \\
&= \frac{1}{N!(2\pi)^N} \int_0^{2\pi} s_\lambda(e^{-i\theta_1}, \dots, e^{-i\theta_N}) s_\mu(e^{i\theta_1}, \dots, e^{i\theta_N}) \times \\
&\quad \times \prod_{j=1}^N f(e^{i\theta_j}) \prod_{1 \leq j < k \leq N} |e^{i\theta_j} - e^{i\theta_k}|^2 d\theta_j \\
&= \det (d_{j-\lambda_j-k+\mu_k})_{j,k=1}^N .
\end{aligned} \tag{1.75}$$

One can recognize the pattern of striking rows and columns involved in the construction of $T_N^{\lambda,\mu}(f)$, as the index j is shifted to $j - \lambda_j$ and k to $k - \mu_k$.

We write the expectation value $\langle \dots \rangle$ with respect to the matrix model with weight function f as

$$\langle s_\lambda(U) s_\mu(U^{-1}) \rangle = \frac{\int s_\lambda(U) s_\mu(U^{-1}) \tilde{f}(U) dU}{\int \tilde{f}(U) dU} . \tag{1.76}$$

We will often neglect to write $U^{\pm 1}$ explicitly, instead writing $\langle s_\lambda s_\mu \rangle$ or, more generally, $\langle AB \rangle$ for symmetric polynomials A and B . For two functions of the form

$$a(z) = \sum_{k \leq 0} a_k z^k \quad , \quad b(z) = \sum_{k \geq 0} b_k z^k \quad , \tag{1.77}$$

the associated Toeplitz matrix satisfies

$$T(ab) = T(a)T(b) . \tag{1.78}$$

Let us therefore write $f(e^{i\theta})$ as follows

$$f(z) = H(x; z) H(y; z^{-1}) \quad , \tag{1.79}$$

where $H(x; z)$ is the generating function of the homogeneous symmetric polynomials h_k given in (1.6) and where we assume that $h_k(x)$ and $h_k(y)$ are square-summable, i.e. $\sum_k |h_k|^2 < \infty$. We can also define our weight function as

$$f(z) = E(x; z)E(y; z^{-1}) , \quad (1.80)$$

at the cost replacing h_j by e_j everywhere, which is equivalent to transposing all diagrams on either the left or right hand side of the equation. The unique $U(N)$ -invariant (Haar) measure corresponds to $f = 1$, which corresponds to $x_j = 0$ for all j for both $f(z) = H(x; z)H(y; z^{-1})$ and $f(z) = E(x; z)E(y; z^{-1})$. This is known as the circular unitary ensemble (CUE) in random matrix theory, which will be treated in section 1.4. We will consider the case where $f(z) = H(x; z)H(y; z^{-1})$ for general x and y unless stated otherwise.

It was shown by Gessel [37] that $D_N(f)$ can be expressed in terms of Schur polynomials as

$$D_N(f) = \sum_{\ell(\nu) \leq N} s_\nu(x)s_\nu(y) . \quad (1.81)$$

Equation (1.75) can be similarly expressed in terms of (skew) Schur polynomials [40], [41], [42],

$$\int s_\lambda(U)s_\mu(U^{-1}) \det f(U) dU = \sum_{\ell(\rho) \leq N} s_{\rho/\lambda}(x)s_{\rho/\mu}(y) . \quad (1.82)$$

We now take the limit $N \rightarrow \infty$. From (1.82) and the fact that [Chapter I.5, example 26 in [33]]

$$\sum_{\rho} s_{\rho/\lambda}(x)s_{\rho/\mu}(y) = \sum_{\nu} s_{\mu/\nu}(x)s_{\lambda/\nu}(y) \sum_{\eta} s_{\eta}(x)s_{\eta}(y) , \quad (1.83)$$

where the sums run over all partitions, it follows that [41], [42]

$$\langle s_\lambda(U)s_\mu(U^{-1}) \rangle = \sum_{\nu} s_{\lambda/\nu}(y)s_{\mu/\nu}(x) , \quad (1.84)$$

where the sum runs over all ν such that $\nu \subseteq \lambda, \mu$. As noted at equation (1.80), we can also define $f(z) = E(x; z)E(y; z^{-1})$ at the cost of transposing diagrams. In this case, one has

$$\langle s_\lambda(U)s_\mu(U^{-1}) \rangle = \sum_{\nu} s_{(\lambda/\nu)^t}(y)s_{(\mu/\nu)^t}(x) , \quad (1.85)$$

We will consider $f(z) = H(x; z)H(y; z^{-1})$ and apply (1.84) unless stated otherwise. If we take $\mu = \emptyset$ in (1.84), the only choice for ν that contributes to the above sum is $\nu = \emptyset$ as well, and we have

$$\langle s_\lambda(U) \rangle = s_\lambda(y) , \quad \langle s_\mu(U^{-1}) \rangle = s_\mu(x) . \quad (1.86)$$

We also define the connected expectation value ,

$$\langle s_\lambda(U)s_\mu(U^{-1}) \rangle_c := \langle s_\lambda(U)s_\mu(U^{-1}) \rangle - \langle s_\lambda(U) \rangle \langle s_\mu(U^{-1}) \rangle , \quad (1.87)$$

which corresponds to subtracting the contribution corresponding to $\nu = \emptyset$ in (1.84).

We now consider what the assumptions of Szego's theorem imply for a function of the form $f(z) = H(x; z)H(x; z^{-1})$ or $f(z) = E(x; z)E(x; z^{-1})$. Consider first the case $f(z) = H(x; z)H(x; z^{-1})$. From the bottom line of (1.6), we see that

$$f(z) = \exp \left(\sum_{k=1}^{\infty} \frac{p_k(x)}{k} z^k + \frac{p_k(y)}{k} z^{-k} \right) . \quad (1.88)$$

Therefore,

$$c_k = \frac{p_k(x)}{k}, \quad c_{-k} = \frac{p_k(y)}{k}, \quad k \neq 0, \quad (1.89)$$

and (1.66) is written as

$$\sum_{k=1}^{\infty} \frac{|p_k(x)| + |p_k(y)|}{k} < \infty, \quad \sum_{k=1}^{\infty} \frac{|p_k(x)|^2 + |p_k(y)|^2}{k} < \infty, \quad (1.90)$$

where we ignore an irrelevant factor 2. We see that

$$\lim_{k \rightarrow \infty} |p_k| \rightarrow 0, \quad (1.91)$$

for both $p_k(x)$ and $p_k(y)$, as $\sum_{k=1}^{\infty} \frac{|p_k(x)|}{k}$ diverges otherwise. We see that equation (1.91) requires that $x_j, y_j < 1$. In the above expressions, if we replace $E(x; z)$ by $H(x; z)$, we have $p_k \rightarrow (-1)^{k+1} p_k$, so that the assumptions of Szegő's theorem are given by (1.90) as well.

1.2.1 Finite matrix size

Although the expressions given above were derived for $N \rightarrow \infty$, some of them can, in fact, be generalized to finite N in case the number of distinct non-zero variables x_j is smaller than N . From equations (1.81), (1.82), and (1.83), we see that, for finite N and $f(z) = H(x; z)H(x; z^{-1})$,

$$\begin{aligned} \langle s_\lambda(U) s_\mu(U^{-1}) \rangle &= \left(\frac{\sum_{\kappa} (s_\kappa(x))^2}{\sum_{\ell(\rho) \leq N} (s_\rho(x))^2} \right) \sum_{\nu} s_{\lambda/\nu}(x) s_{\mu/\nu}(x) + \\ &\quad - \frac{\sum_{\ell(\nu) > N} s_{\nu/\lambda}(x) s_{\nu/\mu}(x)}{\sum_{\ell(\rho) \leq N} (s_\rho(x))^2}. \end{aligned} \quad (1.92)$$

Let us denote the number of non-zero variables by i_{\max} , i.e. $x_i \neq 0$ for $i \leq i_{\max}$ and $x_i = 0$ for $i > i_{\max}$. In that case, $s_\kappa(x) = 0$ for $\ell(\kappa) > i_{\max}$, see equation (1.28), so that

$$\frac{\sum_{\kappa} (s_{\kappa}(x))^2}{\sum_{\ell(\rho) \leq N} (s_{\rho}(x))^2} = 1 . \quad (1.93)$$

Indeed, in case $N - \ell(\lambda) > i_{\max}$ and $N - \ell(\mu) > i_{\max}$, we can apply (1.28) again to find

$$\sum_{\ell(\nu) > N} s_{\nu/\lambda}(x) s_{\nu/\mu}(x) = 0 . \quad (1.94)$$

From this we conclude that, for $N - |\lambda| > i_{\max}$ and $N - |\mu| > i_{\max}$, we have

$$\frac{\int s_{\lambda}(U) s_{\mu}(U^{-1}) \tilde{f}(U) dU}{\int \tilde{f}(U) dU} = \sum_{\nu} s_{\lambda/\nu}(x) s_{\mu/\nu}(x) , \quad (1.95)$$

i.e. the asymptotic expression (1.84) still holds in this case. Again, the above expressions still hold if we replace $H(x; z)$ by $E(x; z)$ and all representations by their transposes.

1.3 Long-range random walkers

We summarize here the derivation which relates correlation functions of one-dimensional long-range random walkers (LRRW) to weighted unitary integrals over Schur functions. The random walkers considered here are ‘vicious’, that is, non-intersecting. For random walkers which can move only a single site, these can be described either by fermions or hard-core bosons. These were introduced in [46] and studied and generalized by various authors, see e.g. [47], [48], [49], [50]. Bogoliubov [23] found a relation with integrals over Schur polynomials, see also [24], [25]. This was gener-

alized to LRRW models by Pérez-García and Tierz [26], in which case the particles behave as hard-core bosons. The treatment presented here is based mainly on [23], [24], and [26].

Consider what Bogoliubov refers to as the the XX0-model, that is, the XY-model with zero magnetic field,

$$\hat{H} = \sum_{m,n} \Delta_{n,m} \sigma_n^- \sigma_m^+ \quad , \quad \Delta_{m,n} = \delta_{n+1,m} + \delta_{n-1,m} . \quad (1.96)$$

We start with state with holes at all sites

$$|\uparrow\rangle = \otimes_n |\uparrow\rangle_n = \otimes_n \begin{pmatrix} 1 \\ 0 \end{pmatrix}_n , \quad (1.97)$$

which satisfies

$$\hat{H} |\uparrow\rangle = 0 . \quad (1.98)$$

Define the correlation function

$$F_{j;l}(\tau) = \langle \uparrow | \sigma_j^+ e^{-\tau \hat{H}} \sigma_l^- | \uparrow \rangle . \quad (1.99)$$

For now, we consider τ to be a general complex number, but we will mostly be interested in the case where $\tau = it$ where t is a real-valued time parameter. Using

$$[\sigma_n^+, \sigma_m^-] = \sigma_n^z \delta_{m,n} \quad , \quad [\sigma_n^z, \sigma_m^\pm] = \pm 2\sigma_n^\pm \delta_{m,n} , \quad (1.100)$$

we have

$$[\hat{H}, \sigma_k^-] = \sum_m \Delta_{m,k} \sigma_m^- \sigma_k^z , \quad (1.101)$$

which we apply to find

$$\frac{d}{d\tau} F_{j;l}(\tau) = - \left\langle \uparrow \left| \sigma_j^+ e^{-\tau \hat{H}} \hat{H} \sigma_l^- \right| \uparrow \right\rangle = \sum_m \Delta_{l,m} F_{j;m}(\tau) . \quad (1.102)$$

In particular, for the XX0-model, where $\Delta_{m,n} = \delta_{n+1,m} + \delta_{n-1,m}$,

$$\frac{d}{d\tau} F_{j;l}(\tau) = F_{j;l+1}(\tau) + F_{j;l-1}(\tau) . \quad (1.103)$$

We will generally consider the case where $\Delta_{m,n} = \Delta_{m-n} = a_{m-n}$, i.e. the hopping amplitude depends only on the (positive or negative) distance between lattice sites m and n . In this case, $\Delta_{m,n}$ is a Toeplitz matrix, i.e. it is constant along its diagonals. Taking $L + 1$ lattice sites, as in [23], the hamiltonian is generally of the form,

$$\hat{H} = - \sum_{m=0}^L \sum_{n=1}^{(L-1)/2} (a_n \sigma_m^- \sigma_{m+n}^+ + a_{-n} \sigma_m^- \sigma_{m-n}^+) + \frac{h}{2} \sum_{m=0}^L (\sigma_m^z - \mathbf{1}) , \quad (1.104)$$

where we demand that $a_{-k} = a_k^*$, the complex conjugate of a_k . We then have

$$\left[\hat{H}, \sigma_k^- \right] = - \sum_n (a_n \sigma_{k-n}^- \sigma_n^z + a_{-n} \sigma_{k+n}^- \sigma_n^z) - h \sigma_k^- , \quad (1.105)$$

so that

$$\frac{d}{d\tau} F_{j;l}(\tau) = \sum_n (a_n F_{j-n;l} + a_{-n} F_{j+n;l}) + h F_{j;l} . \quad (1.106)$$

It is clear that $F_{j;l}$ only depends on $|j - l|$. The generating function $f(z; \tau) = \sum_{j \in \mathbb{Z}} F_{j;l} z^{j-l}$ is given by [23], [26]

$$f(z; \tau) = \exp \left(\tau \sum_{k \in \mathbb{Z}} a_k z^k \right) , \quad (1.107)$$

where we set $a_0 = h$. Consider now the multi-particle correlation function, with $N \leq L$,

$$F_{j_1, \dots, j_N; l_1, \dots, l_N}(\tau) = \left\langle \uparrow \left| \sigma_{j_1}^+ \dots \sigma_{j_N}^+ e^{-\tau \hat{H}} \sigma_{l_1}^- \dots \sigma_{l_N}^- \right| \uparrow \right\rangle . \quad (1.108)$$

We impose periodic boundary conditions for simplicity. However, we will be taking the thermodynamic limit and considering only configurations which contain an infinite sequence of adjacent holes, with the particles either confined to a finite interval in their initial configuration or starting with an infinite sequence of adjacent particles. As such, imposing periodic boundary conditions will have no effect on our final result. We then have,

$$\begin{aligned} \frac{d}{d\tau} F_{j_1, \dots, j_N; l_1, \dots, l_N}(\tau) &= \sum_{k, m} (a_k F_{j_1, \dots, j_N; l_1, \dots, l_m+k, \dots, l_N}(\tau) + a_k F_{j_1, \dots, j_N; l_1, \dots, l_m-k, \dots, l_N}(\tau)) + \\ &+ Nh F_{j_1, \dots, j_N; l_1, \dots, l_N}(\tau) . \end{aligned} \quad (1.109)$$

Remember that the summations over k and m are over different ranges. The solution to equation (1.109) is of determinantal form [23], [24], [26],

$$F_{j_1, \dots, j_N; l_1, \dots, l_N}(\tau) = \det (F_{j_r; l_s}(\tau))_{r, s=1}^N . \quad (1.110)$$

From the initial condition $F_{j;l}(0) = \delta_{j,l}$, it follows that,

$$F_{j;l}(\tau) = \frac{1}{L+1} \sum_{s=0}^L \exp(\tau a_k e^{ik\theta_s}) e^{i(j-l)\theta_s} , \quad (1.111)$$

where $\theta_s = \frac{2\pi}{L+1} (s - L/2)$. Using the determinantal expression for Schur functions

in equation (1.46), $F_{j_1, \dots, j_N; l_1, \dots, l_N}(\tau)$ is given by

$$F_{j_1, \dots, j_N; l_1, \dots, l_N}(\tau) = \frac{1}{(L+1)^N} \sum_{\{s_j\}} \exp \left(\tau \sum_{j=1}^N \sum_k^{(L-1)/2} a_k e^{ik\theta_{s_j}} \right) \prod_{1 \leq j < k \leq N} |e^{i\theta_{s_j}} - e^{i\theta_{s_k}}|^2 \times \\ \times s_\lambda(e^{i\theta_{s_1}}, \dots, e^{i\theta_{s_N}}) s_\mu(e^{-i\theta_{s_1}}, \dots, e^{-i\theta_{s_N}}), \quad (1.112)$$

with $\lambda_r = j_r - N + r$ and $\mu_s = l_s - N + s$. We shift j_r and l_r by N , such that

$$\lambda_r = j_r + r, \quad \mu_s = l_s + s. \quad (1.113)$$

This is merely a convenient relabelling of our lattice sites. We now take $L \rightarrow \infty$. Demanding that the hopping parameters a_k decay at least as $a_k \sim k^{-1-\epsilon}$ for some $\epsilon > 0$, we then have [23], [24], [26],

$$F_{j_1, \dots, j_N; l_1, \dots, l_N}(\tau) = \mathcal{N} e^{Nh\tau} \int_{-\pi}^{\pi} d\theta_1 \dots \int_{-\pi}^{\pi} d\theta_N \prod_{1 \leq r < s \leq N} |e^{i\theta_r} - e^{i\theta_s}|^2 \prod_{k=1}^M f(e^{i\theta_k}; \tau) \times \\ \times s_\lambda(e^{i\theta_1}, \dots, e^{i\theta_N}) s_\mu(e^{-i\theta_1}, \dots, e^{-i\theta_N}), \quad (1.114)$$

where the weight function $f(z; \tau)$ is in (1.107). We include in equation (1.114) a normalization factor \mathcal{N} which is determined by demanding

$$F_{j_1, \dots, j_N; l_1, \dots, l_N}(0) = \prod_{k=1}^M \delta_{j_k, l_k}. \quad (1.115)$$

Note that (1.114) is the expression for an integral over $U(N)$ weighted by some weight function f with insertion of Schur polynomials s_λ and s_μ , as mentioned at the start of this section. In particular, writing $s_\lambda(U) = s_\lambda(e^{i\theta_j})$, where $e^{i\theta_j}$ are the

eigenvalues of U , we have

$$F_{j_1, \dots, j_N; l_1, \dots, l_N}(\tau) = \int_{U(N)} dU \tilde{f}(U) s_\lambda(U) s_\mu(U^{-1}) . \quad (1.116)$$

When we take the limit $\tau \rightarrow 0$, we have $f = 1$, which recovers the integral over the Haar measure on $U(N)$. In this case $s_{\lambda/\mu}(x) = 0$ for any $\lambda/\mu \neq \emptyset$, which greatly simplifies many calculations.

If $\lambda = \emptyset = \mu$, we have $j_r = -r = l_r$, and we are simply considering the return probability for N adjacent particles [51], [52], see also [53]. In general, we will write

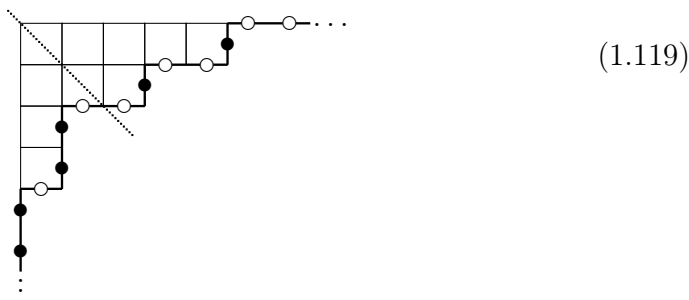
$$F_{\lambda; \mu}(\tau) = F_{j_1, \dots, j_N; l_1, \dots, l_N}(\tau) , \quad (1.117)$$

where equation (1.113) expresses the relation between λ , μ and $\{j_r\}$, $\{l_r\}$, respectively. We will write the state corresponding to an empty diagram as $|\emptyset\rangle$. This can be illustrated as follows, where a particle is indicated by a black dot and hole by a white dot and the vertical line separates lattice sites 0 and 1.

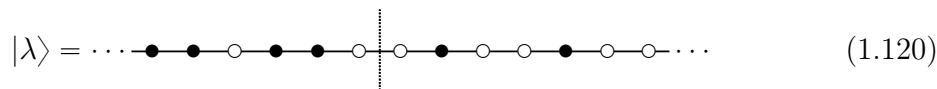
$$|\emptyset\rangle = \cdots \bullet \bullet \bullet \bullet \bullet \begin{array}{c} | \\ \hline \end{array} \circ \circ \circ \circ \circ \cdots \quad (1.118)$$

For non-empty λ, μ , $F_{\lambda; \mu}$ corresponds to a correlation function where certain particles are shifted by a finite number of sites. The well-known association between Young diagrams and 1D configurations of spins (or fermions, or any other binary variable) is as follows. We place a diagram in the corner where an infinitely long horizontal and vertical line meet. We number the edges of these horizontal and vertical lines, as well as external edges (i.e. those on the lower right) of the diagram, such that the main diagonal passes between sites 0 and 1. We then associate a particle to all vertical edges and a hole to all horizontal edges. This association is illustrated

below² for $\lambda = (5, 3, 1^2)$, where we add a dotted diagonal line which separates lattice sites 0 and 1.



The configuration corresponding to the above diagram is illustrated below, with again a dotted line separating sites 0 and 1.



It is clear from the above association between diagrams and spin configurations that λ affects particles from position $j = -\ell(\lambda) + 1$ up to $j = \lambda_1$, which means that there is an interval containing $\ell(\lambda)$ particles and λ_1 holes, the leftmost of which is a hole and the rightmost a particle. In particular, the state $|\lambda\rangle$ has a hole at $j = -\ell(\lambda) + 1$ and a particle at $j = \lambda_1$, and the remaining $\ell(\lambda) - 1$ particles and $\lambda_1 - 1$ holes are distributed over sites $j = \{-\ell(\lambda) + 2, -\ell(\lambda) + 3, \dots, \lambda_1 - 1\}$, which can be seen explicitly for $\lambda = (5, 3, 1^2)$ above.

²We made grateful use of the illustrations in the excellent review [54] by Zinn-Justin, which we adapt here for our purposes.

1.4 Random matrices and spectral statistics

As mentioned in the overview, the original focus of this thesis was random matrix theory and its application to spectral statistics of quantum chaotic and, in particular, intermediate systems. However, our calculations did not reveal intermediate statistics in the CSMM, as opposed to those of earlier authors who worked on this model. This section serves to provide our original motivation and results with some broader context by reviewing the relation between RMT, spectral statistics, and quantum chaos, as well as random matrix treatments of intermediate statistics. This section is somewhat broader and more historical in scope, which sets it apart from other sections in this chapter. This difference is mainly due to the fact that RMT is an enormously rich field with very many applications, although the same may perhaps be said some of the other topics treated here. More importantly, the relation between quantum chaos (or lack thereof) and spectral statistics, as expressed in the Bohigas–Giannoni–Schmit (or Berry–Tabor) conjecture, is one that was gradually established through the consideration of many examples by many authors. As such, any treatment of the relation between chaoticity and spectral statistics is bound to consider this historical context. In spite of the fact that this section is broader in its orientation than other sections in this chapter, the present treatment of RMT and spectral statistics cannot do justice to such a rich area of mathematics and physics. Nonetheless, we hope that it may serve as a helpful introduction and background for our results in chapter 4. There are many excellent books and reviews on the topic which one may consult for more information, including [55], [56], [57], see also e.g. [58] for a more mathematical treatment, including the relation to the Riemann hypothesis.

1.4.1 Random matrix theory and quantum chaos

Random matrix theory provides a phenomenological description of a wide variety of systems appearing in physics and beyond, starting with Wishart’s analysis of covariance matrices in 1928 [59], then apparently lying dormant for some time until it was applied by Wigner to nucleon scattering in the 1950’s [60], and later finding applications in quantum chaos [61], disordered electronic [62] and mesoscopic [63] systems, quantum chromodynamics [64], models of 2d quantum gravity and string theory [65], economics [66], information theory [67], and number theory [68], as well as other fields. RMT has recently received an increasing amount of attention from the high energy physics community, particularly as a result of a remarkable relation between the genus expansion of certain matrix integrals and partition function of JT-gravity [69]. This theory of gravity arises as a low-energy limit of SYK-theory, which is thought to exhibit certain universal low-energy behavior of black holes, see e.g. [70], [71], [72], [73], [74] for this and related applications of RMT.

The application of RMT to black holes is intimately related to the fact that black holes are chaotic objects, see e.g. [71]. This relation between RMT and quantum chaos has been known for much longer. It was most clearly articulated by Bohigas, Giannoni, and Schmit [61], although they were not the first to hint at such a relationship [75], [76]. The content of their statement, which has come to be known as the Bohigas–Giannoni–Schmit (BGS) conjecture, is essentially that quantum chaotic systems have energy spectra which exhibit the same statistics as Gaussian random matrix ensembles (RME’s) of the appropriate symmetry type. These universal eigenvalue statistics are known as Wigner–Dyson (WD) statistics. The BGS-conjecture has been so extensively corroborated that WD-statistics are nowadays seen almost as a definition of quantum chaos.

To better explain the BGS-conjecture, we treat the relevant RME’s in a bit more detail. We will generally consider random matrix ensembles which have partition

functions in the form of a matrix integral,

$$\int dM P(M) . \quad (1.121)$$

Here, $P(M)$ is the probability density function associated to a matrix M . We will start by considering those cases where we integrate over all matrices that are either real symmetric, hermitian, or self-dual quaternionic. These matrices have real eigenvalues and can be diagonalized by orthogonal, unitary, or symplectic transformations, respectively. Indeed, these RME's are invariant under these transformations, e.g. the set of all hermitian matrices is invariant under unitary similarity transformations. Writing the eigenvalues as x_j and integrating out the diagonalizing transformations leads to the following eigenvalue expression, see e.g. [77] or [55],

$$Z = C_N \int \prod_{i=1}^N \frac{dx_i}{2\pi} f(x_i) \prod_{i<j} (x_i - x_j)^\beta , \quad (1.122)$$

where C_N is some (typically irrelevant) multiplicative constant and $f(x)$ is called the *weight function*. Further, $\beta = 1, 2$, or 4 for the case where the diagonalizing transformation is orthogonal, unitary, or symplectic, respectively. Choosing

$$P(M) \propto \exp(-\alpha \text{tr} M^2) , \quad (1.123)$$

where α is some positive numerical constant, leads to the Gaussian orthogonal ensemble (GOE), Gaussian unitary ensemble (GUE), or Gaussian symplectic ensemble (GSE) for $\beta = 1, 2$, or 4 , respectively. We see that there appears a so-called Vandermonde determinant, $\prod_{i<j} (x_i - x_j)$, to the power β . This leads to a vanishing probability that two eigenvalues will coincide, which is known as *level repulsion*. In particular, when $N = 2$, the distribution of spacings s between adjacent energy

levels is given by (see e.g. [77] or [55])

$$P(s) = \begin{cases} \frac{\pi}{2} s e^{-\pi s^2/4} & , \quad \text{GOE} , \\ \frac{32}{\pi^2} s^2 e^{-4s^2/\pi} & , \quad \text{GUE} , \\ \frac{2^{18}}{3^6 \pi^3} s^4 e^{-64s^2/9\pi} & , \quad \text{GSE} . \end{cases} \quad (1.124)$$

For $N \rightarrow \infty$, the level spacing distributions are very similar to the case of $N = 2$, see e.g. section 5.12 in [55]. From the proportionality to s^β for $\beta = 1, 2, 4$, we see that $P(s = 0) = 0$ for all three Gaussian RME's. On the other hand, uncorrelated energy levels follows a Poisson distribution. In this case, $P(s) = e^{-s}$, so that energy level have a higher probability of lying close to one another, which is known as *level clustering*. We will show examples of these different types of level statistics below.

The content of the BGS-conjecture is then that the energy eigenvalues of quantum chaotic systems of the appropriate symmetry class exhibit the same eigenvalue statistics (as exhibited e.g. by the level spacing distribution) as the above Gaussian RME's. That is, time-reversal invariant systems are described by the GOE, systems with no time-reversal invariance by the GUE, and systems where the time-reversal operator squares to minus the identity (spin systems) by the GSE. Conversely, it was conjectured by Berry and Tabor [78] that 'generic' integrable systems display Poissonian level statistics. The latter has come to be known as the Berry–Tabor (BT) conjecture. In this case there exist various counterexamples, which is why it should be emphasized that the BT-conjecture applies generically but not universally. Like the BGS-conjecture, it has seen ample corroboration, see e.g. [79] for more information.

We consider an example of the BGS-conjecture for time-reversal invariant systems, which was in fact treated by BGS in their original work [61]. This is the Sinai billiard, which consists of a square billiard with a circle of size R cut out of the middle, see

the inset on the top right of figure 1.2 for an image of ($1/8^{\text{th}}$ of) this billiard. It was analyzed by Yakov Sinai in a seminal paper [80], where he demonstrated its strong chaotic behavior. Upon quantization, one may compare the energy spectrum with that of the GOE, as we are considering a time-reversal invariant system. To make a faithful comparison, we need to define new energy variables in which the average spacing between energy eigenvalues is the same for both spectra, typically set to unity. This process is known as *unfolding*, which ensures that differences in energy level statistics are not due to trivial large scale (compared to the average level spacing) variations in level density. It should be emphasized that the authors of [61] consider $1/8^{\text{th}}$ of the Sinai billiard. This is obtained by reflecting the Sinai billiard across its 4 symmetry axes. As mentioned, the resulting, desymmetrized, billiard is shown in the inset in the top right of figure 1.2. This desymmetrization is done so as to eliminate ‘accidental’ degeneracies in the energy eigenvalues that arise from the reflection symmetries of the Sinai billiard. After doing so, it can be seen in figure 1.2 that the energy eigenvalues of the Sinai billiard follow the level spacing of the GOE very closely. Although the level spacing distribution provides an intuitive measure of the energy level statistics, it is typically very hard to compute and not amenable to analytical methods. For this reason, we will be considering a more convenient known as the spectral form factor (SFF), which we will introduce in section 1.4.3.

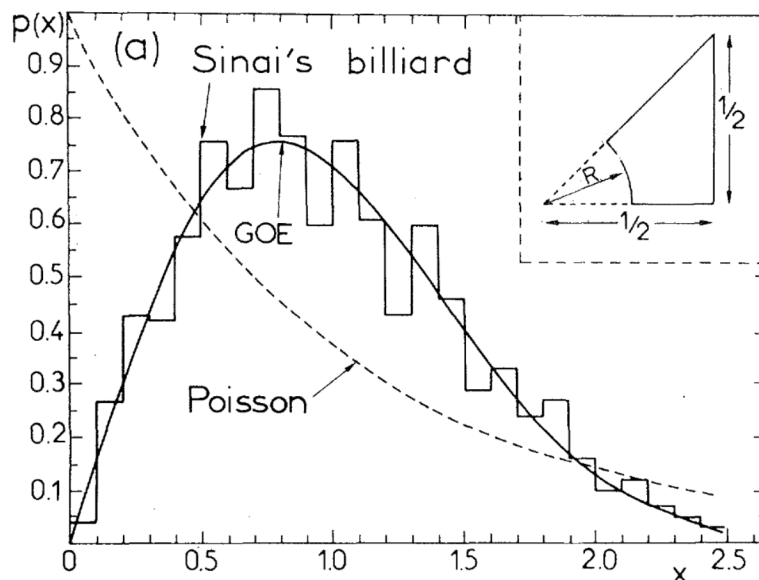


Figure 1.2: The numerically obtained level spacing of the desymmetrized Sinai billiard compared with that of the GOE. One can see that they match closely, which gives a foundational example of the BGS-conjecture. For comparison, the Poisson distribution is indicated with a dotted line. This image is reprinted from [61].

We mentioned above that the BGS (and BT) conjecture ascribe (near) universal eigenvalue statistics to quantum systems based purely on chaoticity (or lack thereof) and symmetry. There exists a similar universality for random matrix ensembles. In particular, upon unfolding, it can be shown that a broad class of weight functions (including but not limited to the Gaussian choice) leads to the WD-statistics exhibited by Gaussian RME's. Moreover, RME's can also be defined in terms of the distribution of their matrix entries, for which it can also be shown that a large class of distributions of matrix entries leads to WD-statistics. For a detailed survey, see e.g. [81]. Not only, then, do quantum chaotic systems display universal WD-statistics, the same is true for a large class of RME's. The latter is known as *random matrix universality*, which is one of the central aspects of RMT [77], [55].

Besides Gaussian RME's, an important and closely related class are those where the matrices themselves are unitary. These are the circular ensembles, so named because the eigenvalues of unitary matrices lie on the complex unit circle. These were first introduced by Freeman Dyson in the early 1960's [82]. The circular analogues of the Gaussian ensembles are known as the circular orthogonal ensemble (COE), the aforementioned circular unitary ensemble (CUE), and the circular symplectic ensemble (CSE) which, as in the Gaussian case, refers to the transformations under which the ensemble is invariant. For example, the CUE is the unique measure on unitary matrices that is invariant under unitary transformations, which is known as the Haar measure. In the asymptotic ($N \rightarrow \infty$) limit, the eigenphases of the circular ensembles exhibit the same eigenvalue statistics as the Gaussian ensembles, which is why this is referred to as Wigner–Dyson statistics, see e.g. [55]. In the remainder of this thesis, we will focus on the CUE and its generalizations. Unitary matrices are themselves diagonalized by a unitary transformation. We again integrate out the diagonalizing transformation to obtain the eigenvalue representation of the partition function,

$$Z = \tilde{C}_N \int \prod_{j=1}^N \frac{d\phi_j}{2\pi} f(e^{i\phi_j}) \prod_{j<k} |e^{-i\phi_j} - e^{-i\phi_k}|^2, \quad (1.125)$$

where we again have a weight function f and where $e^{i\phi_j}$ are the eigenvalues. Taking $f = 1$ gives the CUE. Equation (1.125) features a squared Vandermonde determinant $\prod_{j<k} |e^{-i\phi_j} - e^{-i\phi_k}|^2$, as for the GUE. Likewise, the COE and CSE feature a Vandermonde determinant to the power one and four, respectively. Different choices of f lead to different ensembles which can be treated using the methods outlined in section 1.2, as well as our results which will be presented in chapter 2. Another important tool in the study of RME's are orthogonal polynomials, whose usage was pioneered by Mehta [77]. However, we will only be requiring the expressions in section 1.2, so we will not be treating the orthogonal polynomial approach here.

1.4.2 Intermediate statistics

Certain systems which are somewhere in between chaotic and integrable, such as disordered electrons at the mobility edge of Anderson localization [83], or pseudo-integrable billiards [84], display so-called intermediate statistics. Various random matrix ensembles have been introduced which exhibit these statistics. It appears that the first such model was a solvable random matrix ensemble interpolating between Poisson and WD-statistics that was introduced by Gaudin [85]. The same model was rediscovered later by Yukawa [86] in the context of a so-called Pechukas-Yukawa gas. Another type of RME that was introduced to describe intermediate statistics are the so-called banded RME's [87], for which the entries of the random matrices decay in a power-law fashion away from the main diagonal. There is also the Moshe-Neuberger-Shapiro (MNS) ensemble [88], where the unitary invariance of the ensemble is explicitly broken by a potential term involving a fixed matrix, typically chosen to be diagonal. Bogomolny et al. [89] discovered a number of ensembles which are based on the Lax matrices of various integrable systems. These ensembles exhibit intermediate statistics [90]. Further, a generalization [91] of the Rosenzweig-Porter model [92], as well as standard β -ensembles, introduced in [93] exhibit intermediate statistics [94].

Another class of matrix models was proposed in [4] to describe intermediate level statistics, depending on some parameter q between zero and one. These ensembles are defined in terms of a $U(N)$ -invariant measure, as opposed to the aforementioned ensembles with intermediate statistics. It was observed in [4] that WD-universality is lost, leading instead to the same statistics as the banded and MNS-ensembles mentioned above[7]. The relation of the ($U(N)$ -invariant) RME introduced in [4] to the (non- $U(N)$ -invariant) banded and MNS-ensembles was argued to arise due to a spontaneous breaking of $U(N)$ -invariance [10]. The matrix ensemble proposed in [4] appears in hermitian and unitary guises, analogous to the GUE and CUE. As

noted in the introduction, we analyzed this matrix model in its unitary guise but, to our surprise, did not find any evidence of intermediate statistics. This will be treated in section 4.1. The same RME introduced in [4] was later found by Mariño as a matrix model of type A topological open string theory on the cotangent space of S^3 [5], which is described by $U(N)$ Chern–Simons theory on S^3 [95]. Due to the relation of this RME to Chern–Simons theory, we refer to it as the Chern–Simons matrix model (CSMM). It was famously shown by Witten [96] that Chern–Simons expectation values of Wilson lines are given by knot and link invariants, such as the Jones polynomial for $SU(2)$, or the HOMFLY polynomial for $SU(N)$. The parameter q can be given by a real number or lie on the complex unit circle, see e.g. [97] and [98]. As the previous application of the CSMM to intermediate statistics considered real q between zero and one, we focus on this parameter range as well. In section 1.5, we will review how these matrix models arise from Chern–Simons theory and the matrix model computation of knot and link invariants.

For the hermitian version of the CSMM, the weight function is of the following “log-squared” form, see also e.g. [12],

$$f(x) \propto \exp\left(-\frac{1}{2g_s} \log^2 x\right) \quad , \quad |x| \gg 1 \quad , \quad (1.126)$$

where $g_s = -\log q$. Sufficiently shallow confining potentials, which asymptotically behave as $V(H) \sim \log^2 H$ for $|H| \gg 1$, are associated with indeterminate moment problems. This is to say that the weight function $f(x)$ is not uniquely determined by its moments $m_j = \int x^j f(x) dx$ [6], [99]. In its unitary guise, the CSMM has the following weight function

$$f(e^{i\phi}) = \Theta_3(e^{i\phi}; q) = \sum_n q^{n^2/2} e^{in\phi} \quad . \quad (1.127)$$

That is, f equals Jacobi’s third theta function, which is defined on the complex

unit circle³. One immediately sees that the matrix model with this weight function reduces to the CUE as we take $q \rightarrow 0$. We will consider this limit in more detail below. On the other hand, it was shown in [4] that the hermitian version of the CSMM, after unfolding, displays GUE statistics as one takes $q \rightarrow 1$. Intermediate statistics were found for q away from these limits. These can be seen in figure 1.3, which displays the level statistics found for the hermitian version of the CSMM in [4]. Somewhat confusingly, in [4], $g_s = -\log q$ is denoted by β , which is typically reserved for the symmetry index. As one can see in figure 1.3, the eigenvalue statistics found in [4] range from WD-statistics for $\log q^{-1} = 0$ to increasing intermediacy as we increase $\log q^{-1}$, leading to a level spacing more closely resembling a Poisson distribution. It should be noted that the intermediate level spacing distribution goes to zero at the origin for any value of β , as opposed to the Poisson distribution.

Although our calculations did not reveal any intermediacy in (the unitary version of) the CSMM, we can still be sure that figure 1.3 provides an example of intermediate statistics. This is because the statistics found in [4] were identical to that of the banded and MNS-ensembles, which are known to exhibit intermediacy.

³Note that the definition in (1.170) has $q^{n^2/2}$ rather than q^{n^2} as expansion coefficients, the latter being another common convention.

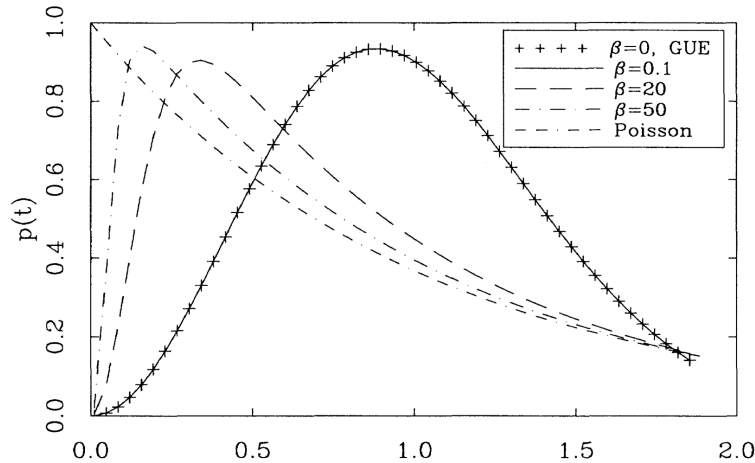


Figure 1.3: The intermediate level spacing distribution, with WD and Poisson distributions for reference, reprinted from [4]. The controlling parameter $\log q^{-1}$ is indicated here by β , where $\beta = 0$ gives WD-statistics. Increasing β leads to greater deviation from WD-statistics and increased similarity to Poisson statistics, although any value of β gives a vanishing probability that two levels coincide.

1.4.3 Level density and spectral form factor

An important object in random matrix theory is the level density (or eigenvalue/eigenphase density, or density of states) given by

$$\rho(\phi) = \frac{1}{N} \sum_{j=1}^N \delta(\phi - \phi_j) = \frac{1}{2\pi N} \sum_{j=1}^N \sum_{n \in \mathbb{Z}} e^{in(\phi - \phi_j)} = \frac{1}{2\pi N} \sum_{n \in \mathbb{Z}} \text{tr} U^n e^{in\phi}, \quad (1.128)$$

where we used the fact that, for a unitary matrix U with eigenvalues $e^{i\phi_j}$,

$$\text{tr} U^n = \sum_{i=1}^N e^{in\phi_j}. \quad (1.129)$$

The level density averaged over an RME, gives the probability of finding an eigenvalue at ϕ . As mentioned above, to faithfully compare different spectra, one has to

transform to a new (energy or eigenphase) variable where the average level spacing is the same everywhere, resulting in a flat level density. Strictly speaking, unfolding involves a change of variables to the staircase function, (see e.g. section 5.19 of [55]),

$$\sigma(\theta) = \int_{\theta_c}^{\theta} d\theta' \rho(\theta') . \quad (1.130)$$

The level density in terms of σ is a perfectly flat function. However, this unfolding procedure is often difficult in practice, necessitating the usage of cruder approaches.

From the level densities, we can construct the n -point density correlation functions for $n = 2, \dots$ and various related quantities. An important example thereof which is often used to characterize the eigenvalue statistics of various ensembles is the spectral form factor (SFF), which is the Fourier transform of the two-point level density correlation function [77]. The two-point correlation function is given by,

$$\langle \rho(\theta) \rho(\phi) \rangle = \frac{1}{N^2} \sum_{k, l \in \mathbb{Z}} \langle \text{tr} U^k \text{tr} U^l \rangle e^{ik\theta + il\phi} - 1 . \quad (1.131)$$

The SFF is then given by the expansion coefficients of $e^{in(\theta-\phi)}$, $n \in \mathbb{Z}^+$, rescaled by a factor N^{-1} , [77], [55],

$$K(n) = \frac{1}{N} \langle |\text{tr} U^n|^2 \rangle . \quad (1.132)$$

The choice of normalization is made so that, for $n/N \geq 1$, the CUE SFF saturates at unity. For future convenience, we also define the connected part of the SFF

$$K(n)_c = K(n) - \frac{1}{N} \langle \text{tr} U^n \rangle^2 . \quad (1.133)$$

We will also occasionally use

$$F(n) = NK(n) , \quad (1.134)$$

and $F(n)_c$ defined as in (1.133).

A well-known, heuristic way to understand the relation between SFF's and spectral statistics is as follows. If we consider a diagonal matrix $V = \text{diag}(e^{i\phi_1}, e^{i\phi_2}, \dots, e^{i\phi_N})$ with all ϕ_j taking random values in $[0, 2\pi)$, and we average over ϕ_j , we get

$$\langle |\text{tr} V^n|^2 \rangle = \left\langle \sum_{k,l=1}^N e^{in(\phi_k - \phi_l)} \right\rangle = N. \quad (1.135)$$

Here, we use the fact that $e^{in(\phi_k - \phi_m)}$ equals 1 for $k = m$, whereas for $k \neq m$ it is a random variable on ($2n$ copies of) the complex unit circle, which averages to zero. A system with eigenphases distributed randomly across the unit circle therefore has a constant SFF. In this case, the SFF, being a sum over complex numbers of unit length, essentially describes a two-dimensional random walk.

On the other hand, random unitary matrices U display level repulsion with overwhelming probability, so that their eigenvalues tend to distribute more evenly across the complex unit circle. Therefore, $\langle |\text{tr} U^n|^2 \rangle$ is much lower than N for small values of n , as evenly spaced complex numbers are more likely to mutually cancel out than complex numbers which are distributed randomly and are thus allowed to cluster. In particular, for systems in the WD-universality class, the connected SFF is given by $F(n)_c = n$ for $n \leq N$, which we refer to as a *linear ramp* (of unit slope). However, for n close to N , we have that n becomes of the order of the average spacing $\phi_{k+1} - \phi_k$. In that case, $e^{in(\phi_k - \phi_l)}$ is an approximately random element of the complex unit circle for all $k \neq l$, so that these again average to zero and only the constant contribution N coming from $k = l$ remains. As a result, we have $K(n) = 1$ for $n > N$, so that the SFF reaches the so-called *plateau*. For Poisson-distributed (uncorrelated) eigenphases, the SFF immediately attains this plateau, as argued above. We will be giving various examples of SFF's, including plots, in chapter 4.

1.5 Chern–Simons theory

We review the construction of Chern–Simons partition functions and knot and link invariants using Heegaard splitting [96] and the knot operator formalism [100]. We will also treat the matrix model description of these objects, referred to as the CSMM, which was introduced in section 1.4.2. One may consult [101] for more information on these topics, as well their application to topological string theory and related questions in geometry.

1.5.1 Knot operator formalism

Heegaard splitting provides a way to calculate the Chern–Simons partition functions of certain three-manifolds, which we generally denote by M . We construct M by taking two separate three-manifolds M_1 and M_2 which share a common boundary Σ , i.e. $\partial M_1 \simeq \Sigma \simeq \partial M_2$. M is then constructed by acting on Σ with some homeomorphism f and then gluing M_1 and M_2 together, which we write as

$$M = M_1 \bigcup_f M_2 . \quad (1.136)$$

In this construction, we take the boundaries of M_1 and M_2 to have opposite orientation, so that M is a closed manifold. Writing the Hilbert space of Σ as $\mathcal{H}(\Sigma)$ and its conjugate as $\mathcal{H}^*(\Sigma)$, performing the path integral over M_1 gives a state $|\Psi_{M_1}\rangle \in \mathcal{H}(\Sigma)$, whereas performing the path integral over M_2 to find a state $\langle\Psi_{M_2}|$ in the conjugate Hilbert space $\mathcal{H}^*(\Sigma)$ due to the fact that the boundaries of M_1 and M_2 have opposite orientation. The homeomorphism f induces a map U_f on $\mathcal{H}(\Sigma)$ whose action we denote by

$$U_f : \mathcal{H}(\Sigma) \rightarrow \mathcal{H}(\Sigma) . \quad (1.137)$$

The partition function is then given by

$$Z(M) = \langle \Psi_{M_1} | U_f | \Psi_{M_2} \rangle . \quad (1.138)$$

In a seminal paper [96], Witten found that $\mathcal{H}(\Sigma)$ is given by the space of conformal blocks of the corresponding Wess-Zumino-Novikov-Witten (WZNW) model on Σ at level k . In case there are no marked points on Σ where Wilson lines are cut, i.e. if all Wilson lines can be embedded on Σ , $\mathcal{H}(\Sigma)$ is given by the characters of the WZNW model on Σ . We will be considering only the latter case.

A relatively simple example of a Heegaard splitting is given by the division of S^3 into two three-balls that share a boundary $\Sigma = S^2$. The only knot that can be embedded on S^2 is the unknot, which is the trivial example of an unknotted circle. We therefore do not consider this example any further. Let us instead consider the case where M_1 and M_2 are given by solid tori $S^1 \times D^2$ which share a boundary torus $\partial M_1 = S^1 \times S^1 = \partial M_2$. The manifolds which can be constructed via such a Heegaard splitting on a torus are known as lens spaces [102]. The simplest example of a lens space is found by taking f to be the identity map. In this case, we glue the two copies of D^2 along their boundaries to form S^2 , so that the resulting space is given by $S^2 \times S^1$. We normalize the Chern–Simons partition function for $S^2 \times S^1$ to unity. Let us consider an example where we act on T^2 with a nontrivial homeomorphism. The group of homeomorphisms of T^2 is given by $SL(2; \mathbb{Z})$, which consists of matrices of the following form

$$\begin{pmatrix} a & b \\ c & d \end{pmatrix}, \quad ad - bc = 1, \quad a, b, c, d \in \mathbb{Z}. \quad (1.139)$$

$SL(2; \mathbb{Z})$ is generated by the modular S and T -transformations. Representing the 1-cycles of the torus by basis vectors $\begin{pmatrix} 1 \\ 0 \end{pmatrix}$ and $\begin{pmatrix} 0 \\ 1 \end{pmatrix}$, the S and T -transformations

can be written as

$$S = \begin{pmatrix} 0 & -1 \\ 1 & 0 \end{pmatrix}, \quad T = \begin{pmatrix} 1 & 1 \\ 0 & 1 \end{pmatrix}. \quad (1.140)$$

That is, S interchanges the 1-cycles and reverses the orientation of the torus, while T cuts open the torus along a 1-cycle to form a cylinder, twists one end of the cylinder by 2π , and glues the two ends of the cylinder back together. Consider the case where we glue two solid tori $M_{1,2}$ along their boundaries after acting with an S -transformation. Since S -transformations exchange the 1-cycles on the torus, the contractible cycle of M_1 is glued to the non-contractible cycle of M_2 and vice versa. We thus find a closed three-manifold with no non-contractible cycles which, from the Poincaré conjecture, is homeomorphic to S^3 .

The construction of torus knots is analogous to the construction of lens spaces in the sense that, if we insert a Wilson line corresponding to an unknot on the boundary torus, we can act with arbitrary $SL(2; \mathbb{Z})$ transformation on the torus which turns the unknot into a non-trivial torus knot. Let us denote the torus knot operators, to be defined more precisely below, by $\mathcal{W}_\lambda^{(p,q)}$, where λ labels the irreducible representation of the Wilson line that is tied into a knot, and p and q are integers which count the winding of the knot around non-contractible and contractible cycle of the torus, respectively. Note that p and q are coprime for torus knots, whereas for p and q not coprime we would get a torus link, which is a generalization of a torus knot with more than one component (i.e. more than one knotted piece of string). The number of components of a torus link equals the greatest common divisor of p and q . From the definition of the S and T -

transformations, it is clear that they act on torus knot as follows

$$\begin{aligned} S^{-1}\mathcal{W}^{(p,q)}S &= \mathcal{W}^{(q,-p)} , \\ T^{-1}\mathcal{W}^{(p,q)}T &= \mathcal{W}^{(p,q+p)} . \end{aligned}$$

For example, if we insert an unknot around the non-contractible cycle of the torus and act n times with the T -transformation, we get a knot which still winds around the non-contractible cycle once but which now also winds around the contractible cycle n times.

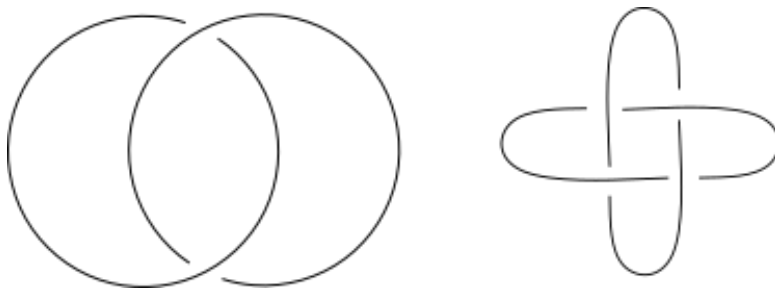


Figure 1.4: Two examples of $(2n, 2)$ -torus links. The Hopf link, on the left, is the $(2, 2)$ -torus link. On the right, we have the $(4, 2)$ -torus link.

It is easy to see that modular transformations map the set of torus knots into itself, as these transformations do not change the number of components. Indeed, for any pair of coprime integers (p, q) , one can easily see that $(p, q + p)$ are also coprime, so that the number of components is unchanged under modular transformations. Further, due to Bézout's lemma [103], there is an $SL(2; \mathbb{Z})$ -transformation corresponding to any pair of coprime integers, so that we can construct any torus knot by acting on an unknot with an $SL(2; \mathbb{Z})$ -transformation.

The explicit form for the knot operators for $SU(N)$ was found by Labastida, Llatas, and Ramallo [100], using the relation to WZNW-models previously found by Witten

[96]. Let us summarize the salient points of the knot operator formalism. As mentioned above, $\mathcal{H}(\Sigma)$ is given by the conformal blocks of the corresponding WZNW-model on Σ with group G at level k . In the case of $\Sigma = T^2$ without marked points, which we will be considering henceforth, $\mathcal{H}(\Sigma)$ consists of the characters of integrable representations of the corresponding WZNW-model. We denote the set of fundamental weights by $\{v_i\}$ and Weyl vector by $\rho = \sum_i v_i$. A representation with highest weight Λ is integrable if $p := \rho + \Lambda = \sum_i p_i v_i$ is in the fundamental Weyl chamber, that is,

$$\sum_i p_i < k + y \quad , \quad p_i > 0 \quad , \quad \forall i \quad , \quad (1.141)$$

where y is the dual Coxeter number of G , which equals N for $G = U(N)$ and $N - 1$ for $G = SU(N)$. Remember that an irrep with highest weight $\Lambda = \sum_i \Lambda_i v_i$ corresponds to a Young tableau where the length of the i^{th} row is given by

$$\Lambda_i + \Lambda_{i+1} + \cdots + \Lambda_I \quad , \quad (1.142)$$

where I equals N in the case of $U(N)$ and $N - 1$ in the case of $SU(N)$. From now on we will take $G = U(N)$ so that $y = N$. We will denote ket states corresponding to p by $|p\rangle$, which can be chosen in such a way that they form an orthonormal basis. The vacuum state, that is, the state without any Wilson line inserted, is given by $|\rho\rangle =: |0\rangle$. If we act with a knot operator corresponding to an unknot in representation corresponding to Λ , the result is [100]

$$\mathcal{W}_\Lambda^{(1,0)} |\rho\rangle = |\rho + \Lambda\rangle = |p\rangle \quad . \quad (1.143)$$

Consider the multiplication properties of knot operators. If we take $\mathcal{W}_\Lambda^{\mathcal{K}}$ to be a

knot operator corresponding to a knot \mathcal{K} in representation λ , we can write

$$\mathcal{W}_\lambda^{\mathcal{K}} \mathcal{W}_\mu^{\mathcal{K}} = \sum_\nu N_{\lambda\mu}^\nu \mathcal{W}_\nu^{\mathcal{K}} . \quad (1.144)$$

The coefficients $N_{\lambda\mu}^\nu$ in (1.144) are the fusion coefficients of the WZNW-model. When the representations under consideration are much smaller than N , $N_{\lambda\mu}^\nu$ are given by Littlewood-Richardson coefficients $c_{\lambda\mu}^\nu$. This allows us to construct the invariants of torus links. We label a torus link by $P, Q \in \mathbb{Z}$, where the number of components is given by $S = \gcd(P, Q)$ and the representations are labelled by $j \in \{1, \dots, S\}$. These links are given by [100], [104], [105]

$$\prod_{j=1}^S \mathcal{W}_{\lambda_j}^{P/S, Q/S} = \sum_\mu c_{\lambda_1, \dots, \lambda_S}^\mu \mathcal{W}_\mu^{P/S, Q/S} , \quad (1.145)$$

where $c_{\lambda_1, \dots, \lambda_S}^\mu$ are generalized Littlewood-Richardson coefficients appearing in the product of representations $\lambda_1, \lambda_2, \dots$.

The only further ingredient we need are the explicit expressions for the Hilbert space operators induced by the modular transformations. We simply state these here, further details may be found in [100]

$$\begin{aligned} T_{pp'} &= \delta_{p,p'} e^{2\pi i(h_p - c/24)} , \\ S_{pp'} &= \frac{i^{N(N-1)/2}}{N^{N/2}} \left(\frac{N}{k+N} \right)^{\frac{N-1}{2}} \sum_{w \in W} \epsilon(w) \exp \left(\frac{-2\pi i p \cdot w(p')}{k+N} \right) . \end{aligned} \quad (1.146)$$

In the above expressions, W is the Weyl group, $\epsilon(w)$ is the signature of Weyl reflection w , c is the central charge of the WZNW-model, and h_p is the conformal weight

of the primary field corresponding to p , which is given by

$$h_p = \frac{p^2 - \rho^2}{2(k + y)}. \quad (1.147)$$

1.5.2 Chern–Simons matrix model

Let us consider how the matrix model description of Chern–Simons theory arises. As explained above, S^3 can be constructed via a Heegaard splitting along a torus on which we act with an S -transformation. We thus find that the Chern–Simons partition function on S^3 is given by

$$Z(S^3) = \langle 0|S|0\rangle = S_{00}. \quad (1.148)$$

We plug in the expression for S_{00} from equation (1.146) and use Weyl’s denominator formula,

$$\sum_{w \in W} \epsilon(w) e^{w(p)} = \prod_{\alpha > 0} 2 \sinh(\alpha/2), \quad (1.149)$$

where α are the positive roots of $U(N)$. Expressing the roots of $U(N)$ in terms of Dynkin coordinates x_i , we find

$$Z(S^3) = \frac{e^{-\frac{g_s}{12}N(N^2-1)}}{N!} \int \frac{dx_i}{2\pi} \prod_{i=1}^N e^{-x_i^2/2g_s} \prod_{i < j} \left(2 \sinh \frac{x_i - x_j}{2} \right)^2. \quad (1.150)$$

Lastly, we define a new set of variables $y_i := e^{Ng_s + x_i}$, in which the partition function is given by [5]

$$Z(S^3) = \frac{e^{-(7N^3g_s/12 + N^2g_s/2 - Ng_s/24)}}{N!} \int_0^\infty \prod_{j=1}^N \frac{dy_j}{2\pi} \prod_{j < k} (y_j - y_k)^2 \exp \left(-\frac{1}{2g_s} \sum_j \log^2(y_j) \right). \quad (1.151)$$

Alternatively, we can use the following expression, involving the third Jacobi Theta function given in (1.127),

$$q^{n^2/2} = \int_0^{2\pi} \frac{d\phi}{2\pi} \Theta_3(e^{i\phi}; q) e^{in\phi} , \quad (1.152)$$

This gives

$$\begin{aligned} \sum_{w \in W} \epsilon(w) q^{\frac{1}{2}(w(\rho) - \rho)^2} &= \frac{1}{|W|} \sum_{w, w' \in W} \epsilon(w) \epsilon(w') q^{\frac{1}{2}(w(\rho) - w(\rho'))^2} \\ &= \frac{1}{|W|} \int \prod_{i=1}^N \frac{d\phi_i}{2\pi} \Theta_3(e^{i\phi_i}; q) \sum_{w, w' \in W} \epsilon(w) \epsilon(w') q^{i(w(\rho) - w(\rho') - \theta)} , \end{aligned} \quad (1.153)$$

where we added another summation over the Weyl group in the first equality and applied (1.152) in the second. Lastly, the Weyl group W is isomorphic to the symmetric group S_N so that $|W| = N!$. Using the Weyl denominator formula again leads to [106][107].

$$Z = \frac{1}{N!} \int_0^{2\pi} \prod_{i=1}^N \frac{d\phi_i}{2\pi} \Theta_3(e^{i\phi_j}; q) \prod_{j < k} |e^{i\phi_j} - e^{i\phi_k}|^2 . \quad (1.154)$$

Note that (1.151) and (1.154) correspond precisely to the matrix ensemble introduced by [4], given in (1.126) and (1.127), respectively.

Torus knots and link invariants

We now outline the computation of torus knot and link invariants using the matrix model for $U(N)$ Chern–Simons on S^3 , for general N and q . The simplest knot, the unknot, is given by the ensemble average of the matrix trace in the corresponding

representation [108]. That is,

$$W_\lambda := \langle \mathcal{W}_\lambda^{(1,0)} \rangle = \langle \text{tr}_\lambda U \rangle , \quad (1.155)$$

where, for a matrix U with eigenvalues $e^{i\phi_j}$,

$$\text{tr}_\lambda U = s_\lambda(U) = s_\lambda(e^{i\phi_j}) . \quad (1.156)$$

We will mostly write traces without specified representations, in which case it is understood to be in the fundamental representation. Denote by $\bar{\lambda}$ the representation conjugate to λ . This can be obtained by rotating the skew partition $((\lambda_1)^N)/\lambda$ by 180 degrees, where $((\lambda_1)^N)$ is the rectangular partition consisting of N rows of size λ_1 . The simplest example is the conjugate of the fundamental representation \square , known as the antifundamental representation, which consists of a column of length $N - 1$. We then have [101]

$$\text{tr}_\lambda U^{-1} = \text{tr}_{\bar{\lambda}} U . \quad (1.157)$$

In the language of knot theory, taking $\text{tr}_\lambda U$ to $\text{tr}_\lambda U^{-1}$ corresponds to inverting the orientation of the component carrying representation λ , see e.g. [101]. Of course, for the unknot, this does not matter, as reverting the orientation can be compensated by a simple parity transformation. The same is true for the Hopf link, as overcrossings can be freely changed into undercrossings. For more complicated knots or links, such as the $(4, 2)$ -torus link on the right hand side of figure 1.4, overcrossings can no longer be turned into undercrossings and inverting the orientation of one component will generally lead to a different expectation value.

One can show [108], [109], [110] that $\langle \text{tr} U^n \rangle$ gives the invariant of an $(n, 1)$ -torus knot [111], which differs from any (n, m) -torus knot only by multiplicative factor given by a rational power of q . Equation (1.21) gives an expansion of $\text{tr} U^n$ in terms

of hook-shaped Schur polynomials which, when averaged over the CSMM as in (1.155), gives the unknot invariant for a hook-shaped representation. Further, one may use equation (1.145) to multiply traces $\text{tr}U^n$ to construct more complicated knot and link invariants, which have been extensively treated in [112], [105]. Using (1.157), we then conclude that $\langle |\text{tr}U^n|^2 \rangle$ give the HOMFLY invariant of a $(2n, 2)$ -torus link, with one component carrying the fundamental and the other carrying the antifundamental representation. This gives a knot-theoretical interpretation to the SFF of the CSMM.

Computation of unknot and Hopf link invariants

To compute unknot and Hopf link invariants for general N and q , we will briefly review some aspects of q -numbers. These are so-called q -deformations of more familiar (generally complex) numbers. We will only be considering q -deformation of positive integers here, which are defined as

$$[n]_q = (1 + q + \cdots + q^{n-1}) = \frac{1 - q^n}{1 - q} \quad , \quad n \in \mathbb{Z}^+ . \quad (1.158)$$

Other definitions of $[n]_q$, such as $\frac{q^{-n/2} - q^{n/2}}{q^{-1/2} - q^{1/2}}$, also appear in the literature. Their common feature is that

$$\lim_{q \rightarrow 1^-} [n]_q = n . \quad (1.159)$$

Note that, for $k, m, n \in \mathbb{Z}^+$ satisfying $\frac{m}{n} = k$, we have

$$\frac{[m]_q}{[n]_q} = [k]_{q^n} \quad , \quad \frac{[r \cdot m]}{[r \cdot n]} = [k]_{q^{nr}} \quad (1.160)$$

for example,

$$\frac{[8]_q}{[2]_q} = \frac{1 + q + \cdots + q^7}{1 + q} = 1 + q^2 + q^4 + q^6 = [4]_{q^2} . \quad (1.161)$$

We will write $[n]_q$ as $[n]$ henceforth and only specify the deformation parameter in case it is different from q . q -Factorials and q -binomials are defined as follows. For $n, k \in \mathbb{Z}^+$, we have

$$[N]! = (1 + q)(1 + q + q^2) \cdots (1 + q + \cdots + q^{N-1}) , \quad (1.162)$$

and

$$\begin{bmatrix} N \\ k \end{bmatrix} = \frac{[N]!}{[N - k]![k]} . \quad (1.163)$$

We then introduce the q -Pochhammer symbol, which is defined as

$$(a; q)_k = (1 - a)(1 - aq) \cdots (1 - aq^{k-1}) . \quad (1.164)$$

Note that

$$(a; q)_n = \frac{(a; q)_\infty}{(aq^n; q)_\infty} . \quad (1.165)$$

Further, we have,

$$[n]! = \frac{(q; q)_n}{(1 - q)^n} , \quad (1.166)$$

from which it follows that

$$\begin{bmatrix} N \\ k \end{bmatrix} = \frac{(q; q)_N}{(q; q)_{N-k}(q; q)_k} = \frac{(1 - q^N)(1 - q^{N-1}) \dots (1 - q^{N-r+1})}{(1 - q)(1 - q^2) \dots (1 - q^k)} . \quad (1.167)$$

We see from this expression that, for $q < 1$, we have

$$\lim_{N \rightarrow \infty} \begin{bmatrix} N \\ k \end{bmatrix} = \frac{1}{(q; q)_k} , \quad (1.168)$$

q -Pochhammer symbols can be generalized as follows

$$(a_1, a_2, \dots, a_m; q)_n = \prod_{j=1}^m (a_j; q)_n . \quad (1.169)$$

These are rather versatile objects. For example, Jacobi's third theta function can be expressed through the Jacobi triple product as

$$\sum_{n \in \mathbb{Z}} q^{n^2/2} z^n = (q, -q^{1/2}z, -q^{1/2}/z; q)_\infty , \quad 0 < |q| < 1 . \quad (1.170)$$

Remember that a Schur polynomial with ones as variables gives the dimension of the corresponding representation, that is, $s_\lambda(1^N) = \dim(\lambda)$, see (1.16). If, instead, we choose variables as $x_j = q^{j-1}$, we get the following q -deformation of the dimension of λ

$$s_\lambda(x_j = q^{j-1}) = q^{n(\lambda)} \prod_{x \in \lambda} \frac{[N + c(x)]}{[h(x)]} =: q^{n(\lambda)} \dim_q(\lambda) . \quad (1.171)$$

The quantity $\dim_q(\lambda)$ is known as the *quantum dimension*, or q -dimension. It is given by the hook-length formula (1.16) where numbers are replaced by q -numbers. Note that (1.160) implies that representations with the same dimension generally have different quantum dimensions. For $|q| < 1$ and $N \rightarrow \infty$, quantum dimensions

for reps with finite column lengths depend only on the hook-lengths. This is because $q^{N-k} = 0$ for k finite, so that, for λ such that $c(x)$ is finite for all $x \in \lambda$,

$$\prod_{x \in \lambda} \frac{[N + c(x)]}{[h(x)]} = \frac{1}{(1-q)^{|\lambda|}} \prod_{x \in \lambda} \frac{1}{[h(x)]} . \quad (1.172)$$

We will now use this to evaluate the matrix integrals for CSMM. In this case, $f(e^{i\theta})$ is equal to $\Theta_3(e^{i\theta})$ in (1.173). Let us therefore consider the Jacobi triple product expansion of the third theta function

$$\begin{aligned} \sum_{n \in \mathbb{Z}} q^{n^2/2} e^{in\theta} &= (q; q)_\infty \prod_{j=1}^{\infty} (1 + q^{k-1/2} e^{i\theta})(1 + q^{k-1/2} e^{-i\theta}) \\ &= (q; q)_\infty E(x; e^{i\theta}) E(x; e^{-i\theta}) , \end{aligned} \quad (1.173)$$

where we define $x = (q^{1/2}, q^{3/2}, \dots)$ in the last line. Then,

$f(e^{i\theta}) = \sqrt{(q; q)_\infty} E(x; e^{i\theta}) E(x; e^{-i\theta})$ is the weight function of the Chern–Simons matrix model.

We saw in section 1.2 how $U(N)$ integrals over symmetric polynomials for general N and weight function can be expressed as a minors of a Toeplitz matrix of symbol $f(z) = \sum_{k \in \mathbb{Z}} d_k z^k$, i.e. a Toeplitz matrix with d_k on the k^{th} diagonal [40]. We repeat part of equation (1.75) for convenience.

$$D_{N-1}^{\lambda, \mu}(f) = \det(d_{\lambda_j - j - \mu_k + k})_{j, k=1}^N = \int_{U(N)} \tilde{f}(U) s_\lambda(U^{-1}) s_\mu(U) dU . \quad (1.174)$$

The weight function under consideration here is the third theta function, to which we apply the triple product expansion (1.170). We then have

$$D_{N-1}^{\lambda, \mu}(\Theta_3) = \det \left(q^{(\lambda_j - j - \mu_k + k)^2/2} \right)_{j, k=1}^N . \quad (1.175)$$

First taking $\lambda = \emptyset = \mu$, we see that the partition function of the CSMM is given by

$$Z = D_{N-1}(\Theta_3) = \det \left(q^{(k-j)^2/2} \right)_{j,k=1}^N = \prod_{j < k} (1 - q^{k-j}) = \prod_{k=1}^{N-1} (1 - q^k)^{N-k} . \quad (1.176)$$

Taking only $\lambda = \emptyset$ gives

$$\begin{aligned} D_{N-1}^\mu(\Theta_3) &= \det (d_{k-\mu_k-j})_{j,k=1}^N = \int_{U(N)} \tilde{f}(U) s_\mu(U) dU \\ &= \det \left(q^{(k-\mu_k-j)^2/2} \right)_{j,k=1}^N . \end{aligned} \quad (1.177)$$

We have (see e.g. the appendix of [113]),

$$\det (q^{(\mu_k+k-j)^2/2})_{j,k=1}^N = q^{\sum_k \mu_k^2/2} \prod_{j > k} (1 - q^{\mu_j - \mu_k + k - j}) . \quad (1.178)$$

Then,

$$W_{\lambda\mu} := \langle s_\lambda(U^{-1}) s_\mu(U) \rangle = \frac{D_{N-1}^{\lambda,\mu}}{D_{N-1}} . \quad (1.179)$$

As mentioned, this equals the Chern–Simons average over a pair of Wilson lines tied into a Hopf link where one Wilson line carries a $U(N)$ representation λ and the other carries μ , up to an irrelevant factor q to some rational power. For $\mu = \emptyset$, the Hopf link reduces to an unknot carrying rep λ , and vice versa for $\lambda = \emptyset$. Using (1.178), we then have

$$\begin{aligned} W_\mu &= \frac{\det \left(q^{(k-\mu_k-j)^2/2} \right)}{\det \left(q^{(k-j)^2/2} \right)} = q^{\sum_j \mu_j^2/2} \frac{\prod_{j < k} (1 - q^{k-j-\mu_k+\mu_j})}{\prod_{j < k} (1 - q^{k-j})} \\ &= q^{-n(\mu) + \sum_j \mu_j^2/2} s_\mu(1, q, \dots, q^{N-1}) , \end{aligned} \quad (1.180)$$

where $n(\mu) = \sum_{j=1}^N (j-1)\mu_j$. When we take $N \rightarrow \infty$, we apply (1.85) to find

$$W_\mu^\infty = s_{\mu^t}(q^{j-1/2}) = q^{|\mu|/2+n(\mu^t)-n(\mu)} s_\mu(q^{j-1}) . \quad (1.181)$$

The power appearing in the prefactor is given by the sum of the content, $c(x)$, over the partition μ . Specifically, $c(x) = j - i$ for $x = (i, j) \in \mu$, and [33]

$$\sum_{x \in \mu} c(x) = n(\mu^t) - n(\mu) , \quad (1.182)$$

For general λ and μ , N , and $|q| < 1$, we have [42], [107],

$$\begin{aligned} W_{\lambda\mu} &= \frac{1}{Z_N} \int s_\lambda(U^{-1}) s_\mu(U) f(U) dU \\ &= q^{\sum_{j=1}^N (\lambda_j^2/2 + \mu_j^2/2 - (j-1)(\lambda_j + \mu_j))} s_\mu(q^{j-1}) s_\lambda(q^{-\mu_1}, q^{1-\mu_2}, \dots, q^{N-1-\mu_N}) \\ &= q^{-n(\lambda) - n(\mu) + \sum_{j=1}^N (\lambda_j^2/2 + \mu_j^2/2)} s_\mu(q^{j-1}) s_\lambda(q^{-\mu_1}, q^{1-\mu_2}, \dots, q^{N-1-\mu_N}) . \end{aligned} \quad (1.183)$$

For $N \rightarrow \infty$ and $|q| < 1$, we apply (1.85) to find

$$W_{\lambda\mu}^\infty = \sum_{\nu} s_{(\lambda/\nu)^t}(q^{j-1/2}) s_{(\mu/\nu)^t}(q^{j-1/2}) . \quad (1.184)$$

We will be applying both equations (1.183) and (1.184) in chapter 4. Consider the Schur polynomial $s_\lambda(q^{j-1})$ appearing in (1.184). As mentioned, this is given by the q -hook length formula in (1.171), and the result equals the quantum dimension of λ . Applying (1.171), the hook-shaped Schur polynomial is found to be

$$s_{(a,1^b)}(x_i = q^{i-1}) = q^{b(b+1)/2} \frac{[N+a-1]!}{[N-b-1]![a-1]![b]![a+b]} . \quad (1.185)$$

For $c(x) \ll N$, $\forall x \in \lambda$ and $N \rightarrow \infty$, (1.171) gives

$$s_\lambda(q^{j-1}) = \frac{q^{n(\lambda)}}{(1-q)^{|\lambda|}} \prod_{x \in \lambda} [h(x)]^{-1} = q^{n(\lambda)} \prod_{x \in \lambda} (1 - q^{h(x)})^{-1} . \quad (1.186)$$

In particular, $s_\lambda(q^{j-1})$ depends only on $n(\lambda)$ and the hook lengths, so that e.g. $\frac{[N+a-1]}{[N-b-1]} = (1-q)^{-(a+b)}$. Therefore, for a partition λ for which

$$\sum_{x \in \lambda} c(x) = n(\lambda^t) - n(\lambda) = 0 , \quad (1.187)$$

the unknot W_λ^∞ is invariant under taking $\lambda \rightarrow \lambda^t$. One can clearly see from equation (1.171) that this is not the case for finite N . These examples illustrate the simplifications which occur as $q^N \rightarrow 0$, which will appear again in section 4.3.

Chapter 2

Unitary matrix integrals

This chapter presents our mathematical results. It is mainly based on [1], which builds on the main result we derived in [2]. There are further results in this dissertation which could be considered of mathematical interest which will not be presented in this chapter, such as the polynomials found in the ‘t Hooft limit, or the implications of the fact that $\chi_{(n^k)}^{\lambda/\mu}$ is cancellation free. However, since these results were derived in the context of physical questions, we present them in the following chapters, in particular in sections 3.6 and 4.5. In this chapter, we focus on identities which provide new ways to compute various objects, in particular unitary integrals over symmetric polynomials, which can be used to tackle other mathematical problems.

2.1 Power sums and hook-shaped diagrams

We will consider here the calculation of the expectation value of a product of two traces $\langle \text{tr} U^n \text{tr} U^{-k} \rangle$, for $k, n \in \mathbb{N}^+$, and weight function f satisfying the strong Szegő

limit theorem. We repeat here equation (1.54)

$$\mathrm{tr}U^n = p_n(e^{i\theta_j}) = \sum_{r=0}^{n-1} (-1)^r s_{(n-r,1^r)}(U) . \quad (2.1)$$

It is clear that this also holds when we replace U with U^{-1} . Using (1.86), we have

$$\langle \mathrm{tr}U^n \rangle = p_n(y) , \quad \langle \mathrm{tr}U^{-n} \rangle = p_n(x) . \quad (2.2)$$

Then,

$$\langle \mathrm{tr}U^n \mathrm{tr}U^{-k} \rangle = \sum_{r=0}^{n-1} (-1)^r s_{(n-r,1^r)/\nu}(y) \sum_{\nu} \sum_{s=0}^{k-1} (-1)^s s_{(k-s,1^s)/\nu}(x) . \quad (2.3)$$

The first sum on the right hand side runs over all representations ν satisfying $\nu \subseteq (n-r, 1^r)$ as well as $\nu \subseteq (k-s, 1^s)$. We list below the contributions arising for various choices of ν . We will often omit the variables x and y henceforth.

1. If ν is the empty partition $\nu = \emptyset$, $s_{\lambda/\nu} = s_{\lambda}$ i.e. the skew Schur polynomials reduces to the usual (non-skew) Schur polynomial. This contributes

$$\sum_{r=0}^{n-1} (-1)^r s_{(n-r,1^r)}(y) \sum_{s=0}^{k-1} (-1)^s s_{(k-s,1^s)}(x) = p_n(y)p_k(x) . \quad (2.4)$$

2. If $\nu = \lambda$, the skew Schur polynomial $s_{\lambda/\nu} = s_{\lambda/\lambda} = 1$. For $\lambda = (n-r, 1^r)$ and $\mu = (k-s, 1^s)$, one can only have $\lambda = \nu = \mu$ if $k = n$ and $r = s$. For $k = n$ and $\nu = (n-r, 1^r)$ and we sum over r , we get a contribution of the following form

$$\sum_{r=0}^{n-1} (s_{\emptyset})^2 = n . \quad (2.5)$$

This is where the term $n\delta_{n,k}$ in (2.8) originates.

3. Take $k \leq n$ without loss of generality. The only remaining choice for ν is $\nu \neq \emptyset$ and $\nu \neq (n-r, 1^r)$. For $\lambda = (a, 1^b)$ and $\nu = (c, 1^d)$ such that $\nu \subseteq \lambda$, we have $\lambda/\nu = (a-c) \times (1^{b-d})$, e.g. for $\lambda = (4, 1^2)$ and $\nu = (2, 1)$, we have the following:

$$\begin{array}{|c|c|c|c|} \hline \square & \square & \square & \square \\ \hline \square & & & \\ \hline \square & & & \\ \hline \end{array} / \begin{array}{|c|c|} \hline \square & \square \\ \hline \square & \\ \hline \end{array} = \begin{array}{|c|c|c|} \hline \square & \square & \square \\ \hline \end{array} \quad (2.6)$$

Fixing $\nu = (a, 1^b)$ and considering only the sum over r in (2.3), we have

$$\sum_{r=0}^{n-1} (-1)^r s_{(n-r, 1^r)/(a, 1^b)} = \sum_{r=b}^{n-a} (-1)^r h_{n-r-a} e_{r-b} = 0, \quad (2.7)$$

where we applied (1.7), see also the diagrams in (1.41). That is, we get zero contribution for all $\nu \neq \emptyset, (n-r, 1^r)$.

Combining the above arguments leads to the following expression, which is the main result in [2],

$$\boxed{\langle \text{tr} U^n \text{tr} U^{-k} \rangle = n\delta_{n,k} + p_n(y)p_k(x)}. \quad (2.8)$$

Of course, the same reasoning as above can be applied to other expectation values involving $\text{tr} U^n$, such as

$$\langle \text{tr} U^{-n} s_\lambda(U) \rangle_c = \sum_{\nu \neq \emptyset} \sum_{r=0}^{n-1} (-1)^r s_{(n-r, 1^r)/\nu} s_{\lambda/\nu}. \quad (2.9)$$

Again, the sum is over all $\nu \neq \emptyset$ such that $\nu \subseteq \lambda, (n-r, 1^r)$. Fixing any $\nu \subseteq (n-r, 1^r)$ in (2.9) with $\nu \neq (n-r, 1^r)$ gives zero when summing over r by application of (2.7). Therefore, we only get a non-zero answer for terms for which $\nu = (n-1, 1^r) \subseteq \lambda$. That is,

$$\langle \text{tr} U^{-n} s_\lambda(U) \rangle_c = \sum_r (-1)^r s_{\lambda/(n-r, 1^r)}, \quad (2.10)$$

where the sum is over $\min(0, n-\lambda_1) \leq r \leq \min(n-1, \lambda_1^t + 1)$. Using (1.44), we can express this as

$$\langle \text{tr} U^{-n} s_\lambda(U) \rangle_c = \sum_\nu (-1)^{\text{ht}(\lambda/\nu)} s_\nu, \quad (2.11)$$

where the sum is over all ν such that λ/ν is a border strip η of size n , which we also write as $\nu = \lambda \setminus \eta$. As an example, take $\lambda = (6, 4, 3^2, 2)$ and $n = 4$. We show the diagrams ν appearing in (2.11) below, where the cells that are removed are again given in black.

(2.12)

2.1.1 Applying Wick's theorem

We will now combine equation (2.8) with Wick's theorem to compute more complicated objects. In particular, for terms of the form $\langle \text{tr} U^{n_1} \text{tr} U^{n_2} \dots \text{tr} U^{-k_1} \text{tr} U^{-k_2} \dots \rangle$, we sum over all ways to contract between copies of $\text{tr} U^{n_j}$ and $\text{tr} U^{k_m}$. This contraction is done using the connected version of equation (2.8), which equals the CUE

result,

$$\langle \text{tr}U^n \text{tr}U^{-k} \rangle_c = n\delta_{n,k} . \quad (2.13)$$

We first consider how Wick's theorem arises from the properties of Young diagrams for some relatively simple cases. For example, we have

$$\langle (\text{tr}U^2)^2 \text{tr}U^{-1} \rangle_c = 2 \langle \text{tr}U \text{tr}U^{-2} \rangle_c \langle \text{tr}U^{-2} \rangle_c = 0 , \quad (2.14)$$

where the factor two in the second expression arises from the fact that there are two ways to contract between $(\text{tr}U^2)^2$ and $\text{tr}U^{-1}$, which both contribute a term proportional to $\langle \text{tr}U \text{tr}U^{-2} \rangle_c = 0$. We will now express the same equation using Young diagrams. Using (1.21), the diagrams corresponding to $\text{tr}U^2$ are as follows:

$$\begin{array}{|c|c|} \hline \square & \square \\ \hline \end{array} - \begin{array}{|c|} \hline \square \\ \hline \square \\ \hline \end{array} \quad (2.15)$$

We take the square of the above expression and apply equation (1.42) (or, in this case, the Pieri formulas (1.33) and (1.34)) to find the diagrams contributing to $(\text{tr}U^2)^2$. These are as follows:

$$\begin{array}{|c|c|c|c|} \hline \square & \square & \square & \square \\ \hline \end{array} - \begin{array}{|c|c|c|} \hline \square & \square & \square \\ \hline \square & & \\ \hline \end{array} + 2 \begin{array}{|c|c|} \hline \square & \square \\ \hline \square & \square \\ \hline \end{array} - \begin{array}{|c|c|} \hline \square & \square \\ \hline \square & \\ \hline \square & \\ \hline \end{array} + \begin{array}{|c|} \hline \square \\ \hline \square \\ \hline \square \\ \hline \square \\ \hline \end{array} \quad (2.16)$$

We will denote the above sum over diagrams as $\sum_{\lambda} b_{\lambda} s_{\lambda}$, i.e. $b_{(4)} = 1$, $b_{(3,1)} = -1$, $b_{(2,2)} = 2$, $b_{(2,1,1)} = -1$, $b_{(1^4)} = 1$. Applying (1.84), we have

$$\langle (\text{tr}U^2)^2 \text{tr}U^{-1} \rangle_c = \sum_{\lambda} b_{\lambda} s_{\lambda/\square} \quad (2.17)$$

That is, we take $\sum_{\lambda} b_{\lambda} s_{\lambda}$ and find the skew diagrams λ/\square , found by removing a single cell from λ which has no cells to its right or below it. From these constraints, it follows that the resulting object after removing an cell is still a valid, non-skew diagram. This gives the following sum over diagrams, which evidently mutually cancel.

$$\begin{aligned}
 & \square\square\square\square_{\blacksquare} - \begin{array}{|c|c|c|} \hline \square & \square & \square \\ \hline \blacksquare & & \\ \hline \end{array} - \begin{array}{|c|c|c|} \hline \square & \square & \blacksquare \\ \hline \square & & \\ \hline \end{array} + 2 \begin{array}{|c|c|} \hline \square & \square \\ \hline \square & \blacksquare \\ \hline \end{array} + \\
 & - \begin{array}{|c|c|} \hline \square & \square \\ \hline \square & \blacksquare \\ \hline \end{array} - \begin{array}{|c|c|} \hline \square & \blacksquare \\ \hline \square & \\ \hline \square & \\ \hline \end{array} + \begin{array}{|c|} \hline \square \\ \hline \square \\ \hline \square \\ \hline \blacksquare \\ \hline \end{array} = 0
 \end{aligned} \tag{2.18}$$

We thus explicitly confirm that Wick’s theorem is satisfied for the case of equation (2.14). Consider now $\langle (\text{tr}U^2)^2 \text{tr}U^{-2} \rangle_c$. Using (2.8), this should give

$$\langle (\text{tr}U^2)^2 \text{tr}U^{-2} \rangle_c = 2 \langle \text{tr}U^2 \text{tr}U^{-2} \rangle_c \langle \text{tr}U^2 \rangle = 4 \langle \text{tr}U^2 \rangle \tag{2.19}$$

We will check this explicitly as well. Applying (2.11) to $\sum_{\lambda} b_{\lambda} s_{\lambda}$ gives

$$\langle (\text{tr}U^2)^2 \text{tr}U^{-2} \rangle_c = \sum_{\lambda} b_{\lambda} [s_{\lambda/(2)} - s_{\lambda/(1^2)}] = \sum_{\lambda} b_{\lambda} \sum_{\nu} (-1)^{\text{ht}(\lambda/\nu)} s_{\nu}, \tag{2.20}$$

where the sum is over all ν such that λ/ν is a border strip of size 2, i.e. $\lambda/\nu = \square\square$ or $\lambda/\nu = \begin{array}{|c|} \hline \square \\ \hline \square \\ \hline \end{array}$. In terms of diagrams, this is given below. The first three diagrams corresponds to $\lambda/\nu = \square\square$ whereas the latter three correspond to $\lambda/\nu = \begin{array}{|c|} \hline \square \\ \hline \square \\ \hline \end{array}$, which

appear with a minus sign due to the factor $(-1)^{\text{ht}(\lambda/\nu)}$.

$$\begin{aligned}
 & \begin{array}{|c|c|c|} \hline \square & \square & \blacksquare \\ \hline \end{array} - \begin{array}{|c|c|} \hline \square & \blacksquare \\ \hline \square & \\ \hline \end{array} + 2 \begin{array}{|c|c|} \hline \square & \square \\ \hline \blacksquare & \blacksquare \\ \hline \end{array} - 2 \begin{array}{|c|c|} \hline \square & \blacksquare \\ \hline \square & \\ \hline \end{array} + \begin{array}{|c|c|} \hline \square & \square \\ \hline \blacksquare & \\ \hline \end{array} - \begin{array}{|c|} \hline \square \\ \hline \square \\ \hline \blacksquare \\ \hline \end{array} \\
 & = 4 \begin{array}{|c|c|} \hline \square & \square \\ \hline \end{array} - 4 \begin{array}{|c|} \hline \square \\ \hline \square \\ \hline \end{array} \quad (2.21)
 \end{aligned}$$

We see that $\langle (\text{tr}U^2)^2 \text{tr}U^{-2} \rangle_c = 2 \langle \text{tr}U^2 \text{tr}U^{-2} \rangle_c \langle \text{tr}U^2 \rangle = 4 \begin{array}{|c|c|} \hline \square & \square \\ \hline \end{array} - 4 \begin{array}{|c|} \hline \square \\ \hline \square \\ \hline \end{array} = 4 \langle \text{tr}U^2 \rangle$, thus confirming (2.19). Lastly, we will briefly check

$$\langle (\text{tr}U^2)^2 (\text{tr}U^{-1})^2 \rangle_c = 0. \quad (2.22)$$

We have

$$\begin{array}{|c|} \hline \square \\ \hline \end{array} \times \begin{array}{|c|} \hline \square \\ \hline \end{array} = \begin{array}{|c|c|} \hline \square & \square \\ \hline \end{array} + \begin{array}{|c|} \hline \square \\ \hline \square \\ \hline \end{array} \quad (2.23)$$

Note that $\begin{array}{|c|} \hline \square \\ \hline \end{array}$ appears with a positive sign, instead of with a minus sign as it does for $\text{tr}U^2$. Then,

$$\langle (\text{tr}U^2)^2 (\text{tr}U^{-1})^2 \rangle_c = s_{\square} \sum_{\lambda} b_{\lambda} s_{\lambda/\square} \overset{0}{\cancel{\lambda}} + \sum_{\lambda} b_{\lambda} [s_{\lambda/(2)} + s_{\lambda/(1^2)}], \quad (2.24)$$

where we applied the fact that $\sum_{\lambda} b_{\lambda} s_{\lambda/\square} = 0$, see the diagrams in equation (2.18). Note that (2.24) gives an equation very similar to (2.20), but now $s_{\lambda/(1^2)}$ carries a positive sign. This gives the same six diagrams as in the top line of equation (2.21), except that the last three diagrams are multiplied by -1 . The result can be seen below.

$$\begin{array}{c}
 \square \square \blacksquare - \begin{array}{|c|c|} \hline \square & \blacksquare \\ \hline \square & \square \\ \hline \end{array} + 2 \begin{array}{|c|c|} \hline \square & \square \\ \hline \blacksquare & \blacksquare \\ \hline \end{array} + 2 \begin{array}{|c|c|} \hline \square & \blacksquare \\ \hline \square & \blacksquare \\ \hline \end{array} - \begin{array}{|c|c|} \hline \square & \square \\ \hline \blacksquare & \square \\ \hline \end{array} + \begin{array}{|c|} \hline \square \\ \hline \blacksquare \\ \hline \end{array} \quad (2.25)
 \end{array}$$

It is easy to see that all diagrams cancel out and the result is zero, which confirms equation (2.22). From these relatively simple examples, one can explicitly see how Wick's theorem arises from equation (1.84) and the multiplication rules for Young diagrams given in section 1.1. We proceed to apply Wick's theorem to the computation of more general objects in the remainder of this section.

2.2 Integrating over generalized power sums

We use Wick's theorem and equation (2.8) to generalize an identity due to Diaconis and Shahshahani [27], see also [28]. Writing $p_\rho = p_{\rho_1} p_{\rho_2} \dots p_{\rho_{\ell(\rho)}}$ and $m_j(\rho) = \text{Card}\{k : \rho_k = j\}$, as in equations (1.9) and (1.10), respectively, we wish to calculate $\langle p_\rho(U) p_\mu(U^{-1}) \rangle$. This is written out as follows,

$$\langle (\text{tr} U^{j_1})^{m_{j_1}(\rho)} (\text{tr} U^{j_2})^{m_{j_2}(\rho)} \dots (\text{tr} U^{-k_1})^{m_{k_1}(\mu)} (\text{tr} U^{-k_2})^{m_{k_2}(\mu)} \dots \rangle . \quad (2.26)$$

We start with a simpler object that we can more easily apply Wick's theorem to. We see that performing n contractions on $\langle (\text{tr} U^j)^a (\text{tr} U^{-j})^b \rangle$ leads to the following expression

$$C_{n,j} := \frac{a! b! j^n}{(a-n)! (b-n)! n!} p_j(x)^{b-n} p_j(y)^{a-n} , \quad n \leq \text{Min}(a, b) . \quad (2.27)$$

Further, we have $C_{n,j} = 0$ for $n \geq \text{Min}(a, b) + 1$. Equation (2.27) arises as follows. There are $\frac{a!b!}{(a-n)!(b-n)!n!}$ ways to perform n contractions between $(\text{tr}U^j)^a$ and $(\text{tr}U^{-j})^b$, and the contracted terms contribute $(\langle \text{tr}U^j \text{tr}U^{-j} \rangle_c)^n = j^n$. The $a + b - 2n$ uncontracted traces contribute $\langle \text{tr}U^j \rangle^{a-n} \langle \text{tr}U^{-j} \rangle^{b-n} = p_j(x)^{b-n} p_j(y)^{a-n}$. We now consider all possible ways to perform n contractions between $p_\rho(U)$ and $p_\mu(U^{-1})$. This leads to a sum over $\alpha = (\alpha_1, \alpha_2, \dots)$ which are partitions of n , which specify the contractions that are performed. In particular, $m_j(\alpha)$ gives the number of $\text{tr}U^j$ and $\text{tr}U^{-j}$ which are contracted. The contribution coming from n contractions in $\langle p_\rho(U) p_\mu(U^{-1}) \rangle$ can then be written as

$$C_n = \sum_{\alpha} \prod_j C_{m_j(\alpha), j} , \quad (2.28)$$

where the sum is over α that are partitions of n . We denote by \tilde{n} is the maximal number of contractions one can perform, which is given by

$$\tilde{n} = \text{Max}(n) = \sum_{j \geq 1} \text{Min}(m_j(\rho), m_j(\mu)) . \quad (2.29)$$

Summing over all possible contractions and applying (2.27) and (2.28), we arrive at our result

$$\langle p_\rho(U) p_\mu(U^{-1}) \rangle = \sum_{n=0}^{\tilde{n}} C_n . \quad (2.30)$$

As mentioned before, this is a generalization of a result in [27], which considered the CUE, where $f = 1$ so that $p_j(x) = 0$ for all $j \neq 0$. Therefore, in the CUE case, one only gets a non-zero result when $\rho = \mu$. In our notation, their result reads

$$\langle p_\rho(U) p_\mu(U^{-1}) \rangle_{\text{CUE}} = z_\rho \delta_{\rho, \mu} , \quad (2.31)$$

where $\delta_{\rho,\mu} = 1$ for $\rho = \mu$ and zero otherwise. Note that (2.31) is only the last term in the full expansion in (2.30), corresponding to $n = \tilde{n} = \sum_j m_j(\rho)$, so that all power sums in $p_\rho(U)$ and $p_\mu(U^{-1})$ are contracted.

2.3 Schur polynomials and border strips

We will derive two expressions for general $\langle s_\lambda(U)s_\nu(U^{-1}) \rangle$ which rely on removing border strips from λ and ν . The first of these, equation (2.46), relates $\langle s_\lambda(U)s_\nu(U^{-1}) \rangle$ to sums over $\langle s_\mu(U) \rangle \langle s_\rho(U^{-1}) \rangle$, where μ and ρ are related to λ and ν by the removal of border strips, respectively. The second expression, in equation (2.62), provides an expansion of $\langle s_\lambda(U)s_\nu(U^{-1}) \rangle$ in terms of the power sums $p_k(x)$ and $p_k(y)$. The latter expression appears to be particularly useful, as power sums are simpler objects than general Schur polynomials. In the context of LRRW models, $p_k(x)$ and $p_k(y)$ are given by $\pm \tau k a_{\pm k}$, where $a_{\pm k}$ are the hopping parameters in (1.104). Equation (2.62) therefore provides an expansion in τ , where the expansion coefficients depend on a_k which can be read off from the hamiltonian. We will treat the application of these formulas to LRRW models in sections 3.7 and 3.8.

2.3.1 Expansion in Schur polynomials

From (1.44), (1.48), and (2.11), we have

$$\langle s_\lambda p_n \rangle_c = \sum_{\eta} (-1)^{\text{ht}(\eta)} \langle s_{\lambda \setminus \eta} \rangle = \sum_{\mu} \frac{\chi_{\mu}^{\lambda}}{z_{\mu}} \langle p_{\mu - (n)} \rangle n m_n(\mu), \quad (2.32)$$

where the sum is over all μ containing a row of size n and $\mu - (n)$ is the remainder of μ after removing a row of size n . We remind the reader that $\lambda \setminus \eta$ is the diagram that results from λ after removing border strip η with (in this case) $|\eta| = n$. We can also use the recursive definition of χ_{μ}^{λ} in equation (1.55) to see that the second

equality in (2.32) should hold. From (1.10), it is clear that

$$z_\mu = z_{\mu-(n)} n m_n(\mu) . \quad (2.33)$$

Plugging this into the rightmost expression in (2.32) and applying (1.55) leads to

$$\langle s_\lambda p_n \rangle_c = \sum_{\mu} \sum_{\eta} (-1)^{\text{ht}(\eta)} \frac{\chi^{\lambda \setminus \eta}_{\mu-(n)}}{z_{\mu-(n)}} \langle p_{\mu-(n)} \rangle . \quad (2.34)$$

We can then apply equation (1.48), which leads to the second equality in (2.32). If we insert two identical power sums, we find the following

$$\begin{aligned} \langle s_\lambda p_n^2 \rangle_c &= \sum_{\eta, \zeta} (-1)^{\text{ht}(\eta) + \text{ht}(\zeta)} \langle s_{(\lambda \setminus \eta) \setminus \zeta} \rangle + 2 \langle p_n \rangle \langle s_\lambda p_n \rangle_c \\ &= \sum_{\mu} \frac{\chi^\mu}{z_\mu} \langle p_{\mu-(n^2)} \rangle 2n^2 m_n(\mu) (m_n(\mu) - 1) + 2 \langle p_n \rangle \langle s_\lambda p_n \rangle_c , \end{aligned} \quad (2.35)$$

where we consecutively remove border strips η and ζ satisfying $|\eta| = n = |\zeta|$, resulting in the partition $(\lambda \setminus \eta) \setminus \zeta$. The sum on the right hand side runs over all μ containing (at least) two rows of length n , and $\mu - (n^2)$ is the remainder of μ after removing two such rows. The term $2 \langle p_n \rangle \langle s_\lambda p_n \rangle_c$ arises from a single contraction between p_n and s_λ . We can again apply equation (1.55) to demonstrate the second equality in (2.35), where we focus on the term arising from two contractions. Plugging

$$z_\mu = z_{\mu-(n^2)} n^2 m_n(\mu) (m_n(\mu) - 1) . \quad (2.36)$$

into the first term on the right of (2.35) leads to

$$\sum_{\mu} \sum_{\zeta, \eta} (-1)^{\text{ht}(\zeta) + \text{ht}(\eta)} \frac{\chi_{\mu - (n^2)}^{(\lambda \setminus \eta) \setminus \zeta}}{z_{\mu - (n^2)}} \langle p_{\mu - (n^2)} \rangle, \quad (2.37)$$

which, by (1.48), recovers the top line of (2.35).

We then take $\langle s_{\lambda}(p_n)^k \rangle$ and perform all k contractions. This gives an object we denote by $C(n, k; \lambda)$, which equals

$$\begin{aligned} C(n, k; \lambda) &= \sum_{\mu} \frac{\chi_{\mu}^{\lambda}}{z_{\mu}} \langle p_{\mu - (n^k)} \rangle k! n^k \frac{m_n(\mu)!}{(m_n(\mu) - k)!} \\ &= \sum_{\eta_1, \dots, \eta_k} (-1)^{\text{ht}(T_{\eta})} \langle s_{\lambda \setminus \{\eta\}} \rangle. \end{aligned} \quad (2.38)$$

The sum on the left is over all μ containing at least k rows of length n . The sum on the right is over k border strips satisfying $|\eta_j| = n$, where $\lambda \setminus \{\eta\}$ is the diagram obtained after removing all η_j from λ , and T_{η} is the BST consisting of the union of η_1, \dots, η_k . It follows that the term in (2.38) gives zero if it is not possible to construct a subdiagram of λ with k border strips of size n , e.g. simply if $|\lambda| < nk$. Note that $C(n, 1; \lambda) = \langle s_{\lambda} p_n \rangle_c$ and $C(n, 2; \lambda) = \langle s_{\lambda} p_n^2 \rangle_c - 2 \langle p_n \rangle \langle s_{\lambda} p_n \rangle_c$.

We now consider

$$\langle s_{\lambda}(U) s_{\nu}(U^{-1}) \rangle_c = \sum_{\mu, \rho} \frac{\chi_{\mu}^{\lambda}}{z_{\mu}} \frac{\chi_{\rho}^{\nu}}{z_{\rho}} \langle p_{\mu}(U) p_{\rho}(U^{-1}) \rangle. \quad (2.39)$$

When we consider those μ and ρ that contain a row of size n and we contract a single copy of p_n between $p_{\mu}(U)$ and $p_{\rho}(U^{-1})$, we get an object we denote by $A(n, 1; \lambda, \nu)$,

which is given by

$$\begin{aligned} A(n, 1; \lambda, \nu) &:= \sum_{\mu, \rho} \frac{\chi_\mu^\lambda}{z_\mu} \frac{\chi_\rho^\nu}{z_\rho} n m_n(\mu) m_n(\rho) \langle p_{\mu-(n)}(U) \rangle \langle p_{\rho-(n)}(U^{-1}) \rangle \\ &= \frac{1}{n} \langle s_\lambda p_n \rangle_c \langle s_\nu p_n \rangle_c . \end{aligned} \quad (2.40)$$

Using (2.32) gives the following for $A(n, 1; \lambda, \nu)$,

$$\frac{1}{n} C(n, 1; \lambda) C(n, 1; \nu) = \frac{1}{n} \left(\sum_{\eta} (-1)^{\text{ht}(\eta)} \langle s_\lambda \eta \rangle \right) \left(\sum_{\zeta} (-1)^{\text{ht}(\zeta)} \langle s_\nu \zeta \rangle \right) , \quad (2.41)$$

where the sums are again over border strips satisfying $|\eta| = n = |\zeta|$. Consider now μ and ρ that contain at least two rows of length n and contract two copies of p_n between $p_\mu(U)$ and $p_\rho(U^{-1})$,

$$\begin{aligned} A(n, 2; \lambda, \nu) &= \frac{1}{2} \left(\sum_{\mu, \rho} \frac{\chi_\mu^\lambda}{z_\mu} n m_n(\mu) (m_n(\mu) - 1) \langle p_{\mu-(n)}(U) \rangle \right) \times \binom{\mu \rightarrow \rho}{\lambda \rightarrow \nu} \\ &= \frac{1}{2n^2} C(n, 2; \lambda) C(n, 2; \nu) . \end{aligned} \quad (2.42)$$

More generally, performing k contractions between $(\text{tr} U^n)^k$ and $(\text{tr} U^{-n})^k$ results in

$$A(n, k; \lambda, \nu) = \frac{1}{k! n^k} C(n, k; \lambda) C(n, k; \nu) . \quad (2.43)$$

Consider a partition α and, as above, contract over α_1 copies of $p_1(U)$ and $p_1(U^{-1})$, α_2 copies of $p_2(U)$ and $p_2(U^{-1})$, etc. This gives the following,

$$A(n, \alpha; \lambda, \nu) = \frac{1}{z_\alpha} \prod_{j \geq 1} C(n, \alpha_j; \lambda) C(n, \alpha_j; \nu) . \quad (2.44)$$

We can apply the above expression and (2.38), leading to

$$\langle s_\lambda s_\nu \rangle_c = \sum_\alpha \frac{1}{z_\alpha} \prod_{j \geq 1} C(n, \alpha_j; \lambda) C(n, \alpha_j; \nu) , \quad (2.45)$$

which can be written out as

$$\langle s_\lambda(U) s_\nu(U^{-1}) \rangle_c = \sum_\alpha \frac{1}{z_\alpha} \left(\sum_{\{\eta\}} (-1)^{\text{ht}(T_\eta)} s_{\lambda \setminus \{\eta\}}(y) \right) \times \begin{pmatrix} y \rightarrow x \\ \lambda \rightarrow \nu \end{pmatrix} . \quad (2.46)$$

The second sum above is over all border strips η_j satisfying $|\eta_j| = \alpha_j$. The above equation can be interpreted as follows. For any α , consider all ways to remove α_1 border strips of unit size (single cells) from λ and ν , α_2 border strips of size 2, α_3 of size 3, and so on. The resulting diagrams are written as $\lambda \setminus \{\eta\}$ and idem for $\lambda \rightarrow \nu$. Remember from equation (1.55) and the comments below that $\lambda \setminus \{\alpha\}$ does not depend on the order of the entries of α , that is, on the order in which we remove border strips of various sizes. Indeed, $\lambda \setminus \{\alpha\}$ only depends on λ and the set of cardinalities $m_j(\alpha)$.

Equation (2.46) expresses general expectation values $\langle s_\lambda s_\nu \rangle_c$ in terms of the non-skew Schur polynomials corresponding to $\lambda \setminus \{\eta\}$ and $\nu \setminus \{\eta\}$. On the other hand, equation (1.84), which we started with, gives an expansion in terms of skew Schur polynomials. There are various applications where an expression in terms of non-skew Schur polynomials is desirable. In general, this may be due to the fact that there are many more skew diagrams than non-skew ones, so that an expansion in non-skew diagrams may reveal underlying structures that are otherwise difficult to discern. This is also the case for the LRRW correlation functions we will be considering in the next section, where equation (2.46) will reveal relations between various correlation functions.

We consider now the special case where one can form BST's of shapes λ and ν from α_j border strips of size j , summed over j , such that we can fully contract between $p_\mu(U)$ and $p_\rho(U^{-1})$. That is, we consider the case where we can completely tile both λ and ν with α_1 single cells, α_2 border strips of size 2 (dominoes), and so on, for the same α . This clearly requires $|\lambda| = |\nu| = \sum_{j \geq 1} j\alpha_j$, which is a necessary (but not sufficient) condition for $\chi_\alpha^\lambda, \chi_\alpha^\nu \neq 0$. Consider the CUE, where $s_{\lambda/\mu} = 0$ for any $\lambda/\mu \neq \emptyset$. Applying the Murnaghan-Nakayama formula,

$$\sum_{\alpha_1, \dots, \alpha_k} (-1)^{\text{ht}(T_\alpha)} = \chi_\alpha^\lambda, \tag{2.47}$$

we then find that

$$\langle s_\lambda s_\nu \rangle_{\text{CUE}} = \sum_\alpha z_\alpha^{-1} \chi_\alpha^\lambda \chi_\alpha^\nu = \delta_{\lambda, \nu}. \tag{2.48}$$

This is just the orthonormality property for symmetric group characters, e.g. [Proposition 7.17.6b, [31]]. Another way to arrive at the same expression is to directly plug equation (2.31),

$$\langle p_\mu p_\rho \rangle_{\text{CUE}} = z_\mu \delta_{\mu, \rho}, \tag{2.49}$$

into equation (2.39) to find the orthonormality relation in (2.48).

We work out the explicit example for $\lambda = (3, 2)$, which is a sufficiently small partition that we can still apply (1.84) for comparison. Indeed, applying (1.84) to $\langle s_{(3,2)} s_{(3,2)} \rangle_c = \sum_\nu s_{(3,2)/\nu} s_{(3,2)/\nu}$ gives the following diagrams $(3, 2)/\nu$:

$$\begin{array}{c} \square & \square & \square \\ \square & \square & \square \end{array}, \quad \begin{array}{c} \square & \square \\ \square & \square \end{array}, \quad \square \square \square, \quad \square \square, \quad \square \square, \quad 2 \square \tag{2.50}$$

One also gets the empty diagram for $\nu = (3, 2) = \lambda$, which we did not indicate above. Note that \square appears with multiplicity 2 as it arises from $\nu = (3, 1)$ and $\nu = (2^2)$. By applying (1.44) for $n = 1$ (or, equivalently, (1.35) or (1.36)) to the leftmost diagram, we find the following:

$$\begin{array}{|c|c|c|} \hline & \square & \square \\ \hline \square & \square & \\ \hline \end{array} = \begin{array}{|c|c|} \hline \square & \square \\ \hline \square & \square \\ \hline \end{array} + \begin{array}{|c|c|c|} \hline \square & \square & \square \\ \hline \square & & \\ \hline \end{array} \tag{2.51}$$

This leads to

$$\begin{aligned}
 \langle s_{(3,2)} s_{(3,2)} \rangle_c &= (s_{(2,2)} + s_{(3,1)})^2 + (s_{(3)} + s_{(2,1)})^2 + s_{(2,1)}^2 + \\
 &+ (s_{(2)} + s_{(1^2)})^2 + s_{(2)}^2 + 2s_{(1)}^2 + 1 . \tag{2.52}
 \end{aligned}$$

Note that the above equation is strictly speaking only correct when $x = y$. For $x \neq y$, we have e.g. $(s_{(2,2)}(x) + s_{(3,1)}(x))(s_{(2,2)}(y) + s_{(3,1)}(y))$ instead of $(s_{(2,2)} + s_{(3,1)})^2$, but we write it in this way to avoid clutter.

We now apply (2.46) to compute $\langle s_{(3,2)} s_{(3,2)} \rangle_c$. To do so, we successively remove border strips from $(3, 2)$ to find the various partitions $(3, 2) \setminus \{\alpha\}$ in (2.46). This is illustrated below, where two diagrams connected by an arrow as $\xrightarrow{p_j}$ again indicates that partitions λ and μ are related by the removal of a border strip of size j . The graph below contains all information about the removal of border strips from $(3, 2)$, except for those cases where the removal of a border strip leads to the empty diagram. All diagrams in figure 2.1 except for $(3, 2)$ and $(2, 2)$ are hook shapes and therefore border strips, so that they are related to \emptyset by the removal of a single border strip. The number of ways to arrive at a diagram by following the arrows in figure gives the multiplicity of that diagram in (2.46). For example, for $\begin{array}{|c|c|c|} \hline \square & \square & \square \\ \hline \square & & \\ \hline \end{array}$, the diagram \square has multiplicity 5 for $\alpha = (1^5)$, as there are 5 distinct ways to arrive at \square following arrows indicated by p_1 in figure 2.1. For α containing elements of different sizes, a

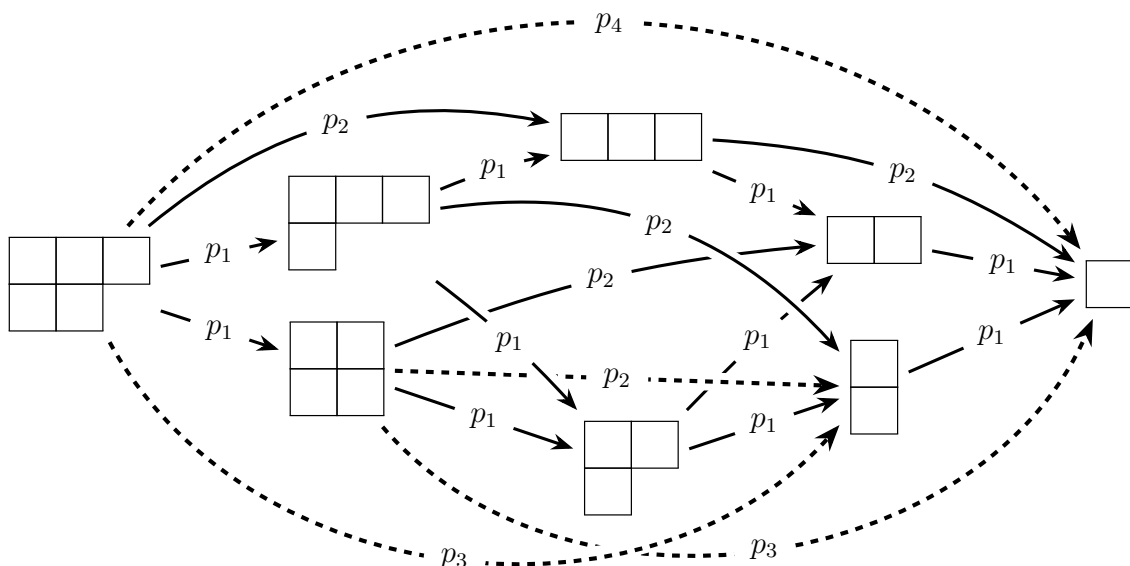
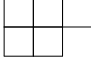





Figure 2.1: The diagrams for $\lambda = (3, 2)$ and those obtained by removal of border strips of size j , which is indicated by p_j . The solid and dashed lines again indicate the removal of border strips of even and odd heights, respectively. This graph indicates all ways to remove border strips from $(3, 2)$ and the resulting diagrams, except for those cases where the removal of a border strip leads to the empty diagram.

single ordering should be fixed to find the correct multiplicity i.e. we do not sum over different compositions of the same cycle type. Applying equation (2.46) then leads to (2.53), where we indicate the compositions α of the power sums p_α over which we contract. That is, to arrive at a term indicated by some α , one should start from $\begin{array}{|c|c|c|} \hline \square & \square & \square \\ \hline \square & \square & \square \\ \hline \end{array}$ and follow arrows indicated by the α_j in any order, keeping in

mind the sign given by $(-1)^{\text{ht}(\eta_j)}$ with $|\eta_j| = \alpha_j$.

$$\begin{aligned} \langle s_{(3,2)} s_{(3,2)} \rangle_c &= \overset{(1)}{(s_{(2,2)} + s_{(3,1)})^2} + \overset{(2)}{\frac{1}{2} s_{(3)}^2} + \overset{(1^2)}{\frac{1}{2} (2s_{(2,1)} + s_{(3)})^2} + \overset{(3)}{\frac{1}{3} s_{(1^2)}^2} + \overset{(2,1)}{\frac{1}{2} s_{(2)}^2} + \\ &+ \overset{(1^3)}{\frac{1}{3!} (3s_{(2)} + 2s_{(1^2)})^2} + \left(\frac{1}{3} + \frac{1}{8} + \frac{1}{4} + \frac{1}{4} + \frac{5^2}{4!} \right) s_{(1)} + 1. \end{aligned} \quad (2.53)$$

The last two terms on the bottom line of the expression above arise from $|\alpha| = 4, 5$. In the latter case, following arrows indicated by p_{α_j} leads to \emptyset . One can see that there is only a single way to start at  and arrive at \emptyset for $\alpha = (4, 1), (3, 2), (3, 1^2), (2^2, 1), (2, 1^3)$ by following the corresponding arrows in the graph above. However, we already noted that there are 5 distinct ways to start from  and arrive at  following arrows with p_1 . This implies there is an equal number of ways to arrive at \emptyset by removing single elements, simply by taking the additional step  $\xrightarrow{p_1} \emptyset$. We thus find $\frac{1}{z_{(4,1)}} + \frac{1}{z_{(3,2)}} + \frac{1}{z_{(3,1^2)}} + \frac{1}{z_{(2,1^3)}} + \frac{1}{z_{(2^2,1)}} + \frac{5^2}{z_{(1^5)}}$, which equals

$$\frac{1}{4} + \frac{1}{6} + \frac{1}{6} + \frac{1}{12} + \frac{1}{8} + \frac{5^2}{5!} = 1, \quad (2.54)$$

leading to the unit contribution in equation (2.53). Via this reasoning, one may check that expression (2.53) and (2.52) are identical. The above example may not appear to give a very convincing argument in favor of equation (2.46) over (1.84), as the application of (2.46) appears to be more complicated than (1.84) for the case of $\lambda = (3, 2)$. Indeed, for partitions containing few cells, such as $\lambda = (3, 2)$, it is convenient to use (1.84), as the skew partitions λ/ν can easily be related to non-skew partitions, as in (2.52). However, for larger partitions, this is no longer the case, as (1.35), (1.36), and (1.44) can no longer be applied. When considering larger partitions, then, equation (2.46) can still be used to express general objects $\langle s_\lambda s_\nu \rangle_c$ in terms of non-skew Schur polynomials. This will allow us to express complicated

correlation functions in terms of simpler ones in section 3.7, but can be used more generally in situations where an expression for $\langle s_\lambda s_\nu \rangle$ in terms of non-skew Schur polynomials is desirable.

2.3.2 Expansion in power sum polynomials

For certain applications, such as the LRRW models we will be considering in the next section, expanding $\langle s_\lambda(U) s_\nu(U^{-1}) \rangle$ in terms of power sums $p_k(x)$ and $p_k(y)$ may be particularly useful. One way to do so is to use the expansion in (1.48), calculate all $\chi_\alpha^\lambda, \chi_\alpha^\nu$, and contract power sums using (2.8). However, this is rather inconvenient as the computation of all the symmetric group characters is rapidly becomes more complicated for larger λ, ν . Instead, it would be more effective to once more use equation (1.55) to find a recursive expansion in terms of power sum polynomials. We will do so here, ultimately leading to equation (2.62). For comparison, we will also consider the more complicated method that involves the calculation of all $\chi_\alpha^\lambda, \chi_\alpha^\nu$ at the end of this section to demonstrate its inconvenience compared to equation (2.62).

The expression that we will be deriving provides an iterative method for expanding in $p_\gamma(x)$ and $p_\omega(y)$ that does not require us to find χ_α^λ and χ_α^ν for all α and then contract over all combinations of power sum polynomials. Essentially, we apply equations (2.30) and (1.48) to $\langle s_\lambda(U) s_\nu(U^{-1}) \rangle$ and make use of the orthogonality properties of the symmetric group characters. In particular, we will revert the order of expansion in section 2.3.1 and start from the term with all p_μ contracted, see equation (2.48), then consider the term where a single p_j is not contracted, then two uncontracted power sums, and so on. For simplicity, we start by considering

autocorrelation function up to the subleading term, which gives

$$\begin{aligned} \langle s_\lambda(U) s_\lambda(U^{-1}) \rangle &= \sum_{\mu, \rho} \frac{\chi_\mu^\lambda}{z_\mu} \frac{\chi_\rho^\lambda}{z_\rho} \langle p_\mu(U) p_\rho(U^{-1}) \rangle \\ &= 1 + \sum_{j \geq 1} \sum_{\mu} \frac{(\chi_\mu^\lambda)^2}{z_\mu} \frac{m_j(\mu)}{j} p_j(x) p_j(y) + \dots \end{aligned} \quad (2.55)$$

where sum is over all μ containing a row of size j . We have $\mu = \rho$ since this is the only way to contract all of p_μ with p_ρ except for two copies of p_j (one from p_μ and the other from p_ρ). Using the recursive formula for χ_μ^λ in (1.55) and the orthogonality of symmetric group characters in (2.48), we then find

$$\begin{aligned} \sum_{j \geq 1} \sum_{\mu} \frac{(\chi_\mu^\lambda)^2}{z_\mu} \frac{m_j(\mu)}{j} p_j(x) p_j(y) &= \sum_j \frac{1}{j^2} \sum_{\mu} \frac{\left(\sum_{\eta} (-1)^{\text{ht}(\eta)} \chi_{\mu-(j)}^{\lambda \setminus \eta} \right) \times (\eta \rightarrow \zeta)}{z_{\mu-(j)}} p_j(x) p_j(y) \\ &= \sum_{j \geq 1} \frac{p_j(x) p_j(y)}{j^2} \sum_{\eta} 1, \end{aligned} \quad (2.56)$$

where η and ζ are border strips of size j . Equation (2.56) then tells us that the coefficient $p_j(x) p_j(y)$ in the power sum expansion of $\langle s_\lambda(U) s_\lambda(U^{-1}) \rangle$ is given by $\frac{1}{j^2}$ times the number of ways to remove a border strip of size j from λ . Consider another term in this expansion, where $\mu = (j, \alpha)$, $\rho = (k^2, \alpha)$ with $j = 2k$, and contract over p_α leading to the term proportional to $p_j(x) p_k(y)^2$. Via the same reasoning as above, this is given by

$$\frac{p_j(x) p_k(y)^2}{2j k^2} \sum_{\eta, \zeta, \xi} (-1)^{\text{ht}(\eta) + \text{ht}(\zeta) + \text{ht}(\xi)} \delta_{\lambda \setminus \eta, (\lambda \setminus \zeta) \setminus \xi}, \quad (2.57)$$

where the sums are over all η , border strips of size j , and ζ and ξ , border strips of size k . We see that the terms appearing in the power sum expansion of $\langle s_\lambda(U) s_\lambda(U^{-1}) \rangle$ are found by removing border strips $\{\eta\}$ and $\{\zeta\}$ from λ such that $\lambda \setminus \{\eta\} = \lambda \setminus \{\zeta\}$.

Continuing this procedure gives the following. Consider not contracting $p_\omega(U)$ and $p_\gamma(U^{-1})$ for some ω and γ , leading to the term proportional to $p_\omega(y)p_\gamma(x)$. In general this leads to a sum over μ and ρ (in the middle expression in (2.56)) of the form

$$\mu = (\omega, \alpha) \quad , \quad \rho = (\gamma, \alpha) \quad , \quad (2.58)$$

so that $m_j(\mu) - m_j(\omega) = m_j(\alpha) = m_j(\rho) - m_j(\gamma)$ for all j , and $|\omega| = |\eta|$. Since we sum over μ and ρ for a fixed choice of ω and γ , this effectively leads to a sum over α . Since there are $\frac{1}{m_j(\alpha)!} \frac{m_j(\mu)! m_j(\rho)!}{m_j(\omega)! m_j(\gamma)!}$ ways to perform $m_j(\alpha)$ contractions of p_j appearing in p_μ and p_ρ , we have

$$\begin{aligned} \langle p_\mu p_\rho \rangle = & \cdots + p_\omega(y)p_\gamma(x) \prod_{j \geq 1} \frac{1}{m_j(\alpha)!} \frac{m_j(\mu)!}{(m_j(\mu) - m_j(\alpha))!} \frac{m_j(\rho)!}{(m_j(\rho) - m_j(\alpha))!} j^{m_j(\alpha)} + \\ & + \dots \end{aligned} \quad (2.59)$$

where we explicitly show only the term proportional to $p_\omega(y)p_\gamma(x)$. Using the fact that,

$$z_\mu = z_\alpha \prod_{j \geq 1} j^{m_j(\mu) - m_j(\alpha)} \frac{m_j(\mu)!}{m_j(\alpha)!} \quad , \quad (2.60)$$

and again applying the orthogonality of symmetric group characters, we find that the term proportional to $p_\omega(y)p_\gamma(x)$ in the expansion of $\langle s_\lambda(U)s_\lambda(U^{-1}) \rangle$ is given by

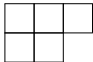
$$\frac{p_\omega(y)p_\gamma(x)}{z_\omega z_\gamma} \sum_{\{\eta\}, \{\xi\}} (-1)^{\text{ht}(T_\eta) + \text{ht}(T_\xi)} \delta_{\lambda \setminus \{\eta\}, \lambda \setminus \{\xi\}} \quad , \quad (2.61)$$


where the sum is over border strips η_1, η_2, \dots satisfying $|\eta_j| = \omega_j$, as well as border strips ξ_j satisfying $|\xi_j| = \gamma_j$. Further, T_η and T_ξ are the (generally disconnected) skew diagrams consisting of the unions of the border strips in η and ξ , respectively,

and $\text{ht}(T)$ is defined in (1.51). It is clear that the examples in (2.56) and (2.57) arise as special cases of (2.61). The autocorrelation function can then be expanded as a sum ω and γ , each contributing a term of the form appearing in (2.61). The same reasoning can evidently be applied to more general correlation functions, which are then given by

$$\langle s_\lambda(U) s_\nu(U^{-1}) \rangle = \sum_{\omega, \gamma} \frac{p_\omega(y) p_\gamma(x)}{z_\omega z_\gamma} \sum_{\{\eta\}, \{\xi\}} (-1)^{\text{ht}(T_\eta) + \text{ht}(T_\xi)} \delta_{\lambda \setminus \{\eta\}, \nu \setminus \{\xi\}}. \quad (2.62)$$

The above expression can be straightforwardly applied by considering the different ways to remove border strips from λ and ν such that the resulting diagrams are identical, as expressed by the presence of $\delta_{\lambda \setminus \{\eta\}, \nu \setminus \{\xi\}}$. This provides a recursive expression which significantly simplifies various computations, especially when λ, ν are large diagrams for which the computation of the symmetric group characters rapidly grows more difficult. Equation (2.62) is particularly useful for applications where one has access to $p_k(x)$ and $p_k(y)$. This includes LRRW models, where $p_k(x)$ and $p_k(y)$ are proportional to the time parameter and the hopping parameters, as we will see in the next chapter.

We now apply (2.62) to $\langle s_\lambda(U) s_\lambda(U^{-1}) \rangle$ for $\lambda = (3, 2)$. Consider all distinct ways to remove a single cell from . As can be seen in figure 2.1, this results in the following diagrams.


(2.63)

Removing a single cell twice results in the following diagrams.

$$\begin{array}{|c|c|c|} \hline \square & \square & \square \\ \hline \blacksquare & \blacksquare & \blacksquare \\ \hline \end{array} \quad 2 \quad \begin{array}{|c|c|c|} \hline \square & \square & \blacksquare \\ \hline \square & \blacksquare & \square \\ \hline \end{array} \tag{2.64}$$

We get multiplicity two for $\begin{array}{|c|c|} \hline \square & \square \\ \hline \square & \square \\ \hline \end{array}$ on the right as one can remove the single cells indicated in black in either order, as can be seen from the fact that there are two distinct ways to arrive at $\begin{array}{|c|c|} \hline \square & \square \\ \hline \square & \square \\ \hline \end{array}$ from $\begin{array}{|c|c|c|} \hline \square & \square & \square \\ \hline \square & \square & \square \\ \hline \end{array}$ by following p_1 in figure 2.1. Removing border strips of sizes 2, 3, 4 results in the diagrams below.

$$\begin{array}{|c|c|c|} \hline \square & \square & \square \\ \hline \blacksquare & \blacksquare & \blacksquare \\ \hline \end{array} \quad \begin{array}{|c|c|c|} \hline \square & \blacksquare & \blacksquare \\ \hline \square & \blacksquare & \blacksquare \\ \hline \end{array} \quad \begin{array}{|c|c|c|} \hline \square & \blacksquare & \blacksquare \\ \hline \blacksquare & \blacksquare & \blacksquare \\ \hline \end{array} \tag{2.65}$$

Note that the height ht of the border strips of sizes 3 and 4 is given by 1, so that $(-1)^{ht} = -1$. It is easy to see that no border strips of size ≥ 5 can be removed from $\begin{array}{|c|c|c|} \hline \square & \square & \square \\ \hline \square & \square & \square \\ \hline \end{array}$, since it is a partition of 5 that is not a border strip. From the fact that there are two distinct ways to remove a single cell from λ , and only a single way to remove border strips of sizes 2, 3, 4, we see that the the corresponding contributions are given by

$$2p_1(x)p_1(y) + \frac{p_2(x)p_2(y)}{4} + \frac{p_3(x)p_3(y)}{9} + \frac{p_4(x)p_4(y)}{16} . \tag{2.66}$$

Consider now the term proportional to $p_1(x)^2 p_1(y)^2$. The two diagrams which arise from consecutively removing two single cells are $\begin{array}{|c|c|} \hline \square & \square \\ \hline \square & \square \\ \hline \end{array}$ and $\begin{array}{|c|c|c|} \hline \square & \square & \square \\ \hline \square & \square & \square \\ \hline \end{array}$, where the former appears with multiplicity two, as demonstrated above. We thus see that there are four ways to take two copies of $\begin{array}{|c|c|c|} \hline \square & \square & \square \\ \hline \square & \square & \square \\ \hline \end{array}$, consecutively remove two single cells, and end up with $\begin{array}{|c|c|} \hline \square & \square \\ \hline \square & \square \\ \hline \end{array}$. Conversely, there is only a single way to end up with $\begin{array}{|c|c|c|} \hline \square & \square & \square \\ \hline \square & \square & \square \\ \hline \end{array}$.

via this procedure. Combined with $(z_{(1^2)})^2 = 4$, this demonstrates that we have

$$\frac{5p_1(x)^2 p_1(y)^2}{4} \tag{2.67}$$

appearing in the expansion of $\langle s_{(3,2)} s_{(3,2)} \rangle$. Lastly, we consider $p_2(x)p_1(y)^2 + p_1(x)^2 p_2(y)$. One may remove either a border strip of size two or two single cells and end up in $\square\square\square$, see the leftmost diagrams in (2.64) and (2.65). Combined with $z_{(1^2)} = 2 = z_{(2)}$, this results in

$$\frac{p_2(x)p_1(y)^2 + p_1(x)^2 p_2(y)}{4}. \tag{2.68}$$

Although the effectiveness of (2.62) is already clear for $\begin{array}{|c|c|c|} \hline \square & \square & \square \\ \hline \square & & \\ \hline \end{array}$, this is still a rather small partition. For larger λ , it becomes progressively harder to compute χ_α^λ , increasing the advantage of (2.62). We will work out more complicated examples in section 3.8, where we apply the above results to correlation functions of LRRW models.

We now proceed to compute $\langle s_{(3,2)}(U) s_{(3,2)}(U^{-1}) \rangle$ via the more laborious method briefly outlined at the start of this subsection, where we compute $\chi_\alpha^{(3,2)}$ for all α , apply (1.48), and perform all possible contractions between the power sum polynomials appearing in (1.48). This provides both an explicit check of equation (2.62) as well as a demonstration of its relative effectiveness for computing $\langle s_\lambda(U) s_\lambda(U^{-1}) \rangle$. We will see in the following section, below equation (3.52), that one may calculate χ_α^λ by using a relation with fermionic particles hopping on a one-dimensional lattice. One may then apply Wick's theorem to the resulting expression to find an expansion of LRRW correlation functions in terms of power sums. Although this may provide a convenient method for calculating χ_α^λ , we will see here that its application to the computation of $\langle s_\lambda(U) s_\nu(U^{-1}) \rangle$ is much less convenient than simply applying equation (2.62). Using (1.55) and looking at figure 2.1, we see that the non-zero

characters χ_α^λ are given by

$$\begin{aligned} \chi_{(1^5)}^{(3,2)} &= 5, & \chi_{(2,1^3)}^{(3,2)} &= 1, & \chi_{(2^2,1)}^{(3,2)} &= 1, \\ \chi_{(3,1^2)}^{(3,2)} &= 1, & \chi_{(3,2)}^{(3,2)} &= -1, & \chi_{(4,1)}^{(3,2)} &= 1. \end{aligned} \quad (2.69)$$

Applying (1.48) gives

$$\begin{aligned} s_{(3,2)} &= \frac{p_1^5}{24} + \frac{p_1^3 p_2}{12} + \frac{p_1^2 p_3}{6} + \frac{p_2^2 p_1}{8} - \frac{p_2 p_3}{6} + \frac{p_1 p_4}{4} \\ &= \frac{p_{(1^5)}}{24} + \frac{p_{(2,1^3)}}{12} + \frac{p_{(3,1^2)}}{6} + \frac{p_{(2^2,1)}}{8} - \frac{p_{(3,2)}}{6} + \frac{p_{(4,1)}}{4}. \end{aligned} \quad (2.70)$$

We then apply Wick's theorem to $\langle s_{(3,2)}(U) s_{(3,2)}(U^{-1}) \rangle_c$. We give three examples below, again indicating the compositions α corresponding to the p_α which are contracted.

$$\begin{aligned} \frac{1}{4} p_1^{(4)}(x) p_1^{(4)}(y) + \frac{1}{8^2} p_1^{(2^2)}(x) p_1^{(2^2)}(y) + \frac{3}{6^2} (p_2^{(3)}(x) p_2^{(3)}(y) - p_2^{(3)}(y) p_1^{(3)}(x)^2) + \\ + \frac{3}{6^2} (p_1^{(3)}(x)^2 p_1^{(3)}(y)^2 - p_2^{(3)}(x) p_1^{(3)}(y)^2) + \dots \end{aligned} \quad (2.71)$$

We will use the above method to find the prefactors of $p_\omega(y) p_\gamma(x)$ for some examples of ω, γ . Consider first $\gamma = \omega = (4)$, leading to a term proportional to $p_4(x) p_4(y)$. This term is rather simple to find as we only get a contribution from the rightmost term in (2.70). In particular, we have

$$\frac{1}{4^2} \langle p_{(4,1)}(U) p_{(4,1)}(U^{-1}) \rangle_c = \frac{p_4(x) p_4(y)}{4^2} + \frac{p_1(x) p_1(y)}{4} + \frac{1}{4}, \quad (2.72)$$

so that $p_4(x) p_4(y)$ appears with a prefactor $\frac{1}{4^2}$ in the expansion of $\langle s_{(3,2)}(U) s_{(3,2)}(U^{-1}) \rangle$. We consider now those terms proportional to $p_3(x) p_3(y)$ arising from (2.70), where the dots below refer to terms not proportional to $p_3(x) p_3(y)$ and where we omit

writing $(U^{\pm 1})$ explicitly henceforth.

$$\begin{aligned} \frac{1}{6^2} \langle p_{(3,1^2)} p_{(3,1^2)} \rangle + \frac{1}{6^2} \langle p_{(3,2)} p_{(3,2)} \rangle &= \frac{p_3(x)p_3(y)}{36} (2+2) + \dots \\ &= \frac{p_3(x)p_3(y)}{9} + \dots \end{aligned} \quad (2.73)$$

We find that the terms whose contribution is proportional to $p_2(x)p_2(y)$ are given by $\frac{\langle p_{(2,1^3)} p_{(2,1^3)} \rangle}{(12)^2} + \frac{\langle p_{(2^2,1)} p_{(2^2,1)} \rangle}{8^2} + \frac{\langle p_{(3,2)} p_{(3,2)} \rangle}{6^2}$, which equals

$$p_2(x)p_2(y) \left(\frac{3!}{12} + \frac{8}{8^2} + \frac{3}{6^2} \right) + \dots = \frac{1}{4} p_2(x)p_2(y) + \dots \quad (2.74)$$

Considering the term proportional to $p_1(x)p_1(y)$, we find the following expression

$$\frac{\langle p_{(1^5)} p_{(1^5)} \rangle}{(24)^2} + \frac{\langle p_{(2,1^3)} p_{(2,1^3)} \rangle}{(12)^2} + \frac{\langle p_{(3,1^2)} p_{(3,1^2)} \rangle}{6^2} + \frac{\langle p_{(2^2,1)} p_{(2^2,1)} \rangle}{8^2} + \frac{\langle p_{(4,1)} p_{(4,1)} \rangle}{4^2} \quad (2.75)$$

is given by

$$p_1(x)p_1(y) \left(\frac{(5!)^2}{(4!)^3} + \frac{6^2}{(12)^2} + \frac{12}{6^2} + \frac{8}{8^2} + \frac{4}{4^2} \right) + \dots = 2p_1(x)p_1(y) + \dots \quad (2.76)$$

Combining equations (2.72), (2.73), (2.74), and (2.76) then leads to equation (2.66), albeit via a much less convenient method.

Consider the term proportional to $p_1(x)^2 p_1(y)^2$, which receives contributions from

$$\frac{\langle p_{(1^5)} p_{(1^5)} \rangle}{(24)^2} + \frac{\langle p_{(2,1^3)} p_{(2,1^3)} \rangle}{(12)^2} + \frac{\langle p_{(3,1^2)} p_{(3,1^2)} \rangle}{6^2}. \quad (2.77)$$

In particular, this contributes

$$p_1(x)^2 p_1(y)^2 \left(\frac{(5!)^2}{(4!)^2 (2!)^2 3!} + \frac{(12)^2}{12} + \frac{3}{6^2} \right) = \frac{5p_1(x)^2 p_1(y)^2}{4}, \quad (2.78)$$

thus confirming equation (2.67). Lastly, we consider a mixed term, namely, the term proportional to $p_2(x)p_1(y)^2 + p_1(x)^2p_2(y)$. This is given by

$$\begin{aligned} \frac{\langle p_{(1^5)}p_{(2,1^3)} \rangle}{12 \cdot 24} - \frac{\langle p_{(3,1^2)}p_{(3,2)} \rangle}{6^2} + \frac{\langle p_{(2,1^3)}p_{(2^2,1)} \rangle}{12 \cdot 8} &= p_2(x)p_1(y)^2 \left(\frac{5}{24} - \frac{1}{12} + \frac{1}{8} \right) + \dots \\ &= \frac{p_2(x)p_1(y)^2}{4} + \dots \end{aligned} \quad (2.79)$$

Of course, inverting the order of $p_\mu(U)$ and $p_\rho(U^{-1})$ in $\langle p_\mu(U)p_\rho(U^{-1}) \rangle$ above gives the same contribution with $x \leftrightarrow y$. The end result is therefore $\frac{p_2(x)p_1(y)^2 + p_1(x)^2p_2(y)}{4}$, thereby confirming (2.68). It is clear from this simple example that the method applied here is much less powerful than the application of equation (2.62), and this becomes more acute when we consider larger partitions than $\lambda = (3, 2)$ as the χ^λ_α are then a lot harder to compute.

Chapter 3

Long-range random walks

We will now apply some of the results derived in the previous chapter, as well as standard identities from symmetric polynomial theory, to LRRW correlation functions. The relation between unitary matrix integral and LRRW models was reviewed in section 1.3, particularly equation (1.116). Here, we first consider identities relating to elementary and complete homogeneous symmetric polynomials, before moving on to power sum polynomials and border strips. We will generally take $N \rightarrow \infty$ here, although the presentation in sections 3.3, 3.5, and 3.6 is valid for finite N as well. This chapter is based on [1].

3.1 Correlation functions

In the relation between unitary matrix integral and LRRW models, the weight function is given by equation (1.107), which we repeat here

$$f(e^{i\theta}; \tau) = \exp \left(\tau \sum_{k \in \mathbb{Z}} a_k e^{i\theta} \right) . \quad (3.1)$$

where a_k are the hopping parameters of the hamiltonian in (1.104). As noted before, the hamiltonian is a Toeplitz matrix, and a_k is the number on its k^{th} diagonal. By comparing with (1.6), we see that we can write the weight function as

$$f(z) = H(x; z)H(y; z^{-1}) , \quad (3.2)$$

with the following identification, for $k \geq 1$,

$$\begin{aligned} \tau a_k &= \frac{p_k(x)}{k} , \\ \tau a_{-k} &= \frac{p_k(y)}{k} . \end{aligned} \quad (3.3)$$

Alternatively, we can write

$$f(z) = E(x; z)E(y; z^{-1}) , \quad (3.4)$$

by identifying, for $k \geq 1$,

$$\begin{aligned} \tau a_k &= \frac{(-1)^{k+1} p_k(x)}{k} , \\ \tau a_{-k} &= \frac{(-1)^{k+1} p_k(y)}{k} , \end{aligned} \quad (3.5)$$

and by transposing the diagrams as in (1.85). When $\tau \rightarrow 0$, i.e. the CUE limit, we have

$$F_{\lambda; \mu}(0) = \langle s_\lambda(U) s_\mu(U^{-1}) \rangle_{\text{CUE}} = \delta_{\lambda, \mu} , \quad (3.6)$$

which is again simply the orthonormality of Schur polynomials as the irreducible characters of $U(N)$. By using the strong Szegő limit theorem, we can compute

$F_{\emptyset;\emptyset}$. Assuming $a_0 = 0$, i.e. zero on-site energy, we have

$$F_{\emptyset;\emptyset}(\tau) = \exp\left(\tau^2 \sum_{k=1}^{\infty} k a_k^2\right) . \quad (3.7)$$

If we have $a_0 \neq 0$, we get an additional multiplicative term $e^{-N\tau a_0}$ on the right, where one should remember that we take $N \rightarrow \infty$. Considering $a_1 = -1 = a_{-1}$ and $a_k = 0$ otherwise, i.e. the XX0-model, and choosing $\tau = it$, we recover the result of [52] and [51], see also [53],

$$F_{\emptyset;\emptyset}(it) = e^{-t^2} . \quad (3.8)$$

Remember that equations (1.83) and (1.84) state that

$$F_{\lambda;\mu}(\tau) = F_{\emptyset;\emptyset}(\tau) \langle s_{\lambda}(U) s_{\mu}(U^{-1}) \rangle_{\tau} , \quad (3.9)$$

where $\langle \dots \rangle_{\tau}$ is given in equation (1.76) with weight function given by $f(z; \tau)$ in (1.107). We therefore define

$$G_{\lambda;\mu}(\tau) := \frac{F_{\lambda;\mu}(\tau)}{F_{\emptyset;\emptyset}(\tau)} = \langle s_{\lambda}(U) s_{\mu}(U^{-1}) \rangle_{\tau} , \quad (3.10)$$

i.e. we express correlations in terms of their proportionality to $F_{\emptyset;\emptyset}(\tau)$. We will also write this as

$$G_{\lambda;\mu}(\tau) =: \langle \lambda | \mu \rangle_{\tau} . \quad (3.11)$$

If $\mu = \emptyset$ (or $\lambda = \emptyset$), we will simply write

$$G_{\lambda;\emptyset}(\tau) = \langle \lambda | \emptyset \rangle_{\tau} =: \langle \lambda \rangle_{\tau} . \quad (3.12)$$

We also define the following - connected - correlation function,

$$G_{\lambda;\mu}^c(\tau) =: \langle \lambda | \mu \rangle_{\tau} - \langle \lambda \rangle_{\tau} \langle \mu \rangle_{\tau}^* . \quad (3.13)$$

3.2 Row and column diagrams

We consider now some explicit examples. Using (1.12), we can express

$$\langle e_n \rangle_{\tau} = e_n(y) = G_{(1^n); \emptyset} , \quad \langle h_n \rangle_{\tau} = h_n(y) = G_{(k); \emptyset} , \quad (3.14)$$

and their complex conjugates $G_{\emptyset;(1^n)}$ and $G_{\emptyset;(n)}$, in terms of $p_k(y)$ with $k \leq n$. For h_n and e_n with $n = 4$, the diagrams and corresponding configurations are given below on the left and right, respectively.

$$(3.15)$$

That is, h_n correspond to taking only the single rightmost particle and moving it n sites to the right, whereas e_n corresponds to taking the n rightmost particles and moving them all a single site to the right. We noted above that with $x = (x_1, \dots, x_K)$, we have $e_j(x) = 0$ for $j > K$ (and likewise for y). This means that, for any $n, m > K$,

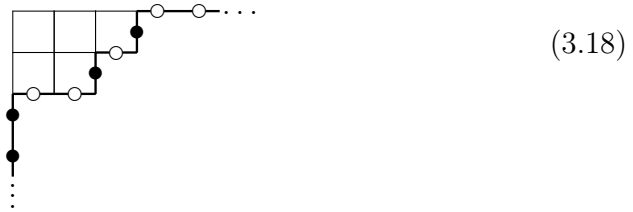
$$F_{(1^m);(1^n)} = \sum_{j=0}^K e_j e_j \quad (3.16)$$

That is, when we move $n > K$ adjacent particles by a single site, the effect is the same as to move K adjacent particles a single site.

Not only can we read off $G_{(n);\emptyset}$ and $G_{(1^n);\emptyset}$ (and their complex conjugates). From the corollary of the Pieri formula in (1.35), we have that, for any λ ,

$$G_{\lambda;(n)}^c = \langle s_\lambda(U)h_n(U^{-1}) \rangle_c = \sum_{j=1}^n h_{n-j} s_{\lambda/(j)} = \sum_{j=1}^n h_{n-j} \sum_{\nu^j} s_{\nu^j} , \quad (3.17)$$

where the rightmost sum is over all ν^j such that λ/ν^j is a horizontal strip of length j . Take, for example, $\lambda = (3, 2)$,



which corresponds to

$$|(3, 2)\rangle = \cdots \bullet \bullet \circ \circ \bullet \circ \bullet \circ \circ \cdots \quad (3.19)$$

We remind the reader that the dots on the left (right) refer to a string of particles (holes). We take $\lambda = (3, 2)$ and $n = 2$. For this choice of λ , the diagrams contributing to the sum over ν^1 and ν^2 in (3.17) are given by equation (2.63).

We assign particles and holes to these diagrams and remind ourselves that the fact that a diagram consisting of a single element corresponds to moving the rightmost particle a single site to the right, that is,

$$G_{(1);\emptyset}(\tau) = \langle \cdots \bullet \circ \bullet \circ \cdots \rangle_\tau . \quad (3.20)$$

We then see that equation (3.17) is given by the following expression. For each configuration, the dots on the left and right again indicate a sequence of particles and holes, typically infinitely long, of which we show only the left- and rightmost, respectively.

$$G_{(3,2);(2)}(\tau) = \langle \cdots \bullet \circ \circ \bullet \circ \bullet \circ \cdots \mid \cdots \bullet \circ \circ \bullet \circ \cdots \rangle_{\tau}, \quad (3.21)$$

which can be expanded as follows

$$\begin{aligned} & \left(\langle \cdots \bullet \circ \circ \bullet \bullet \circ \cdots \rangle_{\tau} + \langle \cdots \bullet \circ \bullet \circ \circ \bullet \circ \cdots \rangle_{\tau} \right) \times G_{(1);\emptyset}(\tau) + \\ & + \langle \cdots \bullet \circ \bullet \circ \bullet \circ \cdots \rangle_{\tau} + \langle \cdots \bullet \circ \circ \circ \bullet \circ \cdots \rangle_{\tau} \end{aligned} \quad (3.22)$$

The first line above corresponds to ν^1 in (3.17), whereas the second line corresponds to ν^2 . By comparing with equation (3.18), we see that the sum over ν^1 contains all diagrams related to $\begin{array}{|c|c|c|} \hline \square & \square & \square \\ \hline \square & & \square \\ \hline \end{array}$ by moving a single particle a single site to the left. The sum over ν^2 consists of all ways to move one or two particles by a total of two sites, with the restriction that we cannot move two adjacent particles. This is the interpretation of the corollary of the Pieri formula in (1.35), and it generalizes to h_n for any $n \in \mathbb{Z}^+$. In particular, we can assign a particle-hole interpretation as follows,

$$s_{\lambda/(n)} = \sum \left\{ \begin{array}{l} \text{Distinct ways to move } \leq n \text{ particles a total of } n \text{ sites} \\ \text{to the left without moving any two adjacent particles.} \end{array} \right\} \quad (3.23)$$

We can apply the same reasoning to $\langle s_{\lambda}(U)e_n(U^{-1}) \rangle$ by using (1.36). Similar to (3.17), we have

$$G_{\lambda;(1^n)} = \sum_{j=1}^n e_{n-j} s_{\lambda/(1^j)} = \sum_{j=1}^n e_{n-j} \sum_{\nu^j} s_{\nu}, \quad (3.24)$$

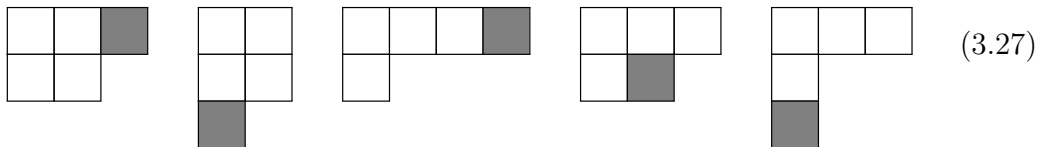
where \sum_{ν^j} is now a sum over all ν such that λ/ν is a vertical strip of length j . This can be interpreted as follows,

$$s_{\lambda/(1^n)} = \sum \left\{ \begin{array}{l} \text{Distinct ways to move } n \text{ particles} \\ \text{a single site to the left.} \end{array} \right\} \quad (3.25)$$

Consider the case where $x = y$ (e.g. $\tau = \beta \in \mathbb{R}$ and $a_k = a_{-k}$). We can then apply the Pieri formula once again, in this case to the products $h_{n-j}s_{\lambda/(j)}$ in (3.17), as

$$h_{n-j}s_{\lambda/(j)} = \sum_{\nu} s_{\nu} , \quad (3.26)$$

where the sum is over all ν obtained from λ by removing a horizontal strip of size j and then adding to the resulting diagram a horizontal strip of size $n - j$. We consider again $G_{(3,2);(2)} = s_{(3,2)/(1)}h_1 + s_{(3,2)/(2)}$, where $(3,2)/(2) = (2,1) + (3)$. Applying the Pieri formula to $s_{(3,2)/(1)}h_1 = s_{(3,2)/(1)}s_{(1)}$ gives the following diagrams, where the cell that is added again indicated in gray. It is clear that $\lambda = (3,2)$ appears twice, as there are two ways to remove (and then add again) a single cell from λ .



We now briefly consider the single particle correlation functions $F_{j;l}$. The generating function $f(z) = \sum_j F_{j;l}z^{j-l}$ for one-particle correlations is written in (1.107). Writing

again $f(z) = H(x; z)H(x; z^{-1})$ for some x , we have

$$\begin{aligned} f(z) &= \prod_j (1 - x_j z)^{-1} (1 - y_j z^{-1})^{-1} \\ &= \sum_{j,k=0}^{\infty} h_j(x) h_k(y) z^{j-k} =: \sum_{m=0}^{\infty} d_m (z^m + z^{-m}), \end{aligned} \quad (3.28)$$

where h_j are complete homogeneous symmetric polynomials. Then,

$$d_m = \sum_{j=m}^{\infty} h_j(y) h_{j-m}(x) = \langle h_M(U) h_{M-m}(U^{-1}) \rangle = G_{j;l}(\tau), \quad j-l = m. \quad (3.29)$$

where M is the largest number k such that $h_k \neq 0$, which is typically infinite. Remember that the $G_{j;l}(\tau)$ are the single-particle wavefunctions at site j and time τ for a particle released from site l . The last two equalities in (3.29) relate $F_{j;l}(\tau)$ to single-particle wavefunctions at site M and time τ for a particle released from site $M - m$. Since M is infinite for most choices of hopping parameters $a_k \sim p_k$, this correspond to releasing a particle at infinity and finding its wavefunction m lattice sites away from where it was released at some Euclidean time τ . The fact that $h_{M-m}(U^{-1}) = G_{j;l}(\tau)$ for $M \rightarrow \infty$ agrees with the intuition that a single particle at infinity does not feel the presence of the other remaining particles, which are infinitely far away from it.

Lastly, we note that one can apply the Jacobi-Trudi identity (1.47) to h_n and e_n to find any skew Schur polynomials on the right hand side of (1.84). This, in effect, provides a way to compute any correlation function. Although the resulting expressions generally grow quickly as one considers large partitions, the application of this method itself is rather simple as it only requires the computation of a determinant. In 3.4, we will outline various other, closely interrelated, methods to calculate any $\langle s_\lambda s_\mu \rangle$, based on power sum polynomials rather than elementary and

complete homogeneous symmetric polynomials.

3.3 Quasi-local particle-hole duality

As mentioned before, we can replace the generating function $f_1(z) = H(x; z)H(y; z^{-1})$ by $f_2(z) = E(x; z)E(y; z^{-1})$ at the cost of transposing the partitions appearing in the correlation functions, see (1.84) and (1.85). This leads to a duality between models related by $a_n \rightarrow (-1)^{n+1}a_n$, as we demonstrate here. Though mathematically quite trivial, the physical interpretation of this duality is rather surprising. As mentioned at the start of this chapter, this duality holds for finite as well as infinite N . From (1.6), it follows that switching between $f_1(z)$ and $f_2(z)$ corresponds to taking

$$p_k(x) \rightarrow (-1)^{k+1}p_k(x) . \quad (3.30)$$

From equations (3.3) and (3.5), it is clear that replacing as $p_k(x) \rightarrow (-1)^{k+1}p_k(x)$ corresponds to $a_k \rightarrow (-1)^{k+1}a_k$. In particular, we consider two hamiltonians for the same a_n ,

$$\begin{aligned} \hat{H}_1 &= - \sum_{m=0}^{\infty} \sum_n a_n (\sigma_m^- \sigma_{m+n}^+ + \sigma_m^- \sigma_{m-n}^+) , \\ \hat{H}_2 &= - \sum_{m=0}^{\infty} \sum_n (-1)^{n+1} a_n (\sigma_m^- \sigma_{m+n}^+ + \sigma_m^- \sigma_{m-n}^+) . \end{aligned} \quad (3.31)$$

Correlation functions for \hat{H}_1 correspond to weight function $f_1(z)$, whereas those for \hat{H}_2 correspond to $f_2(z)$. Let us compare correlation functions for \hat{H}_1 and \hat{H}_2 , which we will write as $F_{\lambda; \mu}^{(1)}(\tau)$ and $F_{\lambda; \mu}^{(2)}(\tau)$, respectively. From Szegő's theorem, we know that $F_{\emptyset; \emptyset}$ only depends on $p_k(x)p_k(y)$, so taking $p_k \rightarrow (-1)^{k+1}p_k$, has no effect on

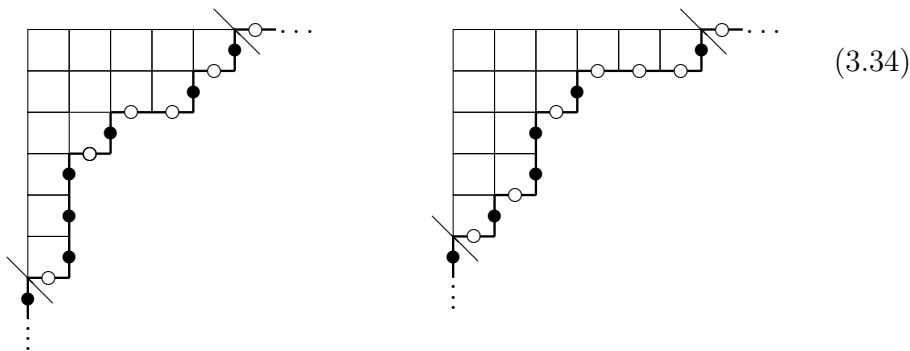
$F_{\emptyset;\emptyset}$. Therefore,

$$F_{\emptyset;\emptyset}^{(1)}(\tau) = F_{\emptyset;\emptyset}^{(2)}(\tau) , \tag{3.32}$$

that is, the return probability for N adjacent particles for \hat{H}_1 is identical to that of \hat{H}_2 for any τ . Moreover, by comparing (1.84) and (1.85), we see that, for general λ and μ ,

$$F_{\lambda;\mu}^{(1)}(\tau) = F_{\lambda^t;\mu^t}^{(2)}(\tau) . \tag{3.33}$$

This establishes the following duality between correlations functions of \hat{H}_1 and \hat{H}_2 . It is well known that transposition of diagrams induces a particle-hole and parity transformation on the corresponding particle-hole configuration. This simply follows from the fact that transposition exchanges left and right, and that it maps vertical edges to horizontal ones (and vice versa). However, we are not implementing particle-hole symmetry in (3.33) but instead we establish an equality between different correlation functions corresponding to different models. Let us consider the configurations associated to $\lambda = (5, 4, 2, 1^3)$ and $\lambda^t = (6, 3, 2^2, 1)$, given on the left and right below, respectively.



These correspond to the following configurations,

$$\begin{aligned}
 |\lambda\rangle &= \cdots \left| \bullet \circ \bullet \bullet \bullet \circ \bullet \circ \circ \bullet \circ \bullet \right| \circ \cdots , \\
 |\lambda^t\rangle &= \cdots \left| \bullet \circ \bullet \circ \bullet \circ \bullet \circ \bullet \circ \bullet \circ \bullet \right| \circ \cdots .
 \end{aligned} \tag{3.35}$$

where the vertical lines on the left and right correspond to the diagonal lines at the lower left and upper right corners of λ and λ^t in (3.34), respectively. We see that the regions in between the vertical lines for $|\lambda\rangle$ and $|\lambda^t\rangle$ are related by performing a parity transformation and exchanging between particles and holes. Only a finite interval $\ell(\lambda) \leq r \leq \lambda_1$ is affected non-trivially by this combination of particle-hole and parity transformations. We thus establish a bijection between the correlation functions corresponding to \hat{H}_1 and \hat{H}_2 , given by the transposition of diagrams, which we refer to as *quasi-local particle-hole duality*. It follows trivially from the above treatment that if $a_{2k} = 0$, $\forall k \in \mathbb{Z}^+$, then $H(x; z) = E(x; z)$, as can be seen immediately from (1.6). It follows that when all even hopping parameters a_{2k} are zero, we have $F_{\lambda; \mu}^{(1)} = F_{\lambda; \mu}^{(2)}$, so we can suppress the superscript. In this case, it follows from (3.33) that

$$F_{\lambda; \mu}(\tau) = F_{\lambda^t; \mu^t}(\tau) . \tag{3.36}$$

That is, any system with $a_{2k} = 0$ satisfies quasi-local particle-hole duality with itself.

3.4 Power sums and border strips

We consider now the particle-hole configurations corresponding to power sum polynomials p_k , which are a very natural basis for the application to LRRW models due to their proportionality to τa_k . Consider specifically the case where $\tau = it$. Then,

from (3.3), we have

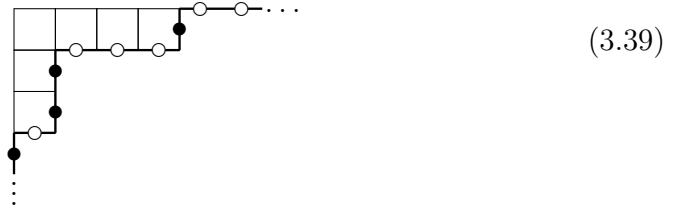
$$p_k(y) = -itka_k^* = (-p_k(x))^* = e^{i\phi} p_k(x) \quad , \quad \phi := \pi - 2 \arg(p_k(x)) \quad . \quad (3.37)$$

Since $p_k(x)$ only differs from $p_k(y)$ by a phase, we can apply the usual multiplication rules to objects of the form $s_\lambda(x)s_\mu(y)$, which is an advantage over the usage of h_j , e_j .

Remember that power sum polynomials are expanded as an alternating sum over hook-shaped Schur polynomials, see equation (1.21). Note that

$$\langle \text{tr} U^n \rangle_\tau = p_n = \sum_{r=0}^{n-1} (-1)^r G_{(n-r, 1^r); \emptyset} \quad , \quad (3.38)$$

can be read off from the hamiltonian by the identification in either (3.3) or (3.5). As an example, the configuration corresponding to a hook shape $\lambda = (4, 1^2)$ is as follows:



That is, a hook-shaped diagram corresponds to taking the particle at site $-b$ and moving it $a + b$ sites to the right. More generally, consider

$$\langle p_n | s_\lambda \rangle = \sum_{r=0}^{n-1} (-1)^r G_{\lambda; (n-r, 1^r)}^c = \sum_{r=0}^{n-1} (-1)^r \langle (n-1, 1^r) | \lambda \rangle \quad . \quad (3.40)$$

Using equation (1.44), this is given by

$$\sum_{r=0}^{n-1} (-1)^r s_{\lambda/(n-r,1^r)} = \sum_{\eta} (-1)^{\text{ht}(\eta)} s_{\lambda \setminus \eta}, \quad (3.41)$$

where the sum is over all η which are border strips of size n , see e.g. the example in (2.12) for $n = 4$. Note that there is only a single Schur polynomial appearing on the right hand side, as opposed to (3.17) and (3.24), which contain factors of e_{n-j} and h_{n-j} , respectively. We consider a few specific examples of (3.41), already noted in [2], before treating it in generality. In particular, consider $\langle s_{\lambda p_n} \rangle_c$ with $(n-r, 1^r) \not\subseteq \lambda \forall r \in \{0, \dots, n-1\}$, such that $\lambda_1 + \lambda_1^t - 1 < n$. This gives

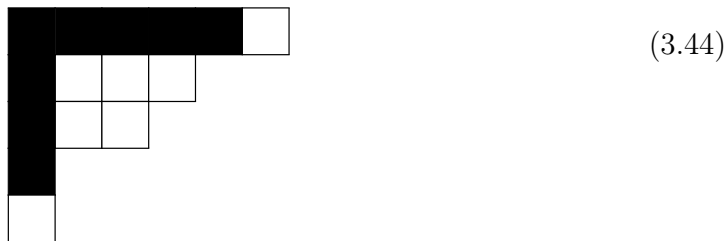
$$\langle \text{tr} U^{-n} \text{tr}_{\lambda} U \rangle_c = 0. \quad (3.42)$$

Writing λ in Frobenius notation as $\lambda = (a_1, \dots, a_k | b_1, \dots, b_k)$ with a_j satisfying $a_1 > \dots > a_k$ and similar for b_j . In this case, $a_1 + b_1 + 1$ equals the hook-length of the top left cell of λ . Equation (3.42) then states that $\langle \text{tr} U^{-n} \text{tr}_{\lambda} U \rangle_c = 0$ if $a_1 + b_1 + 1 < n$. In terms of particle-hole configurations, (3.42) states that $\sum_{r=0}^{n-1} (-1)^r G_{\lambda; (n-r, 1^r)}^c = 0$ if n is greater than the distance (in units of lattice spacing) between the leftmost hole and rightmost particle in the configuration corresponding to λ .

Further, write $m = a_1 + b_1 + 1 - n$ and consider $\lambda = (a|b) = (a_1, \dots, a_k | b_1, \dots, b_k)$ such that $m \leq a_1 - a_2 - 1$ and $m \leq b_1 - b_2 - 1$, respectively. Take $\mu = (a_2, \dots, a_k | b_2, \dots, b_k)$, obtained by removing the first row and column from λ . Any $(n-r, 1^r) \subseteq \lambda$ then satisfies

$$\begin{aligned} \lambda / (n-r, 1^r) &= (a_1 + 1, 1^{b_1}) / (n-r, 1^r) \times \mu \\ &= (a_1 + 1 - n + r) \times (1^{b_1 - r}) \times \mu. \end{aligned} \quad (3.43)$$

Consider the example of $(6, 4, 3, 1^2) / (5, 1^3)$, which is given by the diagram below.

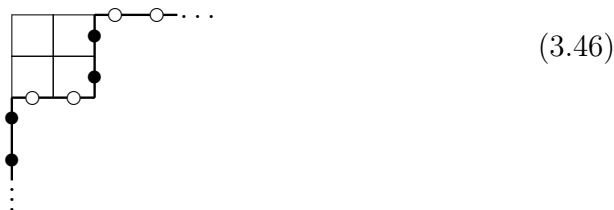


We then apply (1.7) to find

$$\langle s_\lambda(U) \text{tr} U^{-n} \rangle_c = \sum_{r=n-a_1-1}^{b_1} (-1)^r s_{\lambda/(n-r, 1^r)} = \pm s_\mu \sum_{k=0}^m (-1)^k h_{m-k} e_k = 0 . \quad (3.45)$$

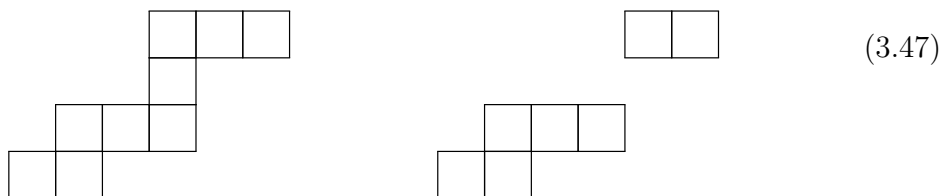
Assigning particle-hole configurations to the diagrams above, we see that the correlation function corresponding to $\langle s_\lambda(U) \text{tr} U^{-n} \rangle_c$ vanishes when the distance between the leftmost hole and rightmost particle, as well as the distance between the rightmost particle and the second-to-rightmost particle (and vice versa for holes), are sufficiently small compared to n .

We now consider (3.41) more generally. In this expression, ν is related to λ by the removal of a border strip, i.e. a connected skew diagram not containing a subdiagram that is a 2 by 2 block. In terms of particles and holes, a 2 by 2 block corresponds to moving two adjacent particles by two sites to the right, see below.

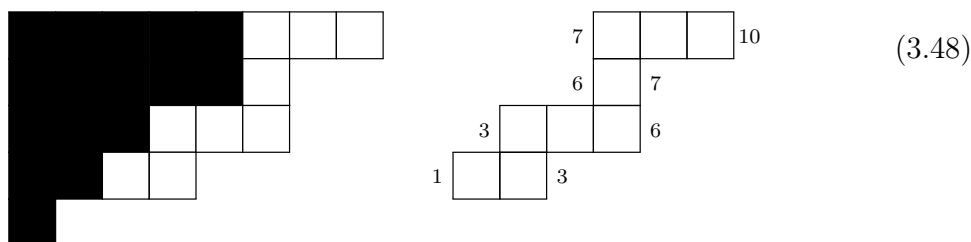


In equation (3.41), fact that a border strip has no 2 by 2 subdiagram therefore states that (the configuration corresponding to) ν is related to λ by moving (a) particle(s) left by n sites without moving two or more adjacent particles by two or more sites.

The number of rows that λ/ν occupies (which is $\text{ht}(\lambda/\nu) + 1$) equals the number of particles that are involved in this process, which follows immediately from the fact that vertical edges on the boundary of a diagram correspond to particles. From the fact that the border strip is connected, it follows that it occupies only consecutive rows. For example, the skew diagram on the left is a border strip, whereas the one on the right clearly is not.



This means that only consecutive (but not necessarily adjacent) particles are affected. However, connectedness is a stronger condition, and in the case of border strips this leads to the following observation. For a skew diagram λ/ν , we call the *outer rim* the (horizontal and vertical) edges on the bottom right of the diagram of λ/ν , as in e.g. [35]. Conversely, the *inner rim* consists of the edges on the top left of λ/ν . For a border strip containing n cells, we number the edges of the inner and outer rims by $j = \{1, \dots, n + 1\}$. We will refer to the j^{th} edge on the outer rim as the j^{th} outer edge, and likewise for the inner rim. We consider an explicit example, where $\lambda = (8, 6^2, 4, 1)$ and $\nu = (5^2, 3, 2, 1)$, leading to a border strip of size $n = 9$ below. On the right hand side, we number the vertical edges of the inner and outer rims of λ/ν .



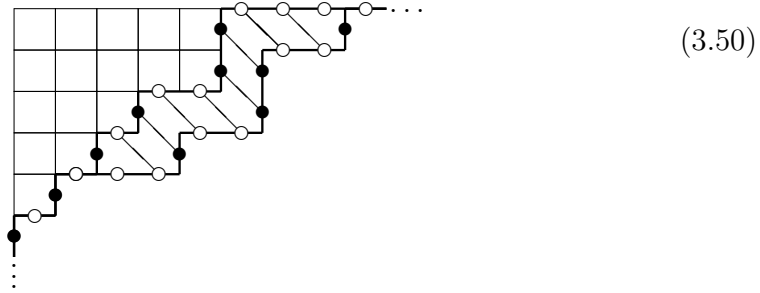
One can see in the above example that the first edge on the inner rim and the ledge edge on the outer rim are both vertical, which is clearly true for any (skew) diagram. Further, we see that all other vertical edges occupy the same positions on the inner and outer rims, namely $\{3, 6, 7\}$. If e.g. the third edge on the inner rim were horizontal, the resulting skew diagram would be disconnected and therefore not a valid border strip, shown below.



It is clear that this holds generally for border strips. In particular, the inner and outer edges of any border strip are identical for $j = 2, 3, \dots, n$, and the outer (inner) edge for $j = 1$ is horizontal (vertical), whereas the outer (inner) edge for $j = n + 1$ is vertical (horizontal).

The configurations corresponding to λ and ν are related by taking the configuration on the outer rim of λ/ν (as a subset of the outer rim of λ) and replacing it by the configuration corresponding to the inner rim of λ/ν . What we effectively get is the following. We take a particle at some site k and move it to site $k - n$, and we get a factor $(-1)^{\text{ht}(\lambda/\nu)}$. Here, $\text{ht}(\lambda/\nu)$ equals the number of particles the affected particle jumps over, that is, the number of particles occupying sites $\{k - n + 1, \dots, k - 1\}$.

We thus see that $(-1)^{\text{ht}(\lambda/\nu)}$ simply implements *fermionic statistics*. Below, we show the border strip λ/ν with empty cells as a subset of λ , where we indicate particles and holes. The inner edge j and outer edge j for $j = 2, \dots, n$ are connected by diagonal lines.



The configurations corresponding to λ and ν are given by

$$\begin{aligned}
 |\lambda\rangle &= \dots \bullet \text{---} \circ \text{---} \bullet \text{---} \circ \text{---} \circ \text{---} \circ \text{---} \bullet \text{---} \circ \text{---} \circ \text{---} \bullet \text{---} \bullet \text{---} \circ \text{---} \circ \text{---} \bullet \text{---} \circ \text{---} \dots, \\
 |\nu\rangle &= \dots \bullet \text{---} \circ \text{---} \bullet \text{---} \circ \text{---} \bullet \text{---} \circ \text{---} \bullet \text{---} \circ \text{---} \circ \text{---} \bullet \text{---} \bullet \text{---} \circ \text{---} \circ \text{---} \circ \text{---} \circ \text{---} \dots.
 \end{aligned}
 \tag{3.51}$$

It is clear that they are identical except for a single particle which has moved $n = 9$ sites to the left, whereby it jumps over 3 other particles, leading to a factor $(-1)^3$. Summarizing the above, we have

$$\sum_{r=0}^{n-1} (-1)^r G_{\lambda; (n-r, 1^r)}^c = \sum (-1)^P s_{\lambda/\eta}(y) \left\{ \begin{array}{l} \text{Distinct ways to move a} \\ \text{particle in } \lambda \text{ to the left by } n \\ \text{sites, thereby hopping over} \\ P \leq n - 1 \text{ other particles.} \end{array} \right\} \tag{3.52}$$

We can apply the reasoning presented above to the calculation of $\chi_\alpha^{\lambda/\mu}$, by considering $p_\alpha s_\mu$ in terms of fermionic particles hopping on a 1D lattice. In particular, starting

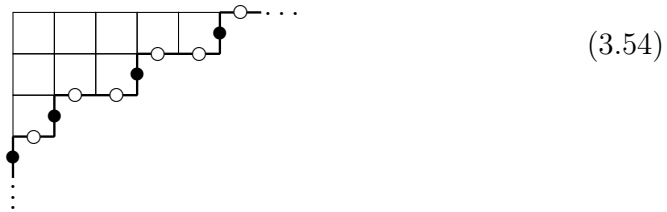
from some partition μ and fixing a choice of α , we consider all way to consecutively take a particle in the configuration corresponding to μ and move it α_j sites to the right, summing over $j \geq 1$, and adding a multiplicative factor -1 for each other particle which it hops over. We then add the resulting numbers (± 1) for all cases where the end result of this process is the configuration λ . The outcome of this computation is precisely $\chi_\alpha^{\lambda/\mu}$. This might provide a convenient method for computing $\chi_\alpha^{\lambda/\mu}$, as it involves moving particles around on a line instead of a border strip tiling problem. Although these two problems evidently identical, the former might be simpler to implement practically.

3.5 Time evolution

When we consider the action of the hamiltonian in (1.104) in terms of diagrams, the following picture arises. We remind the reader that the presentation given here does not depend on taking $N \rightarrow \infty$ and holds for finite N as well. We first consider the XX0-model, in which case the action of H^n on some state with k particles can be described in terms of k non-intersecting (vicious) random walkers that are allowed to move a single site to the left or right at each time step, for n time steps [23]. For the XX0-model, considering $H|\lambda\rangle$ in terms of diagrams then corresponds to summing over all ways to add one cell to and to remove one cell from λ , as this gives vicious random walkers move can take a single site to the right or left. For a general long-range hamiltonian such as in (1.104), the action of H is given by vicious random walkers which can move n sites right or left, weighted by $a_{\pm n}$ and summed over n . We saw above that removing a border strip of size n corresponds to taking a single particle and moving it by n sites to the left, so it appears that

$$H|\lambda\rangle = \sum_n a_n \left(\sum_\eta |\lambda \setminus \eta\rangle + \sum_\nu |\nu\rangle \right), \quad (3.53)$$

where η is a border strip of size n and ν is related to λ by the addition of a border strip of size n , and we sum over all such η and ν . Note that we do not get the minus sign that we get when considering $\langle p_n(U) s_\lambda(U^{-1}) \rangle_c$ as in (3.41). For $n = 1$, when we consider all ways to start with the empty partition and look at all ways to successively add single cells, we simply get Young's lattice. The action of the XX0-model on some state $|\lambda\rangle$ then corresponds to moving from λ along all edges in Young's lattice. For a general hamiltonian as in (1.104), the picture is clearly more involved. Take, for example, the case where $a_4 \neq 0$ and $a_n = 0$ for $n \neq 4$. If we have $\lambda = (5, 3, 1)$, given below,



which corresponds to

$$|\lambda\rangle = \dots \bullet \circ \bullet \circ \circ \bullet \circ \circ \bullet \circ \dots \quad (3.55)$$

It is easy to see that there are two ways to move a single particle four sites to the left, and there are six ways to move a particle four sites to the right. Correspondingly, the action of the hamiltonian $H |\lambda\rangle$ produces the eight diagrams in (3.56).

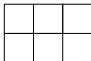

Consider a generalization of the Young's lattice in the form of a graph where each edge connects two diagrams that are related by addition or removal of some size n border strip, for all n . The action $H^n |\lambda\rangle$ of a general long-range hamiltonian as in (1.104) corresponds to an n -site random walk on this graph, where edges corresponding to a border strip of size n carry weight a_n . This provides a general description of the action of a hamiltonian in (1.104) in terms of (addition and re-

moval of) border strips. We know from equation (1.62) how many diagrams there are with some n -core μ and n -weight w , but due to the fact that the graph described above has varying connectivity, the n -site random walk is more likely to end up in some diagrams than others.

3.6 Fermionic models

As in section 3.5, the present treatment up to equation (3.59) does not require $N \rightarrow \infty$. We saw that adding or removing a border strip η and multiplying with $(-1)^{\text{ht}(\eta)}$ implements fermionic statistics, and that this can be applied to the calculation of $\chi_{\alpha}^{\lambda/\mu}$. Inverting this line of reasoning, we will now derive two relations for fermionic

models using the properties of $\chi_{\alpha}^{\lambda/\mu}$. The first of these involves the fact, noted at equation (1.49) and below, that the order in which one adds border strips in the construction of a border strip tableau $\text{BST}(\lambda/\mu, \alpha)$ is irrelevant to its outcome. That is, $\chi_{\alpha}^{\lambda/\mu}$ does not depend on the order of the entries of α . The same is true for the removal of border strips, as can be seen in equation (1.55) and the example in (1.57) and figure 1.1. From the relation between removing or adding border strips in the construction of $\chi_{\alpha}^{\lambda/\mu}$ and fermions hopping on a line, we can make the following observation. Consider a one-dimensional fermion configuration corresponding to some diagram μ , and consider all ways of moving not necessarily distinct fermions to the right by $\alpha_1, \alpha_2, \dots$ sites, where α_j are unordered non-negative integers. We then see that *the order of the step sizes α_j by which we move fermions has no effect on the outcome of this process*. That is, taking a fermion configuration and consecutively moving fermions to the right by various step sizes depend only on the distribution of the step sizes and not the order in which they are taken. It is clear from applying (1.55) and the removal of border strips in the computation of $\chi_{\alpha}^{\lambda/\mu}$ that the same statement holds when we consider fermions that can only hop to the left instead of the right.

Consider a simple example which is partly given in figure 1.1 and in its entirety in figure 2.1. Namely, consider again $\lambda = (3, 2) =$  and now remove twice a single cell and once a border strip of size 2 from λ . We can see this gives ,

regardless of the order of the border strip sizes.

$$\begin{array}{c}
 \begin{array}{|c|c|c|} \hline \square & \square & \square \\ \hline \square & \square & \\ \hline \end{array} \xrightarrow{p_2} \begin{array}{|c|c|c|} \hline \square & \square & \square \\ \hline \square & \square & \\ \hline \end{array} \xrightarrow{p_1} \begin{array}{|c|c|} \hline \square & \square \\ \hline \square & \\ \hline \end{array} \xrightarrow{p_1} \square \\
 \end{array} \tag{3.57}$$

$$\begin{array}{c}
 \begin{array}{|c|c|c|} \hline \square & \square & \square \\ \hline \square & \square & \\ \hline \end{array} \xrightarrow{p_1} \begin{array}{|c|c|c|} \hline \square & \square & \square \\ \hline \square & \square & \\ \hline \end{array} + \begin{array}{|c|c|} \hline \square & \square \\ \hline \square & \\ \hline \end{array} \xrightarrow{p_2} \begin{array}{|c|c|} \hline \square & \square \\ \hline \square & \\ \hline \end{array} + (1-1) \times \begin{array}{|c|} \hline \square \\ \hline \square \\ \hline \end{array} \xrightarrow{p_1} \square \\
 \end{array}$$

$$\begin{array}{c}
 \begin{array}{|c|c|c|} \hline \square & \square & \square \\ \hline \square & \square & \\ \hline \end{array} \xrightarrow{p_1} \begin{array}{|c|c|c|} \hline \square & \square & \square \\ \hline \square & \square & \\ \hline \end{array} + \begin{array}{|c|c|} \hline \square & \square \\ \hline \square & \\ \hline \end{array} \xrightarrow{p_1} 2 \times \begin{array}{|c|c|} \hline \square & \square \\ \hline \square & \\ \hline \end{array} + \begin{array}{|c|c|c|} \hline \square & \square & \square \\ \hline \square & \square & \\ \hline \end{array} \xrightarrow{p_2} \square \\
 \end{array}$$

It is interesting to see that the fact that we arrive at \square follows either from the cancellation between two different ways to arrive at $\begin{array}{|c|} \hline \square \\ \hline \square \\ \hline \end{array}$, in the second line of (3.57), or the fact that one cannot remove a size 2 border strip from $\begin{array}{|c|c|} \hline \square & \square \\ \hline \square & \\ \hline \end{array}$, in the third line of (3.57). Assigning particle-hole configurations to the diagrams above, given in (3.18) for $\begin{array}{|c|c|c|} \hline \square & \square & \square \\ \hline \square & \square & \\ \hline \end{array}$, and treating the particles as fermions gives an example of the irrelevance of the order of step sizes.

Our second result for fermionic systems arises from equations (1.60), (1.61). These state that $\chi_{(n^k)}^{\lambda/\mu}$ is cancellation-free, where μ is the n -core of λ [34], [35]. This leads to the following observation. Take a fermionic hamiltonian \hat{H}_f , where fermions are only allowed to hop n sites, and denote a fermionic state corresponding to the n -core μ of some λ as $\|\mu\rangle\rangle$. The result of $\hat{H}_f\|\mu\rangle\rangle$ can then be expressed in terms of symmetric functions as

$$s_\mu p_n + \sum_{r=0}^{n-1} (-1)^r s_{\mu/(n-r,1^r)} = \sum_{\nu} (-1)^{\text{ht}(\nu/\mu)} s_\nu + \sum_{\nu_n} (-1)^{\text{ht}(\eta)} s_{\mu \setminus \eta}, \tag{3.58}$$

where, as before, ν and $\mu \setminus \eta$ are related to μ by the addition and removal of a border strip of size n , respectively. Compare with equation (3.53), especially the factors

$(-1)^{\text{ht}}$. We can keep iterating this step by adding and removing border strips of size n to and from the resulting diagrams. From (1.60) and the comments below, it then follows that all diagrams appearing in the expansion of $\left(\hat{H}_f\right)^k \|\mu\rangle\rangle$ have the same sign *for any* k . Further, we saw that adding or removing border strips μ/ν and multiplying by $(-1)^{\text{ht}(\mu/\nu)}$ corresponds to letting fermions hop over a distance of $|\mu/\nu|$ lattice sites. It follows that, for a fermionic model where particles can only hop n sites, *all distinct ways to go from some configuration μ to another configuration λ appear with the same sign, with the sign depending only on the choice of μ and λ* . In other words, all different ways to go from any configuration μ to any other configuration λ involves fermions hopping over either an even or an odd number of other fermions. Physically, this means that there is no interference between various ways to arrive at some fermionic state. Fermionic states will spread through Hilbert space rapidly upon time evolution, as they are not restricted by destructive interference.

The same reasoning can be applied to various expectation values of the LRRW models with hamiltonian (1.104). In particular, we will consider $\langle\langle(\text{tr}U^n)^k s_\lambda(U^{-1})\rangle\rangle_c$. Repeatedly applying (1.44), which we have used at various points above, we get

$$\langle\langle(\text{tr}U^n)^k s_\lambda(U^{-1})\rangle\rangle_c = \sum_{j=1}^k \sum_{\nu_{n,j}} (-1)^{\text{ht}(T_j)} s_{\nu_{n,j}}(x) p_n(y)^{k-j} . \quad (3.59)$$

where we use the notation $\nu_{n,j}$ for diagrams related to λ by the consecutive removal of j border strips of size n . For example, consider again $\lambda = (6, 5, 2^2, 1)$ and $(n^k) = (4^4)$. Then, the diagrams $\nu_{4,2}$ are given by removing the green and blue regions from the diagrams in (1.63), for $\nu_{4,3}$ the orange regions are also removed, and after removing the red regions we end up with $\nu_{4,4} = \emptyset$. Note that $\chi_{(n^k)}^\lambda = 0$ for most λ , one sufficient but far from necessary condition for this being that $nk \neq |\lambda|$. In general, consecutively removing border strips of some size n leads eventually to the

aforementioned n -core of λ [31]. From (3.37), we have

$$s_{\nu_{n,j}}(x)p_n^{k-j}(x) = \sum_{\mu} d_{n,j,k}^{\mu} s_{\mu}(x) , \quad (3.60)$$

for some coefficients $d_{n,j,k}^{\mu}$. From (1.42), we know that $s_{\lambda}p_n^k$ is expanded as a sum over all diagrams related to λ by subsequently adding a k border strips of size n . On the other hand, $\nu_{n,j}$ is related to λ by removal of j border strips of size j . Therefore,

$$\langle (\mathrm{tr}U^n)^k s_{\lambda}(U^{-1}) \rangle_c = \sum_{j=1}^k \sum_{\tilde{\nu}_{n,j}^k} e^{i\phi(k-j)} (-1)^{\mathrm{ht}(T_1)+\mathrm{ht}(T_2)} s_{\tilde{\nu}_{n,j}^{k-j}}(x) . \quad (3.61)$$

In the above expression, the sum is over all $\tilde{\nu}_{n,j}^{k-j}$ constructed by first removing j border strips of size n from λ (which results in $\nu_{n,j}$) and then adding $k-j$ border strips of size n , including multiplicities. Further, T_1 is given by the BST constructed of the union of the j border strips that are removed from λ , and T_2 is the tableau that is the union of the $k-j$ border strips that are added to $\nu_{n,j}$ to construct $\tilde{\nu}_{n,j}^{k-j}$. For $\lambda = (6, 5, 2^2, 1)$, we consider

$$\langle (\mathrm{tr}U^4)^2 s_{\lambda}(U^{-1}) \rangle_c . \quad (3.62)$$

As mentioned above, contracting both copies of $\mathrm{tr}U^4$ with s_{λ} gives rise to the diagrams in (1.63) after removing the green and blue border strips. The $\tilde{\nu}_{4,1}^1$ are given by the ways to remove from and then add to λ a border strip of size four. We see from (3.61) that λ appears in the expansion of (3.62) with a multiplicity two, as there are two distinct border strips of size four that one can remove from λ , namely, the green and blue border strips on the top left diagram in (1.63). To find the remaining diagrams appearing in (3.62), one should add border strips of size four to the diagrams obtained after removing the green and blue border strips on the top left diagram in (1.63). In general, we find that $\langle (\mathrm{tr}U^n)^k s_{\lambda}(U^{-1}) \rangle_c$ is given by the

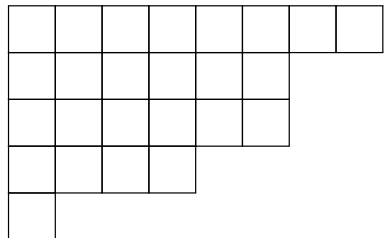
following expression,

$$\pm \sum_{j=1}^k e^{i\phi(k-j)} s_{\nu_{n,j}^{k-j}}(x) \left\{ \begin{array}{l} \text{Distinct ways to consecutively} \\ \text{move } j \text{ particles in } \lambda \text{ to the left} \\ \text{by } n \text{ sites and then move } k-j \\ \text{particles to the right by } n \text{ sites.} \end{array} \right\} \quad (3.63)$$

Note that the particles that are moved by n sites are not necessarily distinct. Further, the right hand side appears with a positive or negative sign depending only on the final configuration. This again follows from the fact that $\chi_{\alpha}^{\lambda/\mu}$ is cancellation-free.

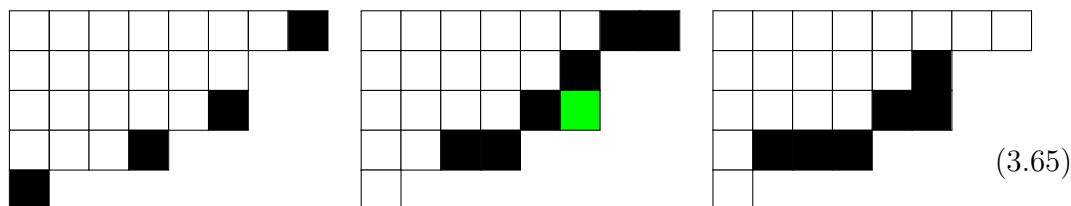
3.7 Schur function expansion

We consider now the expansions for general correlation functions which were derived in section 2.3. We first consider the application of (2.46) here, before moving on to (2.62) in section 3.8. Equation (2.46) expresses $\langle s_{\lambda}(U)s_{\nu}(U^{-1}) \rangle$ as a sum over diagrams obtained from λ and ν by removing border strips of size $\alpha_1, \alpha_2, \dots$ for a partition α , summed over α . In particular, it establishes a relation between $\langle s_{\lambda}s_{\nu} \rangle_c$ and the correlation functions $\langle s_{\lambda \setminus \{\alpha\}} \rangle = \langle \emptyset | s_{\lambda \setminus \{\alpha\}} \rangle$, involving only a single non-trivial configuration $\lambda \setminus \{\alpha\}$ (and likewise for $\nu \setminus \{\alpha\}$). Fixing some α , we sum over all ways to start from λ and ν and move α_j particles j sites to the left with fermionic statistics (in the form of $(-1)^{\text{ht}(T_{\alpha})}$). Consider the autocorrelation for $\nu = \lambda = (8, 6^2, 4, 1)$, which we show below.



$$(3.64)$$

Equation (2.46) gives an expression in terms of diagrams obtained by removing border strips from λ . Below, we show from left to right all border strips of size 1, 2, 3 that can be removed from $\lambda = \nu$.

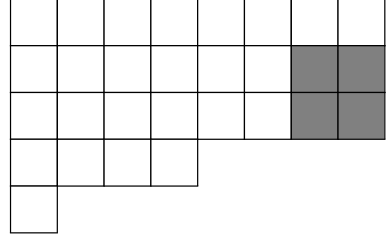


In the middle diagram above, the green cell is shared between both a horizontal and a vertical strip of size two. We can thus remove four border strips of both size 1 and 2, and two of size 3. It is easy to see that there is a single border strip of size 4 that can be removed from λ , three border strips for both sizes 5 and 6, and so on, up to a single border strip of size $\lambda_1 + \ell(\lambda) - 1 = 12$. Applying (2.46) then gives

$$\begin{aligned}
 \langle s_\lambda(U)s_\lambda(U^{-1}) \rangle_c &= (s_{(7,6^2,4,1)} + s_{(8,6,5,4,1)} + s_{(8,6^2,3,1)} + s_{(8,6^2,4)})^2 + \\
 &+ \frac{1}{2} (s_{(6^3,4,1)} - s_{(8,5^2,4,1)} + s_{(8,6,4^2,1)})^2 + \\
 &+ \frac{1}{3} (-s_{(8,5,4,1^2)} + s_{(8,6^2,1^2)})^2 + \dots
 \end{aligned}
 \tag{3.66}$$

In the above expression, the first, second, and third line correspond to the removal of border strips of size one, two, and three, respectively. Further, we again write $(s_\mu + s_\rho + \dots)^2$ instead of $(s_\mu(x) + s_\rho(x) + \dots)(s_\mu(y) + s_\rho(y) + \dots)$.

Consider now $\langle s_\lambda(U)s_\nu(U^{-1}) \rangle$ with λ as above and $\nu = (8^3, 4, 1)$, the latter of which is shown below. We have here $\lambda \subset \nu$, and we indicate ν/λ in gray.


(3.67)

Consider again all ways to remove border strips from ν , and apply (2.46). This then leads to the following terms appearing in the expansion of $\langle s_\lambda(U)s_\nu(U^{-1}) \rangle$,

$$\begin{aligned} & (s_{(7,6^2,4,1)} + s_{(8,6,5,4,1)} + s_{(8,6^2,3,1)} + s_{(8,6^2,4)}) (s_{(8^2,7,4,1)} + s_{(8^3,3,1)} + s_{(8^3,4)}) + \\ & + \frac{1}{2} (s_{(6^3,4,1)} - s_{(8,5^2,4,1)} + s_{(8,6,4^2,1)}) (s_{(8,7^2,4,1)} + s_{(8^2,6,4,1)} + s_{(8^3,2,1)}) + \dots \end{aligned} \quad (3.68)$$

The diagrams appearing on the left (right) in the top and bottom lines of (3.68) are found by removing border strips of sizes 1 and 2 from λ (ν), respectively. This expansion can easily be continued by considering more or larger border strips. From the relation between removal or addition of border strips as in (2.46) and fermionic particles hopping on a line, we see that $\langle s_\lambda(U)s_\nu(U^{-1}) \rangle$ is given by

$$\sum_{\alpha} \frac{1}{z_{\alpha}} \left((-1)^{P_{s_{\lambda \setminus \{\eta\}}}(y)} \left\{ \begin{array}{l} \text{Distinct ways to take } \ell(\alpha) \\ \text{particles in } \lambda \text{ and move} \\ \text{them } \alpha_1, \alpha_2, \dots \text{ sites to} \\ \text{the left, thereby hopping} \\ \text{over } T_{\alpha} \text{ other particles} \end{array} \right\} \right) \times \begin{pmatrix} y \rightarrow x \\ \lambda \rightarrow \nu \end{pmatrix} \quad (3.69)$$

Note that the $\ell(\alpha)$ particles mentioned above are not required to be distinct.

3.8 Power sum expansion

From the fact that, for $\tau = it$, $p_k(x)$ and $p_k(y)$ are related by a phase, it is useful to express LRRW correlation functions as expansions in terms of $p_k(x)$ and $p_k(y)$ in order to reveal these phases. To do so, one may use the relation between Schur and power sum polynomials in equation (1.48) and apply the Murnaghan-Nakayama rule, as done for the relatively simple example of $\langle s_\lambda(U)s_\lambda(U^{-1}) \rangle$ for $\lambda = (3, 2)$ in section 2.3.2. However, as noted there, even this relatively simple example is already somewhat non-trivial, as it requires the computation of χ^λ_α for all α . For these purposes, it is more convenient to employ (2.62), which provides an expansion of $\langle s_\lambda(U)s_\nu(U^{-1}) \rangle$ in terms of $p_k(x)$ and $p_k(y)$. The prefactors appearing in this expansion depend on the number of ways to remove border strips from λ and ν in such a way that the resulting diagram is the same for both λ and ν . Taking again $\nu = \lambda = (8, 6^2, 4, 1)$, for which the diagrams resulting from removal of border strips were treated in section 3.7 above. Applying (2.62) then gives

$$\begin{aligned}
\langle s_\lambda(U)s_\lambda(U^{-1}) \rangle_c &= 4 \left(p_1(x)p_1(y) + \frac{1}{4}p_2(x)p_2(y) \right) + \frac{2}{9}p_3(x)p_3(y) + \frac{1}{16}p_4(x)p_4(y) + \\
&+ 3 \left(\frac{1}{25}p_5(x)p_5(y) + \frac{1}{36}p_6(x)p_6(y) \right) + \\
&+ \frac{1}{2} \left(p_1^2(x)p_2(y) + p_2(x)p_1^2(y) \right) + \\
&+ \frac{1}{6} \left(p_3(x)p_1(y)p_2(y) + p_3(y)p_1(x)p_2(x) \right) + \dots \tag{3.70}
\end{aligned}$$

In the above expression, the first two lines on the right hand side are given by (2.56), which is a special case of (2.62). As we saw previously, the terms $\sim \frac{p_j(x)p_j(y)}{j^2}$ in the first two lines of (3.70) arise as follows. The denominator is given by the inverse of $z_{(j)}z_{(j)} = j^2$, and the numerator equals the number of distinct ways to remove a border strip of size j from $\lambda = (3, 2)$. The third and fourth lines give mixed power sums obtained from not contracting a single $p_j(U^\pm)$ and two copies of

$p_k(U^\mp)$, $p_m(U^\mp)$. From the diagrams in (3.65), one can see that there are four ways to remove two border strips of unit size and arrive at a diagram that can alternatively be obtained by removing a single border strip of size 2. This follows from the fact that there are four ways to remove a border strip of size two, which can alternatively be achieved by removing the two cells of such a border strip successively. However, due to the factors $(-1)^{\text{ht}(T)}$ in (2.62), one of those four contributes with a negative sign, leading to a prefactor of $\frac{2}{z_{(1^2)}z_{(2)}} = \frac{1}{2}$ multiplying $\sim p_1^2 p_2$ in the third line of (3.70). There is a similar cancellation occurring from the term proportional to $p_3 p_1 p_2$. This expansion can then be continued by removing further border strips. Consider again $\langle s_\lambda(U) s_\nu(U^{-1}) \rangle$ with $\lambda = (8, 6^2, 4, 1)$ and $\nu = (8^3, 4, 1)$, as at the end of section 3.7. applying (2.62) leads to

$$\begin{aligned} \langle s_\lambda(U) s_\nu(U^{-1}) \rangle &= -\frac{2}{3} p_1(x) p_3(x) + \frac{1}{4} p_2^2(x) + \\ &\quad \frac{1}{12} p_1(x)^4 + \frac{1}{2} p_2^2(x) p_1(x) p_1(y) + \dots \end{aligned} \quad (3.71)$$

This can be seen by considering diagram corresponding to ν in (3.67), and covering the gray 2 by 2 square with border strips of sizes from 1 to 3. We get no contribution proportional to $p_2(x) p_1(x)^2$ since the two ways to cover a 2 by 2 diagram with a single border strip of size 2 and 2 border strips of size 1 appear with opposite sign. This expansion can be continued by removing more or larger border strips from λ and ν , which can be conveniently done by using the relation to fermionic configurations.

The above examples show that (2.62) can be conveniently applied to $\langle s_\lambda(U) s_\nu(U^{-1}) \rangle$ for larger λ , ν as well, for which χ_α^λ and χ_α^ν would be very hard to compute. Indeed, as hinted at above, it is particularly useful for the following three reasons.

1. Equation (2.62) provides a controlled expansion of general correlation functions $\langle s_\lambda(U) s_\nu(U^{-1}) \rangle$ in terms of power sums. These power sums can be directly read off from the hamiltonian, see (3.3) and (3.5).

2. This expansion can be straightforwardly applied, including to correlation functions involving large diagrams λ, ν . Using the comments below (3.46), the removal of border strips is related to fermionic particles hopping on a line, which could further simplify the application of this method.
3. The power sums $p_k(x)$ and $p_k(y)$ are proportional to τ , so that (2.62) provides an expansion in terms of powers of τ . Depending on the application and the range of τ one would like to consider, this expansion can be truncated at any desirable order that provides sufficient precision. For $\tau = it$, this $p_k(x)$ and $p_k(y)$ are related by a complex phase, leading to various simplifications that are hard to reveal otherwise.

From the treatment above, it follows that the expression for $\langle s_\lambda(U)s_\nu(U^{-1}) \rangle$ in equation (2.62) has the following particle-hole interpretation.

$$\sum_{\omega, \gamma} \frac{p_\omega(y)p_\gamma(x)}{z_\omega z_\gamma} (-1)^P \left\{ \begin{array}{l} \text{Distinct ways to move particles in } \lambda \text{ and } \nu \\ \text{to the left by } \gamma_1, \gamma_2, \dots \text{ and } \omega_1, \omega_2, \dots \text{ sites,} \\ \text{respectively, hopping over } P \text{ other particles} \\ \text{and ending up in the same configuration.} \end{array} \right\} \quad (3.72)$$

3.9 Experimental benchmarking

We provide some suggestions for the benchmarking of experimental setups using correlation functions involving power sum polynomials. In experimental contexts such as trapped ion systems, one could measure the correlation functions corresponding to $\langle p_n(U^{\pm 1}) \rangle = \langle \text{tr} U^{\pm n} \rangle = p_n$ experimentally. Remember that p_n can be read off from the hamiltonian as in (3.3) or (3.5) due to their direct proportionality to $a_{\pm n}$, and is given by a superposition of configurations corresponding to hook-shaped diagrams as in (3.39). Therefore, one could measure $\langle p_n(U^{\pm 1}) \rangle$ and compare them with the intended values of $a_{\pm n}$ to benchmark experimental setups. Further, one can use

equation (2.8),

$$\langle |\text{tr}U^n|^2 \rangle = n + p_n(x)p_n(y) , \quad (3.73)$$

and consider $\text{tr}U^n$ as a superposition of states (when properly normalized), as before. Then, the correlation function corresponding $\langle |\text{tr}U^n|^2 \rangle$ is proportional to $F_{\emptyset;\emptyset}$ with proportionality given by $n + p_n(x)p_n(y)$, up to normalization. When we have certain hopping parameters $a_n \neq 0$, the only way to get independence from time is to have no dependence on the power sums $p_n \sim \tau n a_n$, as they contain a factor of τ . The τ -independence of the connected part of the correlation function corresponding to (2.8) therefore sets it apart from other correlation functions, and might offer an effective way to benchmark experimental setups. Remember that the p_λ form a basis for all symmetric polynomials. In case $\ell(\lambda) \geq 2$ (or $\ell(\nu) \geq 2$) so that $p_\lambda = p_{\lambda_1} p_{\lambda_2} \dots$, Wick's theorem tells us that $\langle p_\lambda p_\mu \rangle_c$ will contain terms where not all p_{λ_j} and p_{μ_k} are contracted. These give contributions containing $p_k(x) \sim \tau$ (and/or $p_j(y) \sim \tau$). Therefore, $\frac{1}{\sqrt{n}} \langle |\text{tr}U^n|^2 \rangle_c$ for any integer n is the only non-zero connected correlation function that does not depend on τ . Lastly, one could use $\langle \text{tr}U^n \text{tr}U^{-k} \rangle_c = n \delta_{n,k}$ (after proper normalization) to see if the system is truly translationally invariant, as its derivation is predicated on the assumption of translational invariance.

Chapter 4

Spectral statistics

This chapter will treat the calculation of SFF, focusing mainly on the CSMM. We will first consider the SFF in the limit $N \rightarrow \infty$ for matrix models satisfying Szegő's strong limit theorem. After that, we will compute the SFF of the CSMM for general N and q and then take the 't Hooft limit. In all cases, we will recover WD-universality, where the CSMM for general N and q as well as in the 't Hooft limit involves some non-trivial unfolding. This chapter is based on [3] which builds on the main result of [2].

4.1 Spectral form factors and universality

Finding the SFF when the strong Szegő limit theorem holds is a simple matter of applying a result derived in chapter 2. In particular, plugging $k = n$ into (2.8), we find that, for $\frac{n}{N} < 1$, the connected SFF of *all* such matrix models is given by a linear ramp of unit slope,

$$F(n)_c = \langle |\text{tr} U^n|^2 \rangle_c = n . \quad (4.1)$$

The disconnected SFF is given by $p_n(x)p_n(y)$ (for both $f(z) = H(x; z)H(y; z^{-1})$ and $f(z) = E(x; z)E(y; z^{-1})$). Eventually, the linear ramp gives way to a plateau, which comes about as follows. Remember that $s_\lambda(x)$ vanishes if the longest column in λ contains more boxes than the number of non-zero variables in the set x (1.28). We saw that we get a contribution equal to unity for every term for which $(n - r, 1^r) = \nu = (n - s, 1^s)$ for $0 \leq r \leq \text{Min}(n - 1, N - 1)$. However, there are only N such reps, as $s_{(a, 1^b)}(x) = 0$ if $b \geq N$. Therefore, we see that

$$NF(n)_c = 1, \quad n/N > 1. \quad (4.2)$$

We thus conclude that, for RME's which satisfy Szegő's strong limit theorem, the connected SFF is exactly given by a linear ramp which saturates at a plateau. Moreover, these RME's have a flat level density, so that we do not have to unfold the spectrum. In particular,

$$\rho(\theta) = \frac{1}{2\pi} \left[1 + \frac{1}{N} \sum_{k \geq 1} (p_k(y)e^{ik\theta} + p_k(x)e^{-ik\theta}) \right] = \frac{1}{2\pi}, \quad (4.3)$$

where the second equality follows from the finiteness of $p_k(x), p_k(y)$, by the assumptions of Szegő's theorem, and the fact that we take $N \rightarrow \infty$. We thus see that RME's satisfying Szegő's strong limit theorem exhibit WD-universality. This includes the CSMM for $q < 1$, in spite of the fact that this was introduced to describe intermediate statistics. We will now consider the SFF of the CSMM for finite N and general q , before taking the 't Hooft limit.

4.2 General matrix size

Before computing the SFF, we first consider the Hopf link for $\lambda = \square = \mu$ as a warm-up exercise. Applying equation (1.183) and using (1.32), we find

$$W_{\square\square} = [N] + q^2[N][N-1] \xrightarrow{N \rightarrow \infty} \frac{1}{1-q} + \frac{q^2}{(1-q)^2}. \quad (4.4)$$

On the right hand side, we consider the limit $N \rightarrow \infty$ and applied $\lim_{N \rightarrow \infty} [N]_q = \lim_{N \rightarrow \infty} \frac{1-q^N}{1-q} = \frac{1}{1-q}$ for $|q| < 1$. On the other hand, applying (1.184)

$$\begin{aligned} W_{\square\square}^\infty &= \sum_{\nu} (s_{(\square/\nu)}(q^{j-1/2}))^2 = (s_{\square}(q^{j-1/2}))^2 + (s_{\emptyset}(q^{j-1/2}))^2 \\ &= q[N]^2 + 1 = \frac{q}{(1-q)^2} + 1 = \lim_{N \rightarrow \infty} W_{\square\square}. \end{aligned} \quad (4.5)$$

As one can see, the fact that terms of the form q^N go to zero as $N \rightarrow \infty$ leads to the agreement between equations (4.4) and (4.5).

We proceed to calculate the SFF, which is given by

$$K(n) := \frac{1}{N} \langle |\text{tr} U^n|^2 \rangle = \frac{1}{N} \sum_{r,s=0}^{n-1} (-1)^{r+s} \langle s_{(n-r,1^r)} s_{(n-s,1^s)} \rangle. \quad (4.6)$$

Plugging equation (1.183) into (4.6), we see that $K(n)$ is given by $\frac{q^{n^2}}{N}$ times

$$\sum_{r,s=0}^{n-1} (-1)^{r+s} q^{-n(r+s)} s_{(n-s,1^s)}(q^{j-1}) s_{(n-r,1^r)}(q^{-n+s}, 1, \dots, q^{s-1}, q^{s+1}, \dots, q^{N-1}). \quad (4.7)$$

The first Schur polynomial appearing in the sum, $s_{(n-s,1^s)}(q^{j-1})$, is given in (1.185). The second Schur polynomial, $s_{\lambda}(q^{j-\mu_j-1})$ for hook-shaped λ and μ , is more complicated. We write $\lambda = (a, 1^b)$ and $\mu = (c, 1^d)$. Defining the sets of variables $x = q^{-c}$,

$y = q^{d+1}, \dots, q^{N-1}$, $z = 1, \dots, q^{d-1}$, we apply (1.32), twice for $\mu = \emptyset$ to give

$$s_\lambda(x, y, z) = \sum_{\rho, \nu} s_{\lambda/\rho}(x) s_{\rho/\nu}(y) s_\nu(z), \quad (4.8)$$

where the sum runs over all partitions satisfying $\nu \subset \rho \subset \lambda$. For $\lambda = (a, 1^b)$ and x, y, z as defined above, we get non-zero contributions only when λ/ρ is a horizontal strip, as $x = q^{-c}$ consists only of a single variable, so that $s_{\lambda/\rho}(x) = 0$ for λ/ρ containing a column of length ≥ 2 . We then have to carefully distinguish between two types of partitions ρ .

1. For $\rho = (e, 1^b)$, we again have $\lambda/\rho = (a - e)$ which is clearly a horizontal strip. Then,

$$s_{\lambda/\rho}(q^{-c}) = q^{-c(a-e)}. \quad (4.9)$$

The requirement that $\nu \subset \rho$ then leads to $\nu = (f, 1^g)$ so that $\rho/\nu = (e - f) \otimes (1^{b-g})$ for $\nu \neq \emptyset$ and $\rho/\nu = \mu$ for $\nu = \emptyset$.

2. For $\rho = (e, 1^{b-1})$, we have $\lambda/\rho = \square \otimes (a - e)$ so that

$$s_{\lambda/\rho}(q^{-c}) = q^{-c(a-e+1)}. \quad (4.10)$$

Then, $\nu = (f, 1^g)$ so that $\rho/\nu = (e - f) \otimes (1^{b-g-1})$ and $\rho/\nu = \rho$ for $\nu = \emptyset$. This situation of course does not occur for $b = 0$, in which case $\lambda = (a)$.

Note that $s_{(a)}(x) = h_a(x)$ and $s_{(1^a)}(x) = e_a(x)$, the complete homogeneous and elementary symmetric polynomials of degree a , respectively. We then have, for $\rho/\nu = (e - f) \otimes (1^{b-g})$

$$s_{\rho/\nu}(y) = h_{e-f}(y) e_{b-g}(y). \quad (4.11)$$

We illustrate these two choices for ρ in equations (4.9) and (4.10) for $\lambda = (4, 1^2)$. As a specific example, we set $e = 2$, so that the first choice of $\rho = (e, 1^b) = (2, 1^2)$. This gives $\lambda/\rho = (4, 1^2)/(2, 1^2) = (2)$. λ/ρ is represented in terms of Young diagrams below.

$$\begin{array}{|c|c|c|c|} \hline \square & \square & \square & \square \\ \hline \square & & & \\ \hline \square & & & \\ \hline \end{array} / \begin{array}{|c|c|} \hline \square & \square \\ \hline \square & \\ \hline \square & \\ \hline \end{array} = \begin{array}{|c|c|} \hline \square & \square \\ \hline \end{array} .$$

Consider now the second choice, $\rho = (e, 1^{b-1}) = (2, 1)$, so that $\lambda/\rho = (4, 1^2)/(2, 1) = (2) \times (1)$, represented in Young diagrams as follows.

$$\begin{array}{|c|c|c|c|} \hline \square & \square & \square & \square \\ \hline \square & & & \\ \hline \square & & & \\ \hline \end{array} / \begin{array}{|c|c|} \hline \square & \square \\ \hline \square & \\ \hline \end{array} = \begin{array}{|c|} \hline \square \\ \hline \end{array} \times \begin{array}{|c|c|} \hline \square & \square \\ \hline \end{array}$$

The result is again a horizontal strip, consisting in this case of two disconnected components. We consider these two choices for μ and sum over all partitions satisfying $\nu \subset \rho \subset \lambda$ to calculate $s_{(n-r, 1^r)}(x, y, z)$. In particular, we sum over g from 0 to $\min(b, d-1)$ or to $\min(b-1, d-1)$, corresponding to $\rho = (e, 1^b)$ or $\rho = (e, 1^{b-1})$, respectively. We then sum over f from 1 to e and lastly over e from 0 to a . This allows the computation of the full SFF, the results of which we discuss below.

4.3 Appearance of the linear ramp

For finite $N > n$, we consider how the linear ramp appears for the connected SFF, which is found by subtracting the disconnected contribution, $\langle \text{tr} U^n \rangle^2$, from the full SFF. The disconnected contribution is thus given by the square of

$$\langle \text{tr} U^n \rangle = q^{n^2/2} \sum_{r=0}^{n-1} (-1)^r q^{-nr} s_{(n-r, 1^r)}(q^{j-1}) . \quad (4.12)$$

For $n = 1, 2, 3$, this equals

$$\begin{aligned}
\langle \text{tr}U \rangle &= q^{1/2}[N] = \frac{q^{1/2}(1 - q^N)}{1 - q} \\
\langle \text{tr}U^2 \rangle &= \frac{(1 - q^N)(-q + q^N + q^{N+1} + q^{N+2})}{1 - q^2} \\
\langle \text{tr}U^3 \rangle &= \frac{q^3 - q^{N+1}(1 + q + q^2)^2 + q^{2N}(1 + q^2)(1 + q + q^2)^2}{q^{3/2}(1 - q^3)} + \\
&\quad - \frac{q^{3N}(1 + q^2)(1 + q + q^2 + q^3 + q^4)}{q^{3/2}(1 - q^3)}
\end{aligned} \tag{4.13}$$

The connected SFF for small n is then given by,

$$\begin{aligned}
F(1)_c &= q s_{(1)}(q^{j-1})s_{(1)}(q^{-1}, q, q^2, \dots) - q(s_{(1)}(1, q, q^2, \dots))^2 \\
&= q[N](1 - q) = 1 - q^N \\
F(2)_c &= \frac{(1 - q^N)(2q - q^N + q^{2N} - q^{2+N} + 2q^{1+2N} + q^{2+2N})}{q}, \\
F(3)_c &= -\frac{1}{q^4}(-3q^4 + q^{3N} - 2q^N + q^{5N} + q^{2+N} + 2q^{3+N} + 3q^{4+N} + 2q^{5+N} + \\
&\quad + q^{6+N} - 2q^{1+2N} - 4q^{2+2N} - 8q^{3+2N} - 8q^{4+2N} - 8q^{5+2N} - 4q^{6+2N} + \\
&\quad - 2q^{7+2N} + 6q^{1+3N} + 10q^{2+3N} + 16q^{3+3N} + 18q^{4+3N} + 16q^{5+3N} + \\
&\quad + 10q^{6+3N} + 6q^{7+3N} + q^{8+3N} - 6q^{1+4N} - 12q^{2+4N} - 16q^{3+4N} - 18q^{4+4N} + \\
&\quad - 16q^{5+4N} - 12q^{6+4N} - 6q^{7+4N} - 2q^{8+4N} + 2q^{1+5N} + 5q^{2+5N} + 6q^{3+5N} + \\
&\quad + 8q^{4+5N} + 6q^{5+5N} + 5q^{6+5N} + 2q^{7+5N} + q^{8+5N})
\end{aligned} \tag{4.14}$$

Examples of the SFF for higher n are too long to print here. One thing one can see from (4.14), which persists for higher (but finite) n , is that the SFF is of the form,

$$F(n)_c = n + \mathcal{O}(q^A), \quad A = N + \dots \tag{4.15}$$

Therefore, for $N \rightarrow \infty$ and $q < 1$ fixed, $q^N \rightarrow 0$ and $F(n)_c \rightarrow n$. This reproduces the exact linear ramp for all RME's satisfying the assumptions of Szegő's theorem.

Linear ramp from Schur bilinears

We saw at the start of this chapter that, for $q < 1$ and $N \rightarrow \infty$, in which case the CSMM satisfies the strong Szegő limit theorem, we get a contribution equal to 1 when considering two identical hook-shaped partitions $(n-r, 1^r) = (n-s, 1^s)$. Since there are n hook-shaped partitions containing n boxes, we get a contribution equal to n , which is the linear ramp. More details can be found in [2].

The above consideration leads us to conclude that, for finite N and for $r = s \leq N-1$, we should have that the summand of the SFF in (4.7) is of the following form

$$\begin{aligned} A(N, n, q, r, r) &:= \langle s_{(n-r, 1^r)} s_{(n-r, 1^r)} \rangle \\ &= q^{n^2 - 2nr} s_{(n-r, 1^r)}(q^{j-1}) s_{(n-r, 1^r)}(q^{-(n-r)}, 1, \dots, q^{r-1}, q^{r+1}, \dots, q^{N-1}) \\ &= 1 + \mathcal{O}(q) . \end{aligned} \tag{4.16}$$

Further, we should have

$$A(N, n, q, r, s) = \mathcal{O}(q) \quad , \quad r \neq s . \tag{4.17}$$

There are two types of terms of $\mathcal{O}(q)$ in the above expressions. First of all, there are terms of the form $q^{N+\dots}$, which go to zero as we take $N \rightarrow \infty$ for fixed $q < 1$. Secondly, there are powers of q not containing factors of N , which do not go to zero as $N \rightarrow \infty$. Therefore, to recover the linear ramp as $N \rightarrow \infty$, all the lower powers of q should mutually cancel out between the various terms in the sum in (4.7).

We start by verifying (4.16). Note that q -numbers and products thereof (such as

q -factorials and q -binomials) are themselves of $\mathcal{O}(1)$. For example,

$$[N]_q = \frac{1 - q^N}{1 - q} = (1 - q^N) \sum_{k=0}^{\infty} q^k = 1 + q + q^2 + \cdots - q^N - q^{N+1} + \dots \quad (4.18)$$

Let us consider $A(N, n, q, 0, 0)$. Plugging the following

$$s_{(n)}(q^{-n}, q, \dots, q^{N-1}) = q^{-n^2} + \mathcal{O}(q^{-n^2+1}) \quad (4.19)$$

into (4.16) leads to

$$\begin{aligned} q^{n^2} s_{(n)}(q^{j-1}) s_{(n)}(q^{-n}, q, \dots, q^{N-1}) &= q^{n^2} \begin{bmatrix} N + n - 1 \\ n \end{bmatrix} (q^{-n^2} + \mathcal{O}(q^{-n^2+1})) \\ &= 1 + \mathcal{O}(q) \quad (4.20) \end{aligned}$$

where we use the aforementioned fact that q -binomials are of the form $1 + \mathcal{O}(q)$. When $r = s \neq 0$, the calculation is slightly more involved. First, we read off from (1.171) that

$$s_{(n-r, 1^r)}(q^{j-1}) = q^{r(r+1)/2} (1 + \mathcal{O}(q)) \quad (4.21)$$

We then determine the lowest power of q appearing in

$s_{(n-r, 1^r)}(q^{-(n-r)}, 1, \dots, q^{r-1}, q^{r+1}, \dots, q^{N-1})$. Using (4.8), this Schur polynomial can be expressed as

$$\sum_{\mu, \nu} s_{(n-r, 1^r)/\mu}(q^{-(n-r)}) s_{\mu/\nu}(1, \dots, q^{r-1}) s_{\nu}(q^{r+1}, \dots, q^{N-1}) \quad (4.22)$$

Consider the case where $\mu = (1^r)$ and $\nu = \emptyset$. This gives $\lambda/\mu = (n-r-1) \times (1)$, so that $s_{(n-r, 1^r)/\mu}(q^{-(n-r)}) = q^{-(n-r)^2}$. Further, we have $s_{\mu}(q, \dots, q^{r-1}) = q^{r(r-1)/2}$, and

$s_\nu = s_\emptyset = 1$. Therefore,

$$s_{(n-r, 1^r)}(q^{-(n-r)}, 1, \dots, q^{r-1}, q^{r+1}, \dots, q^{N-1}) = q^{-(n-r)^2} q^{r(r-1)/2} (1 + \mathcal{O}(q)) . \quad (4.23)$$

Plugging this into (4.16) gives

$$A(N, n, q, r, r) = q^{n^2 - 2nr} q^{r(r+1)/2} q^{-(n-r)^2} q^{r(r-1)/2} (1 + \mathcal{O}(q)) = 1 + \mathcal{O}(q) . \quad (4.24)$$

One can readily check that any other choice of μ and ν leads to higher powers of q . For example, choosing $\nu = (1)$ increases the power of q by 2, and choosing a different partition for μ either increases the power of q by $n - r$ or gives zero (when $\ell((n - r, 1^r)/\mu) > 1$). This leads to equation (4.16).

Let us now consider the case where $r \neq s$, to derive equation (4.17). We take $r < s$ without loss of generality. Taking first $r = 0$, we have

$$\begin{aligned} A(N, n, 0, s, q) &= q^{n^2 - ns} s_{(n-s, 1^s)}(q^{j-1}) s_{(n)}(q^{-(n-s)}, y, z) \\ &= q^{n^2 - ns} q^{s(s+1)/2} q^{-n(n-s)} (1 + \mathcal{O}(q)) \\ &= q^{s(s+1)/2} (1 + \mathcal{O}(q)) = \mathcal{O}(q) . \end{aligned} \quad (4.25)$$

where $y = (1, \dots, q^{s-1})$ and $z = (q^{s+1}, \dots, q^{N-1})$, as before. Lastly, we check the case where $0 \neq s \neq r \neq 0$, choosing again $r < s$ without loss of generality. Following the same procedure that leads to (4.23), we find that

$s_{(n-r, 1^r)}(q^{-(n-s)}, 1, \dots, q^{s-1}, q^{s+1}, \dots, q^{N-1})$ is given by

$$q^{-(n-r)^2} q^{r(r-1)/2} (1 + \mathcal{O}(q)) , \quad (4.26)$$

so that this term, too, appears with a positive power of q ,

$$A(N, n, r, s, q) = q^{((r-s)^2 + r + s)/2} (1 + \mathcal{O}(q)) . \quad (4.27)$$

We have thus shown that terms with $r = s$ contribute $1 + \mathcal{O}(q)$, whereas Schur bilinears with $r \neq s$ contribute terms of $\mathcal{O}(q)$. As mentioned above, powers of q which do not contain a factor N cancel out in the sum over r and s , leaving only a linear ramp plus terms of the form $q^{(N+\dots)}$, as can be seen in some examples in (4.14).

The calculations described here have a simple knot-theoretical interpretation. Remember that $A(N, n, r, s, q)$ is proportional to the HOMFLY invariant of a Hopf link, where the two components of the Hopf link carry $U(N)$ representations corresponding to partitions $(n - r, 1^r)$ and $(n - s, 1^s)$, respectively. The above results entail that Hopf links of Wilson lines carrying hook-shaped representations only give a unit contribution for two identical representations. Therefore, in the limit $q \rightarrow 0$, where the CSMM reduces to the CUE, all Hopf link invariants with different n -box hook-shaped partitions go to zero. On the other hand, those with identical n -box hook-shaped partitions go to one, which is simply the orthogonality of Schur polynomials a characters of $U(N)$. This means, for example, that an unknot carrying $(a, 1^b)$ with $b \neq 0$ has invariant equal to zero, but if we tie two of these unknots together to form a Hopf link the resulting invariant equals one. On the other hand, an unknot carrying representation (a) has invariant equal to one, but if we tie it to an unknot carrying $(a - b, 1^b)$ with $b \neq 0$ to form a Hopf link, the result is again zero.

4.4 Saturation at plateau

If we relax the assumption that $n < N$, the SFF will eventually reach a plateau for large enough n . This can be seen from the simple random walk argument presented in section 1.4.3. Alternatively, the emergence of the plateau can be understood to arise from the fact that $s_\lambda(x) = 0$ for $\ell(\lambda) > |x|$. In particular, the averages appearing on the right hand side of (4.6), are weighted matrix integrals

written in (1.174) over Schur polynomials of the form $s_{(n-r,1^r)}(U) = s_{(n-r,1^r)}(e^{i\phi_j})$. If $\ell(s_{(n-r,1^r)}) = r + 1 > N$, then $s_{(n-r,1^r)}(U) = 0$. Therefore, only Schur bilinears of the form

$$\langle s_{(n-r,1^r)}(U)s_{(n-s,1^s)}(U^{-1}) \rangle \quad , \quad r, s \leq N - 1 \quad , \quad (4.28)$$

give a non-zero contribution to (4.6). It was demonstrated in the previous subsection that, for $r, s \leq N - 1$,

$$\langle s_{(n-r,1^r)}(U)s_{(n-s,1^s)}(U^{-1}) \rangle = \delta_{r,s} + \mathcal{O}(q) \quad , \quad (4.29)$$

from which arises the linear ramp. From equation (4.29), it follows that the linear ramp arising from $r = s \leq N - 1$, saturates at a plateau for $n = N$. However, one should note that this does not take into account terms of $\mathcal{O}(q^N)$, which will turn out to have a significant impact on the shape of the SFF, delaying the onset of the plateau as one increases q^N .

To implement $n > N$ in the expression for the SFF derived at the start of this section, one should take into account that

1. $s_{(e,1^b)}(y) = 0$ for $b > N - d - 2$
2. $e_{b-g}(y) = 0$ for $g > d + b + 1 - N$,

where $x = q^{-c}$, $y = q^{d+1}, \dots, q^{N-1}$, and $z = 1, \dots, q^{d-1}$, as before. Note that the functions above both arise as $s_{\rho/\nu}(y)$ for $\rho = (e, 1^b)$ in equation (4.8), where $e_{b-g}(y)$ is given in equation (4.11), whereas $s_{\rho/\nu}(y)$ reduces to $s_{(e,1^b)}(y)$ for $\nu = \emptyset$. We plot $K(n)$ resulting from this calculation for $N = 10$ and $N = 20$ and various choices of q .

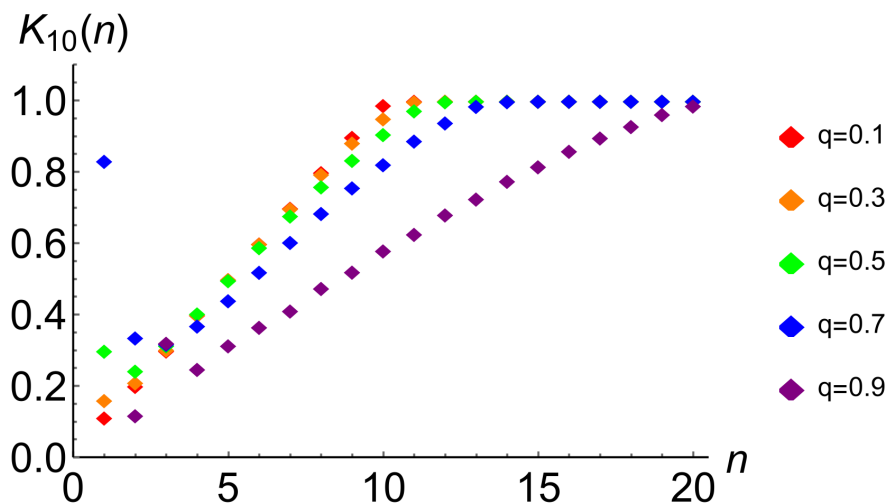


Figure 4.1: The full SFF for $N = 10$ and various values of q .

As one can see, the SFF is closest to a linear ramp for small values of q , which is to be expected as the limit $q \rightarrow 0$ corresponds to the CUE. Further, the disconnected SFF becomes large for small n as we increase q , leading to large, oscillating deviations close to the origin. Comparing figures 4.1 and 4.2 reveals that, for fixed q , deviation from a linear ramp decreases as we increase N .

The aforementioned observations that (for the full SFF), as we increase q , a dip emerges and the slope of the SFF decreases, are not unrelated. In particular, we find that $\sum_{n=1}^k F(n)$ for large enough $k \geq N$ is almost independent of q . That is, as we increase q , we get positive contributions to $A(k)$ arising from the disconnected SFF which are compensated by a decrease in the slope of $F(n)$. We define, for $k > N$, the logarithm of the difference between the sum over the SFF of the CSMM

and the CUE ($q \rightarrow 0$) SFF,

$$A(k) := \log \left[\sum_{n=1}^k F(n) - N^2/2 - N(N-k) \right]. \quad (4.30)$$

We plot the results for $N = 10$ and $k = 10, \dots, 20$ below. It is clear that the difference decreases quite rapidly with k until it stabilizes around some small value. Further, we see that the difference decreases more slowly and acquires a larger minimum value as we increase q .

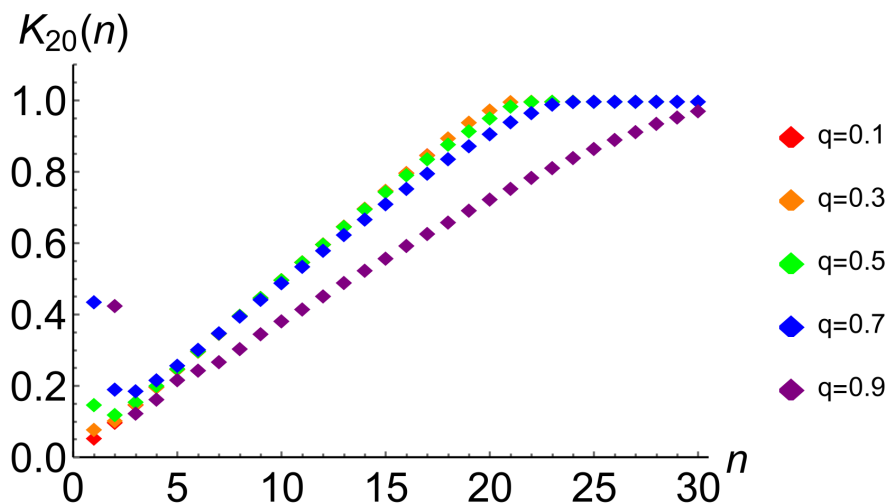


Figure 4.2: The full SFF for $N = 20$ and various values of q .

The SFF's plotted in figures 4.1 and 4.2 were found without unfolding. To see the effect of unfolding, the connected SFF was computed numerically for $N = 10$ and $N = 20$ numerically, using the Metropolis algorithm to generate the spectra. The unfolding is done via Gaussian kernel density estimation using the Silverman rule for bandwidth selection. The data sets for $N = 10$ and $N = 20$ contain at least 10.000 and 5.000 samples, respectively, such that at least 100.000 levels are involved

in the calculation of both SFF's. These are plotted below, where, to distinguish them from the analytically calculated (and non-unfolded) SFF's, we denote the numerically computed SFF's by $L(n)$ ¹. We emphasize once more that these are the connected SFF's, where we omit the disconnected part to enable easier comparison with Wigner–Dyson universality. The SFF's for $N = 10$ and $N = 20$ are distinguished by the fact that they arrive at a plateau at $n = 10$ and $n = 20$, respectively. As we can see, for both $N = 10$ and $N = 20$ and all values of q we consider, the connected SFF's exhibit Wigner–Dyson universality rather than intermediate statistics. We will arrive at similar conclusions for the 't Hooft limit below, albeit via different methods.

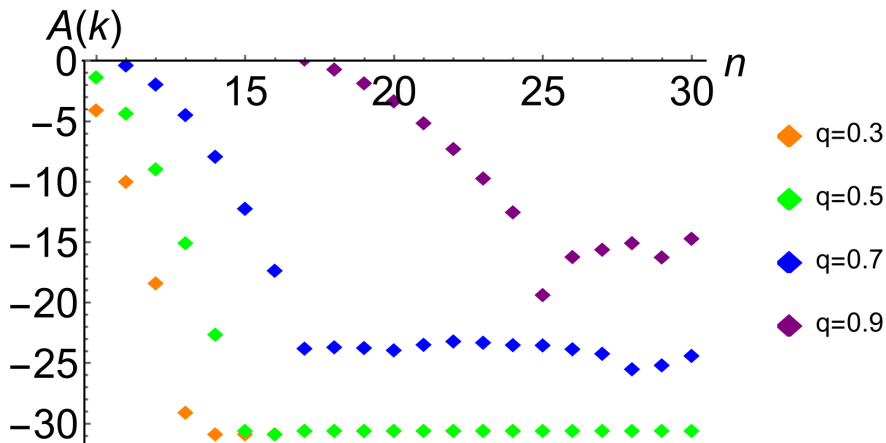


Figure 4.3: The logarithm of the difference between the sum over the CSMM SFF for $N = 10$ and the CUE ($q \rightarrow 0$) SFF, plotted for various values of q . We see that the difference is very small and decreases quite rapidly with k but, conversely, increases with q .

¹We gratefully acknowledge Wouter Buijsman for providing us with the data for these plots.

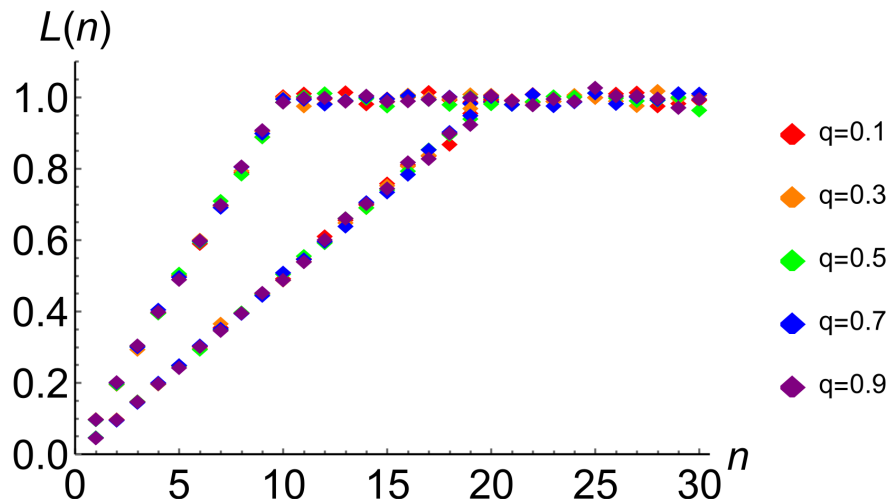


Figure 4.4: The numerically computed connected unfolded SFF’s for $N = 10$ and $N = 20$, which can be distinguished by the fact that they arrive at a plateau at $n = 10$ and $n = 20$, respectively. Note that we plot only the connected SFF here, as opposed to figures 4.1 and 4.2, to simplify comparison with Wigner–Dyson universality. It is clear that Wigner–Dyson universality is recovered to high precision for both $N = 10$ and $N = 20$ and all q considered here.

4.5 Taking the ‘t Hooft-limit

In the string theory literature on the CSMM, the ‘t Hooft limit has been considered, where one takes $N \rightarrow \infty$ and simultaneously $q \rightarrow 1$ such that $y = q^N$ remains finite. This idea goes back to pioneering work by ‘t Hooft in the context of $U(N)$ gauge theories at large N [114]. In the type A topological open string theory on T^*S^3 described by the $U(N)$ Chern–Simons theory, certain large N dualities appear. In particular, it has been argued that the topological A -type open string theory on T^*S^3 undergoes a conifold transition to a *closed* type A topological string theory on the resolved conifold [115]. The magnitude of the B -field on the S^2 blowup of

the conifold is given by $t = Ng_s$, the 't Hooft parameter. The mirror dual of the conifold geometry can be seen to arise from the resolvent of the matrix model in the large N limit [116], [97], see also [117], [118]. These dualities and related results have important applications in enumerative geometry and intersection theory.

As far as the authors are aware, the 't Hooft limit has heretofore not been explicitly considered for the CSMM in the RMT literature. In [119], a closely related limit was considered for a Hermitian version of the q -deformed ensemble considered here, where the weak disorder (GUE) limit corresponds to $q = e^{-\gamma} \rightarrow 1$ and $N \rightarrow \infty$ such that $\gamma N \rightarrow 0$, while the strong disorder limit involves $\gamma N = \text{constant}$. In the latter limit, which is essentially the 't Hooft limit, an approximate expression for the parametric density correlation function was found in [119]. Further, a similar limit was considered for another, closely related, q -deformed circular unitary ensemble in [120], see also [6]. It was found that deviations from the CUE level density only persist in the infinite N limit if one simultaneously scales q such that $(1 - q)N$ remains finite, which is essentially the 't Hooft limit.

The 't Hooft limit is given by the following double scaling,

$$N \rightarrow \infty, \quad g_s \rightarrow 0, \quad \text{such that } t := Ng_s = \text{finite}. \quad (4.31)$$

The 't Hooft limit of the CSMM has been considered in the context of topological string theory in e.g. [115], [97], [117]. In this case, one has $y = q^N = e^{-t} \neq 0$. In this limit, q taken to a finite power will simply give 1, whereas q to the power of multiples of N will give powers of y , which we need to keep track off to calculate the SFF. In the 't Hooft limit, the hook-shaped Schur polynomial in (1.185) goes to

$$\lim_{q \rightarrow 1^-} \frac{1}{(a-1)!b!(a+b)} \left(\frac{1-y}{1-q} \right)^{a+b}, \quad (4.32)$$

which we write as a limit as it is a divergent quantity. However, we will find that the

connected SFF is in fact not divergent for the explicit examples we calculated, which demonstrates that a precise cancellation of these divergent terms has to occur. To reveal this cancellation, we cannot simply use (1.185), as we need to keep track of the powers of q as well. Instead, we will write,

$$\begin{aligned}
 s_{(a,1^b)}(x_i = q^{i-1}) &= \frac{q^{b(b+1)/2}}{\underbrace{[a-1]![b]![a+b]}_{=A_{a,b}}} \frac{[N+a-1]!}{[N-b-1]!} = A_{a,b} \frac{\prod_{k=0}^{a+b-1} (1 - yq^{a-1-k})}{(1-q)^{a+b}}!, \\
 &= \frac{A_{a,b}}{(1-q)^{a+b}} (yq^{a-1}; q^{-1})_{a+b},
 \end{aligned} \tag{4.33}$$

where one should keep in mind that we take the limit $q \rightarrow 1^-$. In particular, for m finite, one can write

$$\begin{bmatrix} N+m \\ k \end{bmatrix} = \frac{(yq^m; q^{-1})_k}{[k]!(1-q)^k}. \tag{4.34}$$

as a convenient way to extract factors of y .

In the ‘t Hooft limit limit, the SFF turns into a remarkable sequence of polynomials of degree $2n - 1$ in y . We will first consider these polynomials and their properties, before turning to the question of unfolding. We have calculated the connected SFF for $n = 1, \dots, 11$, resulting in the expressions on the following pages.

$$F(1)_c = 1 - y ,$$

$$F(2)_c = 2 - 4y + 6y^2 - 4y^3 ,$$

$$F(3)_c = 3 - 9y + 36y^2 - 84y^3 + 90y^4 - 36y^5 ,$$

$$F(4)_c = 4 - 16y + 120y^2 - 560y^3 + 1420y^4 - 1968y^5 + 1400y^6 - 400y^7 ,$$

$$F(5)_c = 5 - 25y + 300y^2 - 2300y^3 + 10150y^4 - 26880y^5 + 43400y^6 + \\ - 41800y^7 + 22050y^8 - 4900y^9 ,$$

$$F(6)_c = 6 - 36y + 630y^2 - 7140y^3 + 47880y^4 - 200592y^5 + 544824y^6 + \\ - 974160y^7 + 1137780y^8 - 834960y^9 + 349272y^{10} - 63504y^{11} ,$$

$$F(7)_c = 7 - 49y + 1176y^2 - 18424y^3 + 173460y^4 - 1042524y^5 + 4187736y^6 + \\ - 11565624y^7 + 22246686y^8 - 29742020y^9 + 27087984y^{10} + \\ - 16024176y^{11} + 5549544y^{12} - 853776y^{13} ,$$

$$F(8)_c = 8 - 64y + 2016y^2 - 41664y^3 + 522480y^4 - 4237632y^5 + 23380896y^6 + \\ - 90830784y^7 + 253846296y^8 - 515838400y^9 + 762521760y^{10} + \\ - 810927936y^{11} + 604107504y^{12} - 299065536y^{13} + 88339680y^{14} + \\ - 11778624y^{15} ,$$

$$F(9)_c = 9 - 81y + 3240y^2 - 85320y^3 + 1372140y^4 - 14394996y^5 + 103900104y^6 + \\ - 535847400y^7 + 2026445850y^8 - 5713765200y^9 + 12118597920y^{10} + \\ - 19364383584y^{11} + 23165382240y^{12} - 20414698920y^{13} + \\ + 12853423440y^{14} - 5468226192y^{15} + 1407913650y^{16} - 165636900y^{17} ,$$

$$\begin{aligned}
F(10)_c = & 10 - 100y + 4950y^2 - 161700y^3 + 3240600y^4 - 42617520y^5 + \\
& + 388588200y^6 - 2556668400y^7 + 12488661900y^8 - 46202499200y^9 + \\
& + 131172321280y^{10} - 287919216000y^{11} + 489596250000y^{12} + \\
& - 642659556000y^{13} + 644511582000y^{14} - 484405727520y^{15} + \\
& + 263957736900y^{16} - 98425126800y^{17} + 22457091800y^{18} + \\
& - 2363904400y^{19} , \\
F(11)_c = & 11 - 121y + 7260y^2 - 287980y^3 + 7031310y^4 - 113142744y^5 + \\
& + 1269259992y^6 - 10345746840y^7 + 63147440070y^8 - 295025713840y^9 + \\
& + 1071727584928y^{10} - 3059501029728y^{11} + 6907003486240y^{12} + \\
& - 12358366232520y^{13} + 17490417413040y^{14} - 19447530019632y^{15} + \\
& + 16771920490182y^{16} - 10982054062980y^{17} + 5272925154640y^{18} + \\
& - 1749762036880y^{19} + 358415185128y^{20} - 34134779536y^{21} . \tag{4.35}
\end{aligned}$$

The complicated form of these polynomials belies the fact that the SFF appears to be very close to a straight line for any y , with decreasing slope for increasing y , see figure 4.5. We emphasize again that the SFF’s plotted in figure 4.5 were found without applying any unfolding. We will consider the issue of unfolding by rescaling the spectrum in section 4.5, see in particular figure 4.7. It turns out that there are three choices of y for which the SFF is a perfectly straight line. Writing $F(n; y)_c$ to indicate dependence on y , we have

$$\begin{aligned}
F(n; 0)_c &= n , \\
F(n; 1/2)_c &= \frac{n}{2} , \\
F(n; 1)_c &= 0 . \tag{4.36}
\end{aligned}$$

The fact that $F(n; 0)_c = n$ was already mentioned in section 4.3. The last equality,

written as a limit for y , can easily be seen to be generally true and will be further commented on in section 4.6. The middle equality, on the other hand, is a priori completely unexpected (at least to the authors).

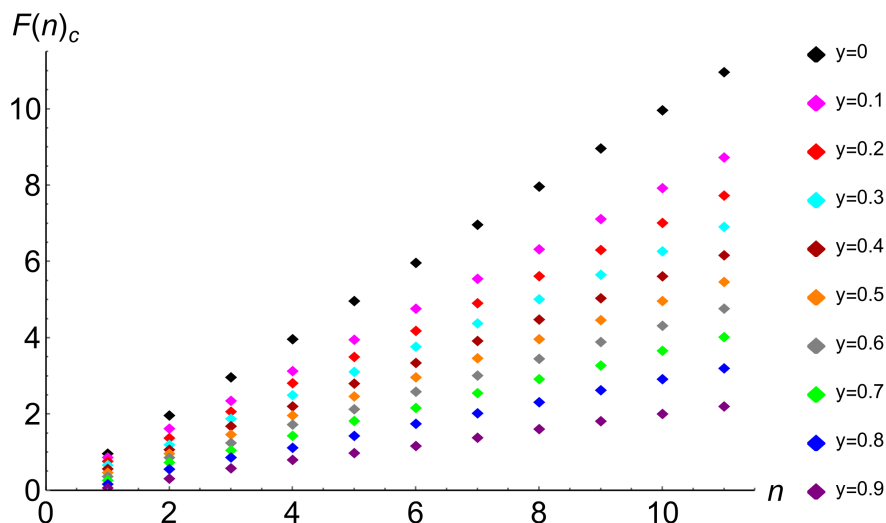


Figure 4.5: The connected SFF in the 't Hooft limit, without unfolding, written in equation (4.35). As one can see, the resulting SFF is very close to a straight line for any choice of y .

One can see from the above plot that the SFF appears to be symmetric around $F(n; 1/2)_c = \frac{n}{2}$. Indeed, we find that

$$F(n; y)_c + F(n; 1 - y)_c = n . \quad (4.37)$$

It can be seen that the polynomials $F(n)_c$ appearing in (4.35) can be factorized into the product of a factor $n(1 - y)$ and polynomials $p_n(y)$ of degree $2n - 2$. The first few of them are given below.

$$\begin{aligned}
p_1 &= 1, \\
p_2 &= 1 - y + 2y^2, \\
p_3 &= 1 - 2y + 10y^2 - 18y^3 + 12y^4, \\
p_4 &= 1 - 3y + 27y^2 - 113y^3 + 242y^4 - 250y^5 + 100y^6, \\
p_5 &= 1 - 4y + 56y^2 - 404y^3 + 1626y^4 - 3750y^5 + 4930y^6 - 3430y^7 + 980y^8, \\
p_6 &= 1 - 5y + 100y^2 - 1090y^3 + 6890y^4 - 26542y^5 + 64262y^6 - 98098y^7 \\
&\quad + 91532y^8 - 47628y^9 + 10584y^{10}, \\
p_7 &= 1 - 6y + 162y^2 - 2470y^3 + 22310y^4 - 126622y^5 + 471626y^6 - 1180606y^7 \\
&\quad + 1997492y^8 - 2251368y^9 + 1618344y^{10} - 670824y^{11} + 121968y^{12}, \\
p_8 &= 1 - 7y + 245y^2 - 4963y^3 + 60347y^4 - 469357y^5 + 2453255y^6 - 8900593y^7 + \\
&\quad + 22830194y^8 - 41649606y^9 + 53665614y^{10} - 47700378y^{11} + 27813060y^{12} \\
&\quad - 9570132y^{13} + 1472328y^{14}. \tag{4.38}
\end{aligned}$$

We were able to identify the coefficients for the following powers of y as

$$\begin{aligned}
y^0 &: 1 \\
y^1 &: -n \\
y^2 &: n^2(n+3)/2 \\
y^3 &: -n(n-1)(2+10n+6n^2+n^3)/6 \\
y^4 &: n(n-1)(-72-224n-28n^2+87n^3+40n^4+5n^5)/144 \\
y^{2n-1} &: -(C_n^{2n})^2(2n-1)/2(n+1) \\
y^{2n} &: (C_n^{2n})^2/(n+1), \tag{4.39}
\end{aligned}$$

where we have the binomial coefficient $C_n^{2n} = (2n)!/(n!)^2$. It seems that no further

information about the expansion coefficients of $p_n(y)$ can be obtained easily. This prevents us from generalizing the connected SFF beyond the 11 terms written in (4.35).

Level density

We now consider the question of unfolding in the 't Hooft limit, where we have

$$N^{-1} \langle \text{tr} U^n \rangle = \frac{1}{2n \log y} [P_n(2y-1) - P_{n-1}(2y-1)] , \quad (4.40)$$

where P_n is the Legendre polynomial. This was already found in [113]. In particular, $\langle \text{tr} U^n \rangle$ diverges in the 't Hooft limit in such a way that $N^{-1} \langle \text{tr} U^n \rangle$ is generally finite, as can be seen from taking $q \rightarrow 1$ in (4.13). We thus have a level density which is no longer flat but contains an oscillatory contribution as well,

$$\rho(\theta; y) = (2\pi)^{-1} \left[1 + \frac{1}{\log y} \sum_{n=1}^{\infty} \frac{P_n(2y-1) - P_{n-1}(2y-1)}{n} \cos(n\theta) \right] . \quad (4.41)$$

For $|t| < 1$, the generating function of the Legendre polynomials reads

$$P(x, t) = \sum_{n=0}^{\infty} P_n(x) t^n = \frac{1}{\sqrt{1-2xt+t^2}} , \quad (4.42)$$

which can be integrated to find, for $|z| < 1$,

$$\int_0^z P(x, t) = \sum_{n=1}^{\infty} \frac{P_{n-1}(x) z^n}{n} = \log \left(z - x + \sqrt{1-2xz+z^2} \right) - \log(1-x) . \quad (4.43)$$

Similarly,

$$\sum_{n=1}^{\infty} \frac{P_n(x) z^n}{n} = \log 2 - \log \left(1 - xz + \sqrt{1-2xz+z^2} \right) . \quad (4.44)$$

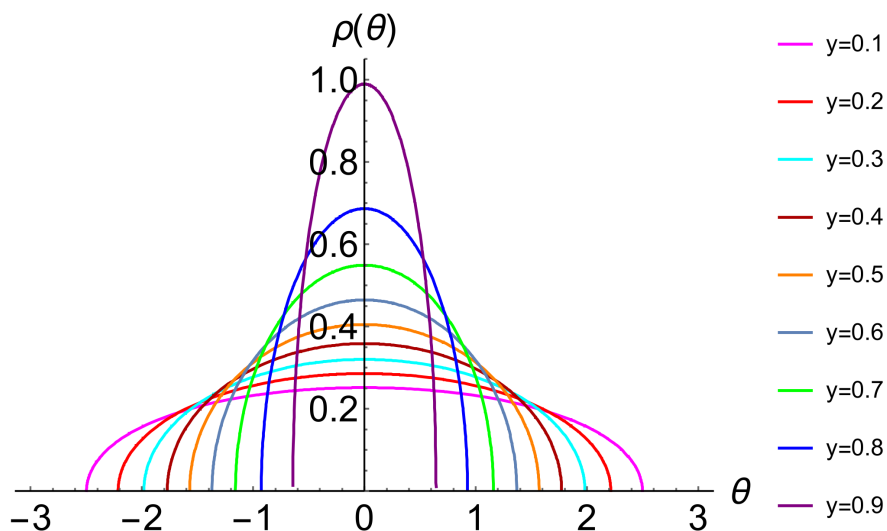


Figure 4.6: The level density in the ‘t Hooft limit plotted for various values of y . For $y > 0$, a gap opens at $\theta_c = \arccos(2y - 1)$ which increases in size with y , with the level remaining a convex function.

Using Abel’s theorem, one may find that

$$\rho(\theta; y) = \frac{1}{2\pi} + \frac{1}{2\pi \log y} [\log 2 - \log R(\cos \theta, 2y - 1)] , \quad (4.45)$$

where

$$R(z, x) = \begin{cases} (\sqrt{1+z} + \sqrt{z-x})^2 , & x < z \\ 1+x , & x \geq z . \end{cases} \quad (4.46)$$

It is easy to see that the second case listed above, $x \geq z$, gives a zero level density, since then $\log R(z, x) = \log 2y$. In particular, a gap opens in the spectrum,

$$\rho(\theta; y) = 0 , \quad \theta > \theta_c = \arccos(2y - 1) . \quad (4.47)$$

This critical angle θ_c was already found in [113], although our level density appears to be different from the expression obtained there. The resulting level densities are plotted in figure 4.6 for $y = .1, .2, \dots, .9$. One can see that these level densities are approximately of semicircular form. Indeed, writing $r(\theta; y) = \rho(0; y)\sqrt{1 - \frac{\theta^2}{\theta_c^2}}$, the difference between $\rho(\theta; y)$ and $r(\theta; y)$ for $y = 0.1, 0.2, \dots, 0.9$ remains smaller than 0.006 for all θ and decreases with y .

Unfolding

To compare the connected SFF in the 't Hooft limit with the CUE result, we have to unfold the spectrum. Strictly speaking, unfolding involves a change of variables to the staircase function, (see e.g. section 5.19 of [55]),

$$\sigma(\theta) = \int_{\theta_c}^{\theta} d\theta' \rho(\theta') . \quad (4.48)$$

The level density in terms of σ is a perfectly flat function. The unfolded SFF is then given by

$$\frac{1}{N} \langle |\sum_{j=1}^N e^{2\pi i \sigma_j}|^2 \rangle . \quad (4.49)$$

However, this unfolding procedure is often difficult in practice, and our case is no exception. Finding $\sigma(\theta)$ using the closed form expression for the level density obtained above is not very complicated, but the expression in (4.49) is not amenable to evaluation. For this reason, we instead perform a constant rescaling to a variable s in terms of which the level density $\rho(s)$ averaged over its support is independent of q^N , that is, we simply rescale so that the average spacing is the same for all y . For any value of y , we take the support of the level density and imagine we can replace the level density by a box-shaped density of the same support. We then rescale the

support so that it is again of size 2π . To do so, we write

$$s(\theta) = \frac{\pi\theta}{\theta_c}, \quad s \in [0, 2\pi), \quad (4.50)$$

so that averaging over its (rescaled) support gives

$$\bar{\rho} = \frac{1}{2\pi} \int_0^{2\pi} ds \rho(s) = \frac{1}{2\pi}. \quad (4.51)$$

In terms of the rescaled eigenphases, the level density $\rho(s)$ is of almost exactly the same shape for any $y > 0$, that is, the various densities in 4.6 are approximately related by rescaling. With this unfolding, the SFF is given by

$$\tilde{F}(n) = \left\langle \left| \sum_{j=1}^N e^{2\pi i s_j} \right|^2 \right\rangle = F\left(\frac{\pi n}{\theta_c}\right). \quad (4.52)$$

The discrete SFF, $F\left(\frac{\pi n}{\theta_c}\right)$, can only be evaluated at integer $\frac{\pi n}{\theta_c}$. However, we saw in figure 4.5 that $F(n)_c$ is very close to a linear ramp with slope ≤ 1 . That is, since

$$F(n)_c \approx f(y)n, \quad 0 \leq f(y) \leq 1, \quad (4.53)$$

the unfolded connected SFF is approximately given by

$$\tilde{F}(n)_c \approx \frac{\pi}{\theta_c} F(n)_c =: G(n), \quad (4.54)$$

which is plotted in 4.7. It is clear that $G(n)$ closely resembles a linear ramp of unit slope for all y except close to unity, with resemblance increasing with n . This entails that $f(y) \approx \frac{\theta_c}{\pi}$. Only for y close to 1 do we get a significant deviation from WD-universality, with $G(n) \rightarrow 0$ for $y \rightarrow 1^-$.

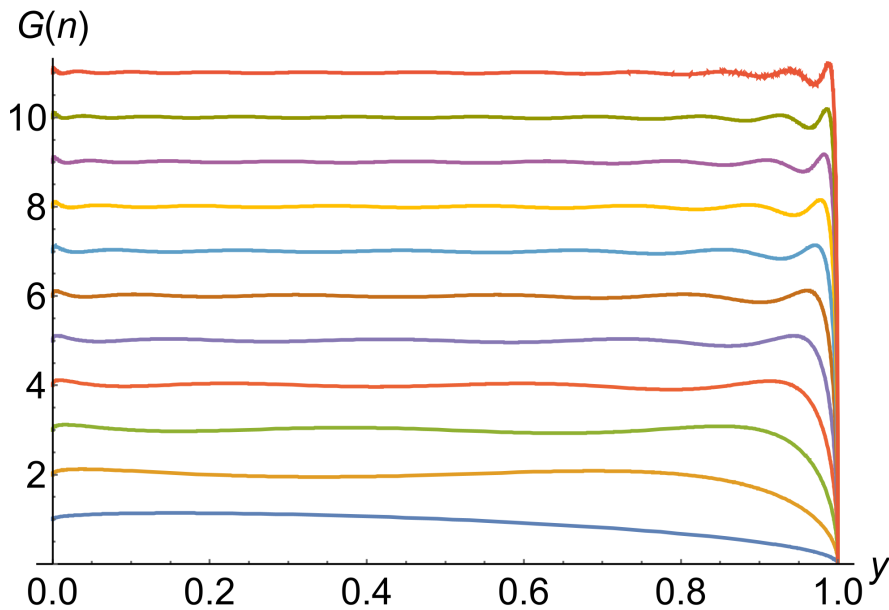


Figure 4.7: The unfolded connected SFF, $G(n) =: \frac{\pi}{\theta_c} F(n)_c$, for $n = 1, \dots, 11$. At $y = 0$, we have exactly $G(n) = n$. For $y > 0$, it is clear that $G(n) \approx n$ remains true to high precision, especially for larger n , so that the unfolded connected SFF is very close to a linear ramp with unit slope. Only for $y \rightarrow 1^-$ does $G(n)$ go to zero and is any resemblance to WD-universality lost.

This demonstrates that the unfolded connected SFF in the 't Hooft limit reproduces WD-universality to high precision for $n = 1, \dots, 11$ and for all y except $y \approx 1$. Although it might be that deviations from WD universality will emerge for lower values of y as we increase n beyond 11, the aforementioned facts that $G(n)$ is close to a linear ramp and that this precision in fact increases with n would appear to render such deviations rather unlikely. Conversely, it may be that deviations from WD will continue to be squeezed into an ever smaller interval below $y = 1$ as we increase n , but here, too, we cannot make definitive statements. We note again that the unfolding implemented here involved only a constant rescaling of the eigenphases. Perhaps unfolding as in (4.49) would remove what deviations from the linear ramp

remain in the plot below. Further, spectral form factors of various systems often display non-universal behavior close to the origin, which then disappears further away from the origin where the SFF approaches a linear ramp. The deviations seen in the plot below, except for the region $y \approx 1$, may be just such an effect.

As mentioned previously, the CSMM reduces to the CUE for $q \rightarrow 0$, where we know WD-universality to hold. We demonstrated that WD-universality holds for any $q < 1$ and $N \rightarrow \infty$ as well. The 't Hooft limit, which involves $q \rightarrow 1^-$, should then constitute the greatest possible deviation from the CUE result, yet WD-universality reappears for all y other than $y \approx 1$ after even a very simple unfolding. This would appear to be rather unexpected, as the CSMM was introduced and extensively studied as a random matrix model for intermediate statistics, as described in more detail in the introduction and section 1.4.2. We further comment on this result and its implications in the conclusion.

4.6 Non-commutativity of limits

One can see from the expression of the SFF that the limits $q \rightarrow 1$ and $N \rightarrow \infty$ do not commute. Such non-commutativity has been discussed in the literature already decades ago, see [113]. In particular, if we take $q \rightarrow 1$ into expression (1.183) for finite N , the Schur polynomials simply give the dimension of the representation, that is

$$s_\lambda(1, 1, \dots, 1) = \dim \lambda . \quad (4.55)$$

Plugging this into (1.183) with $\lambda = (n - r, 1^r)$ and $\mu = (n - s, 1^s)$ shows that the SFF would be simply given by

$$\left(\sum_{r=0}^{n-1} (-1)^r \frac{(N + n - r - 1)!}{(N - r - 1)!(n - r - 1)!r!n} \right)^2 = N^2 . \quad (4.56)$$

for all n . In terms of knot theory, we see that taking $q \rightarrow 1$ for N finite breaks the $(2n, 2)$ -torus link that is the SFF up into its separate $(n, 1)$ -torus knot components, as we have

$$\lim_{q \rightarrow 1} \langle |\text{tr} U^n|^2 \rangle = \lim_{q \rightarrow 1} \langle \text{tr} U^n \rangle \langle \text{tr} U^{-n} \rangle = \lim_{q \rightarrow 1} (\langle \text{tr} U^n \rangle)^2 . \quad (4.57)$$

The connected SFF then equals zero, as was the case in section 4.5. We consider the case where $t = Ng_s \ll 1$ is very small. This allows us to use the following expansion [[33] I.3, example 10],

$$s_\lambda(1 + x_1, 1 + x_2, \dots, 1 + x_N) = \sum_{\mu} d_{\lambda\mu} s_\mu(x_1, \dots, x_N) , \quad (4.58)$$

where we sum over all $\mu \subseteq \lambda$ and where

$$d_{\lambda\mu} = \det \left(\begin{array}{c} \lambda_i + n - 1 \\ \mu_j + n - j \end{array} \right)_{1 \leq i, j \leq N} . \quad (4.59)$$

Some simple examples are given by (see e.g. [121])

$$d_{\lambda\emptyset} = \dim \lambda \quad , \quad d_{\lambda\Box} = \dim \lambda \frac{c_1(\lambda)}{N} , \quad (4.60)$$

where the first Casimir invariant is given by $c_1(\lambda) = |\lambda| = \sum_i \lambda_i$. For $q = e^{-g_s}$ close to 1 and $Ng_s \ll 1$, we see that $s_{(a,1^b)}(q^{j-1})$ is approximately given by

$$s_{(a,1^b)}(1, 1 - g_s, 1 - 2g_s, \dots) = \sum_{\mu} d_{(a,1^b)\mu} s_\mu(0, -g_s, -2g_s, \dots) . \quad (4.61)$$

Expanding up to linear order in g_s , we only get contributions for $\mu = \emptyset$ and $\mu = \square$, which gives

$$\begin{aligned} s_{(a,1^b)}(0, -g_s, -2g_s, \dots) &= \dim(a, 1^b) \left(1 + \frac{a+b}{N}(-g_s - 2g_s - \dots) \right) \\ &= \dim(a, 1^b) \left(1 - \frac{(a+b)(N-1)}{2} g_s \right). \end{aligned} \quad (4.62)$$

Further, $s_{(a,1^b)}(q^{-c}, 1, q, \dots, q^{d-1}, q^{d+1}, \dots, q^{N-1})$ is approximately given by $s_{(a,1^b)}(cg_s, -g_s, \dots, -(d-1)g_s, -(d+1)g_s, \dots)$, which equals

$$\dim(a, 1^b) \left[1 + (a+b) \left(\frac{1-N}{2} + \frac{c+d}{N} \right) g_s \right] \quad (4.63)$$

Plugging this into (1.183) for $\lambda = (n-r, 1^r)$ and $\mu = (n-s, 1^s)$ gives

$$\langle W_{\lambda\mu} \rangle - \langle W_\lambda \rangle \langle W_\mu \rangle = \dim(n-r, 1^r) \dim(n-s, 1^s) \frac{n^2 g_s}{N} + \mathcal{O}(g_s^2) \quad (4.64)$$

We thus see that, to first order in Ng_s , the Wilson loop factorizes, so that

$$F(n)_c = tn^2 + \mathcal{O}(t^2). \quad (4.65)$$

If we now take $N \rightarrow \infty$ in such a way that t remains small, we clearly get a very different result from the linear ramp $F(n)_c = n$ that is found when taking $q \rightarrow 1$ after $N \rightarrow \infty$. Indeed, one may check that the connected SFF in the 't Hooft limit for small n and $y \lesssim 1$ is very close to tn^2 .

Concluding remarks

This thesis treated unitary integrals over symmetric polynomials, their evaluation, and their application to long-range random walkers and the spectral statistics of unitary random matrix ensembles. The introduction and chapter 1 gave an overview of the thesis and reviewed the relevant background material in decreasing order of generality, starting from symmetric functions and the evaluation of their unitary integrals, then treating LRRW models and spectral statistics of RME's, including the particular example of the Chern–Simons matrix model. Chapter 2 proceeded with the derivation of our mathematical results, which focused on the case where the strong Szegő limit theorem applies. Here, we derived three expansions for unitary integrals over symmetric polynomials. Chapter 3 applied these results, as well as basic identities from symmetric function theory, to LRRW models. This leads to various relations between these correlation functions and convenient ways to compute them, as well as auxiliary results on fermionic models. Chapter 4 then considered the application to spectral statistics, focusing in particular on the calculation of the spectral form factor for the CSMM.

The mathematical results presented here generalize previous results in various ways. Our expression for unitary integrals over generalized power sums generalizes a long-standing result due to Diaconis and Shahshahani, whose result for the CUE constitutes the last term in our expansion. The two expansions we found for unitary

integrals over Schur bilinears provide expansions in either non-skew Schur or power sum polynomials. These make use of the iterative structure of the symmetric group characters, allowing for controlled expansions of complicated expectation values, which provides a distinct advantage over the expansion in terms of skew Schur polynomials that was our starting point. This is because there are many more skew diagrams than non-skew ones which tends to obfuscate the underlying structure of an expression in terms of skew Schur polynomials. The unitary integrals considered in this work arise in a wide variety of contexts, some of which were mentioned in the introduction and chapter 1, where the expressions derived here may find further application.

Chapter 3 was mostly concerned with hard-core bosonic LRRW models, which have various physical applications and implementations. First of all, LRRW models such as we consider here have seen increasing activity in both experimental and theoretical contexts due to the experimental accessibility of such systems and the surprising phenomena they exhibit. We believe our work can be applied along some of these lines of research, including the consideration of localization by addition of (diagonal) disorder [16], [17]. Adding such disorder will generally break translational invariance, and the expressions in this work will no longer apply. One may also consider translationally invariant disorder such as random hopping parameters, as in [18], [19], in which case the results derived here would still apply as long as the hopping parameters satisfy the aforementioned asymptotic fall-off conditions. All results in chapter 3 can, in principle, be checked experimentally, where the expressions would be expected to hold up to the time that finite size effects start to occur. Besides checking our results in experimental setups, we identified correlation functions involving power sum polynomials which may be used for experimental benchmarking. Further, we saw that the multiplication properties of power sum polynomials bear close relation to long-range fermionic models. This opens up the possibility of applying the fermionic picture to the computation of symmetric group characters.

Further, this led to the derivation of some results on fermionic models. These have direct physical implications, such as the fact that 1D models where fermions can only hop a distance of n sites are not restricted by destructive interference. These results can also be tested in long-range systems, but then of a fermionic rather than hard-core bosonic type.

We then applied our results to the spectral statistics of unitary RME's. In case Szegő's strong limit theorem applies, we saw that a special case of the first result derived in chapter 2 states that the connected SFF exhibits Wigner–Dyson-universality, consisting of a linear ramp of unit slope which saturates at a plateau. The remainder of chapter 4 focused on the Chern–Simons matrix model, where we first consider general matrix size N and ‘disorder parameter’ q , before taking the ‘t Hooft limit. In all cases, we recover WD-universality upon unfolding. As described in the introduction, the CSMM was originally introduced [4] to describe the intermediate statistics of disordered electrons at the mobility edge, and there is a significant amount of literature on this application of the CSMM and related ensembles, see e.g. [6], [7], [8], [9], [10], [11], [12], [13]. Indeed, the ‘t Hooft limit involves $q \rightarrow 1$, which is the opposite extreme of the CUE limit, $q \rightarrow 0$, yet WD-universality is recovered even here, including for all $y = q^N$ except $y \approx 1$. We do not know at this stage how to reconcile our results with previous works on the CSMM, whose authors did find intermediacy. It should be noted that their analysis centered on the hermitian version of the CSMM where the weight function is $\sim e^{-\alpha \log^2(x)}$ for $x \in \mathbb{R}$, and it employed the theory of orthogonal polynomials and kernels rather than expanding in Schur bilinears. These differences in choice of model and treatment complicate the comparison between our results and earlier work. With Wouter Buijsman, who generated the data for figure 4.4, we are currently working to clarify the question of intermediacy in the CSMM through numerical means.

Some of the results derived in chapter 4 may also be of mathematical interest.

As mentioned in chapter 4, the SFF is proportional to the HOMFLY invariant of a $(2n, 2)$ -torus link with components carrying fundamental and antifundamental representations. The calculation of the SFF thus provides explicit expressions for new link invariants, both for general q, N as well as in the 't Hooft limit. Due to the relation of $U(N)$ Chern–Simons theory at large N with various topological string theories, and its application to enumerative geometry and intersection theory, the results derived here could be of mathematical interest beyond knot theory.

Bibliography

- [1] W.L. Vleeshouwers and V. Gritsev. Unitary matrix integrals, symmetric polynomials, and long-range random walks. *Journal of Physics A: Mathematical and Theoretical*, 56(18):185002, 2023.
- [2] W.L. Vleeshouwers and V. Gritsev. Topological field theory approach to intermediate statistics. *SciPost Phys.*, 10:146, 2021.
- [3] W.L. Vleeshouwers and V. Gritsev. The spectral form factor in the 't Hooft limit – Intermediacy versus universality. *SciPost Phys. Core*, 5:051, 2022.
- [4] K.A. Muttalib, Y. Chen, M.E.H. Ismail, and V.N. Nicopoulos. New family of unitary random matrices. *Phys. Rev. Lett.*, 71:471–475, 1993.
- [5] M. Marino. Chern-Simons theory, matrix integrals, and perturbative three manifold invariants. *Commun. Math. Phys.*, 253:25–49, 2004.
- [6] K. A. Muttalib, Y. Chen, and M. E. H. Ismail. q-random matrix ensembles. In Ismail M.E.H. Garvan F.G., editor, *Symbolic Computation, Number Theory, Special Functions, Physics and Combinatorics.*, pages 199–221. Springer, Boston, MA, 2001.
- [7] V.E. Kravtsov and K.A. Muttalib. New class of random matrix ensembles with multifractal eigenvectors. *Phys. Rev. Lett.*, 79:1913–1916, 1997.

- [8] C.M. Canali. Model for a random-matrix description of the energy-level statistics of disordered systems at the anderson transition. *Phys. Rev. B*, 53:3713–3730, 1996.
- [9] C. Blecken, Y. Chen, and K.A. Muttalib. Transitions in spectral statistics. *Journal of Physics A: Mathematical and General*, 27(16):L563–L568, 1994.
- [10] C.M. Canali and V.E. Kravtsov. Normalization sum rule and spontaneous breaking of $u(n)$ invariance in random matrix ensembles. *Phys. Rev. E*, 51:R5185–R5188, 1995.
- [11] S.M. Nishigaki. Level spacings at the metal-insulator transition in the anderson hamiltonians and multifractal random matrix ensembles. *Physical Review E*, 59(3):2853, 1999.
- [12] E. Bogomolny, O. Bohigas, and M.P. Pato. Distribution of eigenvalues of certain matrix ensembles. *Phys. Rev. E*, 55:6707–6718, 1997.
- [13] V. Kravtsov. Random matrix representations of critical statistics. In *The Oxford Handbook of Random Matrix Theory*. Oxford University Press, 2015.
- [14] A. Friedenauer, H. Schmitz, J. Glueckert, D. Porras, and T. Schätz. Simulating a quantum magnet with trapped ions. *Nature Physics*, 4:757–761, 2008.
- [15] N. Defenu, T. Donner, T. Macrì, G. Pagano, S. Ruffo, and A. Trombettoni. Long-range interacting quantum systems. arXiv:2109.01063, 2021.
- [16] X. Deng, V.E. Kravtsov, G.V. Shlyapnikov, and L. Santos. Duality in power-law localization in disordered one-dimensional systems. *Physical Review Letters*, 120(11), 2018.
- [17] P.A. Nosov, I.M. Khaymovich, and V.E. Kravtsov. Correlation-induced localization. *Physical Review B*, 99(10), 2019.

- [18] E. Bogomolny. Spectral statistics of random toeplitz matrices. *Physical Review E*, 102(4):040101, 2020.
- [19] E. Bogomolny and O. Giraud. Statistical properties of structured random matrices. *Physical Review E*, 103(4):042213, 2021.
- [20] L. Santilli and M. Tierz. Phase transition in complex-time Loschmidt echo of short and long range spin chain. *Journal of Statistical Mechanics: Theory and Experiment*, 2020(6):063102, 2020.
- [21] C. Malyshev and N.M. Bogoliubov. Heisenberg XX chain, non-homogeneously parameterised generating exponential, and diagonally restricted plane partitions. arxiv.2011.05148, 2020.
- [22] E.A. Yuzbashyan and B.L. Altshuler. Migdal-Eliashberg theory as a classical spin chain. *Phys. Rev. B*, 106:014512, 2022.
- [23] N.M. Bogoliubov. XX0 heisenberg chain and random walks. *Journal of Mathematical Sciences*, 138:5636–5643, 2006.
- [24] N.M. Bogoliubov, A.G. Pronko, and J. Timonen. Scaling of many-particle correlations in a dissipative sandpile, 2011.
- [25] N.M. Bogoliubov and C. Malyshev. Correlation functions of xx0 heisenberg chain, q-binomial determinants, and random walks. *Nuclear Physics B*, 879:268–291, 2014.
- [26] D. Pérez-García and M. Tierz. Chern–Simons theory encoded on a spin chain. *J. Stat. Mech.*, 1601(1):013103, 2016.
- [27] P. Diaconis and M. Shahshahani. On the eigenvalues of random matrices. *Journal of Applied Probability*, 31(A):49–62, 1994.

-
- [28] P. Diaconis and S. Evans. Linear functionals of eigenvalues of random matrices. *Transactions of the American Mathematical Society*, 353, 2000.
- [29] I.N. Stewart. *Galois Theory, Fourth Edition*. Taylor & Francis, 2015.
- [30] W. Fulton and W.F.J. Harris. *Representation Theory: A First Course*. Graduate Texts in Mathematics. Springer New York, 1991.
- [31] R.P. Stanley and S. Fomin. *Enumerative Combinatorics: Volume 2*. Cambridge Studies in Advanced Mathematics. Cambridge University Press, 1999.
- [32] R. Bott and L.W. Tu. *Differential forms in algebraic topology*. Graduate texts in mathematics. Springer New York, NY, 1982.
- [33] I.G. Macdonald. *Symmetric Functions and Hall Polynomials*. Oxford classic texts in the physical sciences. Clarendon Press, 1998.
- [34] G. James and A. Kerber. *The Representation Theory of the Symmetric Group*. Encyclopedia of Mathematics and its Applications. Cambridge University Press, 1984.
- [35] D.E. White. A bijection proving orthogonality of the characters of sn . *Advances in Mathematics*, 50(2):160–186, 1983.
- [36] A. Böttcher and B. Silbermann. *Introduction to large truncated Toeplitz matrices*. Springer, 2012.
- [37] I.M. Gessel. Symmetric functions and p -recursiveness. *Journal of Combinatorial Theory, Series A*, 53(2):257 – 285, 1990.
- [38] J. Baik, P. Deift, and K. Johansson. On the distribution of the length of the longest increasing subsequence of random permutations. *Journal of the American Mathematical Society*, 12(4):1119–1178, 1999.

- [39] C.A. Tracy and H. Widom. On the distributions of the lengths of the longest monotone subsequences in random words. *Probability Theory and Related Fields*, 119(3):350–380, 2001.
- [40] D. Bump and P. Diaconis. Toeplitz minors. *Journal of Combinatorial Theory, Series A*, 97(2):252 – 271, 2002.
- [41] D. García-García and M. Tierz. Toeplitz minors and specializations of skew schur polynomials. *Journal of Combinatorial Theory, Series A*, 172:105201, 2020.
- [42] D. García-García and M. Tierz. Matrix models for classical groups and toeplitz \pm hankel minors with applications to chern–simons theory and fermionic models. *Journal of Physics A: Mathematical and Theoretical*, 53(34):345201, 2020.
- [43] G Szegő. Ein Grenzwertsatz über die Toeplitzschen Determinanten einer reellen positiven Funktion. *Math. Ann.*, 76:490–503, 1915.
- [44] H. Weyl. *The Classical Groups: Their Invariants and Representations*. Princeton University Press, 1966.
- [45] C. Andréief. Note sur une relation entre les intégrales définies des produits des fonctions. *Mém. Soc. Sci. Phys. Nat. Bordeaux*, 3:1–14, 1886.
- [46] M.E. Fisher. Walks, walls, wetting, and melting. *Journal of Statistical Physics*, 34:667–729, 1984.
- [47] P. J. Forrester. Vicious random walkers in the limit of a large number of walkers. *Journal of Statistical Physics*, 56(5-6):767–782, 1989.
- [48] P.J. Forrester. Exact solution of the lock step model of vicious walkers. *Journal of Physics A: Mathematical and General*, 23(7):1259–1273, 1990.

- [49] T. Nagao and P.J. Forrester. Vicious random walkers and a discretization of gaussian random matrix ensembles. *Nuclear Physics B*, 620(3):551–565, 2002.
- [50] K. Hikami and T. Imamura. Vicious walkers and hook Young tableaux. *Journal of Physics A: Mathematical and General*, 36(12):3033–3048, 2003.
- [51] J. Viti, J.M. Stéphan, J. Dubail, and M. Haque. Inhomogeneous quenches in a fermionic chain: exact results. *EPL (Europhysics Letters)*, 115, 2015.
- [52] L. Wei, R. Pitaval, and O. Tirkkonen J. Corander. From random matrix theory to coding theory: Volume of a metric ball in unitary group. *IEEE Transactions on Information Theory*, PP, 2015.
- [53] P.L. Krapivsky, J.M. Luck, and K. Mallick. Quantum return probability of a system of n non-interacting lattice fermions. *Journal of Statistical Mechanics: Theory and Experiment*, 2018(2):023104, 2018.
- [54] P. Zinn-Justin. Six-vertex, loop and tiling models: integrability and combinatorics. arXiv:0901.0665, 2009.
- [55] F. Haake, S. Gnutzmann, and M. Kuś. *Quantum Signatures of Chaos*. Physics and astronomy online library. Springer, 2001.
- [56] H.A. Weidenmuller T. Guhr, A. Muller-Groeling. Random matrix theories in quantum physics: Common concepts. *Phys. Rept.*, 299:189–425, 1998.
- [57] H.J. Stöckmann. *Quantum Chaos: An Introduction*. Cambridge University Press, 1999.
- [58] P. Bourgade and J.P. Keating. *Quantum Chaos, Random Matrix Theory, and the Riemann ζ -function*, pages 125–168. Springer Basel, Basel, 2013.
- [59] J. Wishart. The generalised product moment distribution in samples from a normal multivariate population. *Biometrika*, 20A(1-2):32–52, 1928.

- [60] E.P. Wigner. Characteristic vectors of bordered matrices with infinite dimensions. *Annals of Mathematics*, 62(3):548–564, 1955.
- [61] O. Bohigas, M. J. Giannoni, and C. Schmit. Characterization of chaotic quantum spectra and universality of level fluctuation laws. *Phys. Rev. Lett.*, 52:1–4, 1984.
- [62] S. Ma, G. Grinstein, and G. Mazenko. *Directions in Condensed Matter Physics: Memorial Volume in Honor of Shang-keng Ma*. Directions in condensed matter physics. World Scientific, 1986.
- [63] C.W.J. Beenakker. Random-matrix theory of quantum transport. *Reviews of Modern Physics*, 69(3):731–808, 1997.
- [64] J.J.M. Verbaarschot and T. Wettig. Random matrix theory and chiral symmetry in qcd. *Annual Review of Nuclear and Particle Science*, 50(1):343–410, 2000.
- [65] P. Di Francesco, P. Ginsparg, and J. Zinn-Justin. 2d gravity and random matrices. *Physics Reports*, 254(1-2):1–133, 1995.
- [66] J.P. Bouchaud and M> Potters. Financial applications of random matrix theory: a short review. *arXiv:0910.1205*, 2009.
- [67] A. Edelman and Y. Wang. *Random Matrix Theory and Its Innovative Applications*, pages 91–116. Springer US, Boston, MA, 2013.
- [68] H.L Montgomery. The pair correlation of zeros of the zeta function. In *Proc. Symp. Pure Math*, volume 24, pages 181–193, 1973.
- [69] P. Saad, S.H. Shenker, and D. Stanford. A semiclassical ramp in SYK and in gravity. 2019.

-
- [70] A.M. García-García and J.J.M. Verbaarschot. Spectral and thermodynamic properties of the sachdev-ye-kitaev model. *Physical Review D*, 94(12), 2016.
- [71] J.S. Cotler, G. Gur-Ari, M. Hanada, J. Polchinski, P. Saad, S.H. Shenker, D. Stanford, A. Streicher, and M. Tezuka. Black holes and random matrices. *Journal of High Energy Physics*, 2017(5), 2017.
- [72] A. Altland and D. Bagrets. Quantum ergodicity in the syk model. *Nuclear Physics B*, 930:45–68, 2018.
- [73] A. Altland and J. Sonner. Late time physics of holographic quantum chaos. *SciPost Physics*, 11(2), 2021.
- [74] A. Belin, J. de Boer, P. Nayak, and J. Sonner. Generalized spectral form factors and the statistics of heavy operators. 2021.
- [75] G. Casati, F. Valz-Gris, and I. Guarneri. On the connection between quantization of nonintegrable systems and statistical theory of spectra. *Lettere al Nuovo Cimento (1971-1985)*, 28(8):279–282, 1980.
- [76] M.V. Berry. Quantizing a classically ergodic system: Sinai’s billiard and the kkr method. *Annals of Physics*, 131(1):163 – 216, 1981.
- [77] M.L. Mehta. *Random Matrices*. Academic Press, 1991.
- [78] M.V. Berry and M. Tabor. Level clustering in the regular spectrum. *Proceedings of the Royal Society of London. A. Mathematical and Physical Sciences*, 356(1686):375–394, 1977.
- [79] J. Marklof. The berry-tabor conjecture. In Carles Casacuberta, Rosa Maria Miró-Roig, Joan Verdera, and Sebastià Xambó-Descamps, editors, *European Congress of Mathematics*, pages 421–427, Basel, 2001. Birkhäuser Basel.

- [80] Ya G. Sinai. Dynamical systems with elastic reflections. *Russian Mathematical Surveys*, 25(2):137–189, 1970.
- [81] T. Tao and V. Vu. Random matrices: The universality phenomenon for wigner ensembles. 2012.
- [82] F.J. Dyson. Statistical theory of the energy levels of complex systems. *Journal of Mathematical Physics*, 3(1):140, 157, 166, 1962.
- [83] F. Evers and A.D. Mirlin. Anderson transitions. *Rev. Mod. Phys.*, 80:1355–1417, 2008.
- [84] E. B. Bogomolny, U. Gerland, and C. Schmit. Models of intermediate spectral statistics. *Phys. Rev. E*, 59:R1315–R1318, 1999.
- [85] M. Gaudin. Une famille à un paramètre d’ensembles unitaires. *Nuclear Physics*, 85(3):545–575, 1966.
- [86] T. Yukawa. New approach to the statistical properties of energy levels. *Phys. Rev. Lett.*, 54:1883–1886, 1985.
- [87] A. D. Mirlin, Y. V. Fyodorov, F. M. Dittes, J. Quezada, and T. H. Seligman. Transition from localized to extended eigenstates in the ensemble of power-law random banded matrices. *Phys. Rev. E*, 54:3221–3230, 1996.
- [88] M. Moshe, H. Neuberger, and B. Shapiro. Generalized ensemble of random matrices. *Phys. Rev. Lett.*, 73:1497–1500, 1994.
- [89] E. Bogomolny, O. Giraud, and C. Schmit. Random matrix ensembles associated with lax matrices. *Physical Review Letters*, 103(5), 2009.
- [90] E. Bogomolny and O. Giraud. Eigenfunction entropy and spectral compressibility for critical random matrix ensembles. *Phys. Rev. Lett.*, 106:044101, 2011.

- [91] V.E. Kravtsov, I.M. Khaymovich, E. Cuevas, and M. Amini. A random matrix model with localization and ergodic transitions. *New Journal of Physics*, 17(12):122002, 2015.
- [92] N. Rosenzweig and C.E. Porter. "repulsion of energy levels" in complex atomic spectra. *Phys. Rev.*, 120:1698–1714, 1960.
- [93] I. Dumitriu and A. Edelman. Matrix models for beta ensembles. *Journal of Mathematical Physics*, 43(11):5830–5847, 2002.
- [94] W. Buijsman, V. Cheianov, and V. Gritsev. Random matrix ensemble for the level statistics of many-body localization. *Phys. Rev. Lett.*, 122:180601, 2019.
- [95] E. Witten. Chern-Simons gauge theory as a string theory. *Prog. Math.*, 133:637–678, 1995.
- [96] E. Witten. Quantum field theory and the jones polynomial. *Comm. Math. Phys.*, 121(3):351–399, 1989.
- [97] M. Aganagic, A. Klemm, M. Marino, and C. Vafa. Matrix model as a mirror of Chern-Simons theory. *JHEP*, 02:010, 2004.
- [98] E. Witten. Analytic Continuation Of Chern-Simons Theory. *AMS/IP Stud. Adv. Math.*, 50:347–446, 2011.
- [99] M. Tierz. Soft matrix models and Chern-Simons partition functions. *Mod. Phys. Lett. A*, 19:1365–1378, 2004.
- [100] J.M.F. Labastida, P.M. Llatas, and A.V. Ramallo. Knot operators in Chern-Simons gauge theory. *Nucl. Phys.*, B348:651–692, 1991.
- [101] M. Mariño. *Chern-Simons Theory, Matrix Models, and Topological Strings*. Oxford University Press, 2005.

- [102] B.A. Dubrovin, A.T. Fomenko, and S.P. Novikov. *Modern Geometry - Methods and Applications, vol. 1*. Springer-Verlag, 1992.
- [103] J.P. Tignol. *Galois' Theory of Algebraic Equations*. World Scientific, 2001.
- [104] J.M.F. Labastida J.M. Isidro and A.V. Ramallo. Polynomials for torus links from chern-simons gauge theories. *Nuclear Physics B*, 398(1):187 – 236, 1993.
- [105] J.M.F. Labastida and M. Marino. The HOMFLY polynomial for torus links from Chern-Simons gauge theory. *Int. J. Mod. Phys.*, A10:1045–1089, 1995.
- [106] T. Okuda. Derivation of Calabi-Yau crystals from Chern-Simons gauge theory. *JHEP*, 03:047, 2005.
- [107] Y. Dolivet and M. Tierz. Chern-Simons matrix models and Stieltjes-Wigert polynomials. *J. Math. Phys.*, 48:023507, 2007.
- [108] A. Brini, Eynard B, and M. Marino. Torus knots and mirror symmetry. *Annales Henri Poincare*, 13:1873–1910, 2012.
- [109] S. Stevan. Chern-Simons Invariants of Torus Links. *Annales Henri Poincare*, 11:1201–1224, 2010.
- [110] G. Giasemidis and M. Tierz. Torus knot polynomials and susy Wilson loops. *Lett. Math. Phys.*, 104:1535–1556, 2014.
- [111] M. Rosso and V. Jones. On the invariants of torus knots derived from quantum groups. *J. Knot Theor. Ramifications*, 2:97, 1993.
- [112] J.M.F. Labastida and M. Marino. Polynomial invariants for torus knots and topological strings. *Commun. Math. Phys.*, 217:423–449, 2001.
- [113] E. Onofri. $Su(n)$ lattice gauge theory with villain's action. *Il Nuovo Cimento A*, 66, 1981.

- [114] G.'t Hooft. A planar diagram theory for strong interactions. *Nuclear Physics B*, 72(3):461–473, 1974.
- [115] R. Gopakumar and C. Vafa. On the gauge theory / geometry correspondence. *Adv. Theor. Math. Phys.*, 3:1415–1443, 1999.
- [116] M. Aganagic, A. Klemm, and C. Vafa. Disk instantons, mirror symmetry and the duality web. *Z. Naturforsch. A*, 57:1–28, 2002.
- [117] H. Ooguri and C. Vafa. Knot invariants and topological strings. *Nucl. Phys.*, B577:419–438, 2000.
- [118] H. Ooguri and C. Vafa. World sheet derivation of a large N duality. *Nucl. Phys. B*, 641:3–34, 2002.
- [119] C. Blecken and K.A. Muttalib. Brownian motion model of a q-deformed random matrix ensemble. *Journal of Physics A*, 31:2123–2132, 1998.
- [120] K.A. Muttalib and M.E.H. Ismail. Impact of localization on dyson's circular ensemble. *Journal of Physics A: Mathematical and General*, 28(21):L541–L548, 1995.
- [121] B. Fiol and F. Torrents. Exact results for Wilson loops in arbitrary representations. *JHEP*, 1:1029–8479, 2014.

Dankwoord

Het doorlopen van een promotie is voor velen een erg betekenisvol en leerzaam proces en ik ben daarop geen uitzondering. Tegelijkertijd kan het een vrij uitdagende en solistische periode zijn, des te meer als het uitbreken van corona tot gevolg heeft dat het normale maatschappelijk en ook academische leven grotendeels tot stilstand komt. Ondanks dat was deze periode voor mij enorme verrijking, zowel in intellectueel als persoonlijk opzicht. Daarnaast was het ook, over het algemeen, erg leuk om te doen, op uitzonderingen als het nakijken van inleveropgaven na. Ik wil hier graag de mensen bedanken die dat mogelijk hebben gemaakt.

Allereerst wil ik hiervoor mijn eerste begeleider, Vladimir Gritsev, bedanken. Van het begin af aan heeft hij me alle vrijheid en vertrouwen gegeven om mijn eigen ideeën te ontwikkelen, ook als hij zijn bedenkingen had, die over het algemeen achteraf terecht bleken. Daarnaast is hij zeer betrokken en heeft hij me veel gesteund bij mijn persoonlijke keuzes van de afgelopen jaren. Bovenal wil ik hem bedanken voor de interessante en stimulerende maar vooral ook erg gezellige tijd die ik met hem heb doorgebracht. Ook aan mijn tweede begeleider, Cristiane de Morais-Smith, ben ik dank verschuldigd, voor de sfeer in haar groep en de samenwerkingen die ze weet te creëren. De diverse bachelor- en masterscripties die ik samen met haar begeleid heb waren ook voor mij erg leerzaam. Verder wil ik graag Francisco García Flórez bedanken voor zijn goede gezelschap op kantoor en daarbuiten en voor zijn advies

tijdens de laatste maanden van mijn promotietraject. Ook wil ik Wouter Buijsman bedanken, die ik beter heb leren kennen tijdens een conferentie in Bielefeld en dankzij wie het onderzoek van Vladimir en mij met een numeriek perspectief wordt verrijkt. Ook wil ik Jiří Minář bedanken voor zijn goede gezelschap en interessante gesprekken. Hetzelfde geldt voor Diego Liška, met wie Jiří, Vladimir en ik het chaotische gedrag van zwarte gaten proberen te doorgronden. Verder wil ik Miguel Tierz bedanken voor onze uitgebreide en interessante correspondentie en Sebastian de Haro voor zijn advies aan het begin van mijn promotietraject. Verder wil ik Vladimir Kravtsov, Ivan Khaymovich en Peter Forrester bedanken voor het delen van ideeën en literatuur en omdat ze me de kans hebben gegeven om mijn onderzoek bij een conferentie en een online lezing te presenteren. Daarnaast wil ik Geert Kapteijns bedanken, met wie ik erg interessante gesprekken heb gevoerd die vaker niet over natuurkunde gingen dan wel. Andere (oud-)collega's van de UvA die ik zou willen bedanken zijn Daniel Chernowitz, Bart van Voorden, Yuan Miao, Neil Robinson, Bart de Klerk, Rebecca Koch, Jans Henke, Boris Ponsioen, Liam Bond en Antonio Rotundo. Ook wil ik Kareljan Schoutens bedanken, die mijn onafhankelijk begeleider was gedurende de afgelopen vier jaren en in die rol structuur creëerde en goede adviezen kon geven. Ook wil ik Marcel Vonk, Jasper van Wezel en Mikhail Isachenkov bedanken voor de interessante gesprekken die we hebben gehad.

Naast de UvA heb ik ook aan de UU in Utrecht gewerkt, al zij het in mindere mate. Graag wil ik mijn (voormalig) kantoorgenoten Chongchuo Li, Robin Verstraten, Anouar Moustaj, Rodrigo Arouca en Rodrigo Ozela bedanken voor de relatief weinige maar gezellige tijd die we samen hebben doorgebracht, alsook Enea Mauri, Jurriaan Wouters, Peter Sterk, Jette van den Broeke en Emmanuelle Di Salvo. Daarnaast ben ik dankbaar voor de ervaringen die ik heb opgedaan bij het begeleiden van bachelor- en masterstudenten, namelijk die van Joppe Stokvis en Koen van der Zee, die ik samen met Robin Verstraten dagelijkse begeleiding gaf, Stan de Lange, Stefan Boere en Chen Chao, wiens onderzoek we momenteel met

Dankwoord

hem, Cristiane, Vladimir en ikzelf in publiceerbare vorm aan het brengen zijn.

Naast mijn collega's wil ik graag mijn vrienden bedanken, met wie ik de afgelopen jaren veel mooie ervaringen heb gedeeld. Mijn allergrootste dank gaat uit naar mijn verloofde, die zo'n lieve moeder is en wiens dagelijkse steun en aanmoediging een belangrijke bijdrage hebben geleverd aan het tot stand komen van dit proefschrift. Verder wil ik graag mijn familie bedanken, mijn ouders en mijn zus en ook mijn schoonouders, schoonzus en zwagers, voor hun hulp en hun goede adviezen gedurende de afgelopen jaren.

Lekensamenvatting

Deze lekensamenvatting biedt een kort overzicht van de verschillende onderwerpen die in dit proefschrift behandeld worden. Als eerste worden hier Young-diagrammen beschouwd, alsook de rol die ze spelen in het berekenen van bepaalde wiskundige objecten; zogenaamde unitaire matrixintegralen. Deze objecten hebben verschillende natuurkundige toepassingen waarvan er hier twee belicht worden, namelijk lange-afstands-toevalsbewegingen en chaotische kwantumsystemen.

In dit proefschrift worden, in brede zin, toevalsprocessen onderzocht, zoals het opgooien van een munt of een dobbelsteen. De objecten die in dit proefschrift beschouwd worden zijn echter geen munten of dobbelstenen, maar zogenaamde Young-diagrammen. Dit zijn een soort blokkentorens, waarvan er op de volgende pagina een voorbeeld weergegeven is. Stel dat een kind een blokkentoren probeert te bouwen in een kamer waarvan de vloer erg scheef is, zodat dus de enige manier om te voorkomen dat de blokken van elkaar af schuiven is om de toren met één kant tegen de linkermuur van de kamer te bouwen. Dit betekent dat de blokkentoren vanaf links en onder gebouwd wordt, zodat later geplaatste blokken zich rechts en/of boven eerder geplaatste blokken bevinden. Dit leidt bijvoorbeeld tot de blokkentoren die op de volgende pagina is weergegeven. In deze blokkentoren zijn getallen in de blokken geschreven. Dit object wordt strikt gezien een Young-*tableau* genoemd in plaats van een Young-diagram, maar dit is hier verder niet van belang. Men

kan zich voorstellen dat het blokje met het getal 1 als eerste is geplaatst, met 2 als tweede geplaatst, etcetera. Het aantal manieren om een blokkentoren te bouwen is gelijk aan het aantal manieren om de getallen $1, 2, \dots$ in de blokken te schrijven onder voorwaarde dat de getallen naar rechts en naar boven toenemen in grootte. Dat wil zeggen dat het getal in een blokje is groter dan de getallen in blokken die zich links en onder het eerstgenoemde blokje bevinden. Deze eis zorgt ervoor dat de blokkentoren inderdaad vanaf de vloer en de linkermuur wordt opgebouwd.

8					
5	13				
4	6	9	12		
1	2	3	7	10	11

Het is begrijpelijk dat men zich op dit punt begint af te vragen waarom wis- en natuurkundigen zich bezighouden met het bouwen van blokkentorens. Dit soort structuren vervullen echter een centrale rol in tal van toepassingen, waarvan er in dit proefschrift een aantal beschouwd worden. Daarnaast zijn veel belangrijke vraagstukken in de wis- en natuurkunde, zoals hierboven, van ‘combinatorieke’ aard. Dit betekent dat deze vraagstukken in essentie de verschillende manieren beschouwen om een bepaalde structuur, zoals een blokkentoren, te construeren.

In dit proefschrift worden de eigenschappen van deze blokkentorens toegepast op zogenaamde integralen over unitaire matrices. Unitaire matrices beschrijven onder andere hoe kwantummechanische systemen kunnen veranderen, bijvoorbeeld als gevolg van ontwikkeling in de tijd. Integralen zijn wiskundige objecten die, kort gezegd, een bepaald gemiddelde van een wiskundige functie berekenen. In dit proefschrift worden deze functies simpel gezegd gekenmerkt door blokkentorens, wat betekent dat er voor elke blokkentoren een functie bestaat met bepaalde unieke eigenschappen. De matrixintegralen over dit soort functies hebben belangrijke toepassingen in de hi-

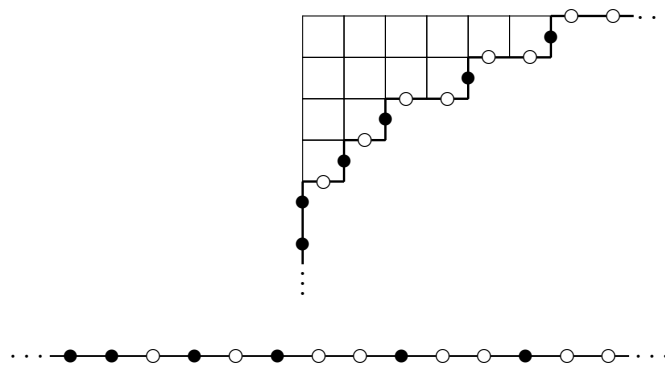
ervoor genoemde toevalsprocessen, maar ook in andere vakgebieden zoals de studie naar priemgetallen, gekromde ruimtes en bepaalde deeltjesfysica. In hoofdstuk 1 wordt de benodigde achtergrondinformatie over Young-diagrammen en gerelateerde objecten behandeld, alsook de rol die deze diagrammen spelen in het oplossen van matrixintegralen en de verschillende natuurkundige toepassingen ervan.

Hoofdstuk 2 beschouwt de wiskundige resultaten, die nieuwe manieren bieden om dit soort ingewikkelde integralen te berekenen. Deze resultaten generaliseren eerder gevonden uitdrukkingen in de wiskundige literatuur op verschillende manieren. De nuttigste resultaten die wij hebben gevonden bieden een manier om een ingewikkeld probleem op te delen in kleinere, minder ingewikkelde problemen. Als men meer van deze kleinere problemen oplost, leidt dat tot een antwoord dat dicht bij het exacte resultaat ligt. Hierdoor kan men de beoogde precisie behalen met simpelere berekeningen zonder een ingewikkeld probleem in zijn totaliteit op te hoeven lossen.

Vervolgens pas ik deze berekeningen toe op natuurkundige vraagstukken. Hoofdstuk 3 behandelt zogenaamde toevalsbewegingen. Dit zijn de bewegingen van deeltjes die willekeurige stappen zetten, waarbij in dit proefschrift gekeken wordt naar deeltjes die ook over grote afstanden kunnen bewegen. Men kan zich dit soort systemen voorstellen als een lange rij met doosjes waar men deeltjes in kan doen. De doosjes zijn klein en kunnen daarom maar één deeltje bevatten. Deze deeltjes kunnen op verschillende manieren over de doosjes verdeeld worden. Bij de studie naar dit soort systemen probeert men hun gemiddelde gedrag te voorspellen. Men kan zich bijvoorbeeld afvragen hoe groot de kans is dat een bepaalde deeltjesconfiguratie - een verdeling van deeltjes over de doosjes - in een andere configuratie overgaat door deeltjes willekeurige stappen te laten zetten.

Interessant genoeg kunnen dit soort deeltjesconfiguraties met de eerder genoemde blokkentorens worden beschreven. Dit doen we door een lijn te volgen die langs de rand van de blokkentoren loopt en daarbij een deeltje toe te kennen aan elke verticale

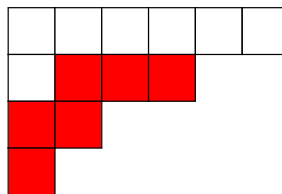
zijde van de rand van de blokkentoren, terwijl er geen deeltjes op de horizontale zijdes geplaatst worden. Ook op de verticale zijdes van de muur en de horizontale zijdes van de vloer worden respectievelijk wél en géén deeltjes geplaatst. Als we doosjes met deeltjes aanduiden met een zwarte stip en doosjes waar zich geen deeltjes bevinden met een witte stip en we het resultaat 180 graden draaien, ziet het er bijvoorbeeld uit zoals hieronder is weergegeven.



Als we de lijn aan de buitenkant van het diagram van linksonder naar rechtsboven volgen, resulteert dit in de opeenvolging van witte en zwarte stippen die eronder is weergegeven. Eerst komen we twee verticale zijdes met zwarte stippen tegen, dan een horizontale zijde met een witte stip, dan een zwarte stip, etc. Door op deze manier de configuratie en de blokkentoren met elkaar te vergelijken, ziet men dat de reeksen zwarte en witte stippen met elkaar overeenkomen.

Ook kunnen blokkentorens gebruikt worden om het rondspringen van deeltjes tussen de doosjes te beschrijven. Zo kan men zich afvragen hoeveel manieren er zijn om een deeltje één, vier of negentien doosjes naar links of rechts te laten springen. Dit soort processen wordt in de taal van diagrammen beschreven door blokken op verschillende manieren op elkaar te stapelen of weg te halen. Eén van de centrale en - voor zover wij weten - nieuwe observaties in dit proefschrift is het feit dat het

verplaatsen van deeltjes over grotere afstanden overeenkomt met het toevoegen of verwijderen van zogeheten *border strips*. Dit zijn reeksen blokken die als een slang langs de rand van de blokkentoren kronkelen. Als we een border strip toevoegen aan een blokkentoren, komt dat overeen met een deeltje een aantal stappen naar rechts te verplaatsen. Als we echter een border strip verwijderen verplaatsen we een deeltje naar links. De afstand waarover het deeltje verplaatst wordt komt overeen met het aantal blokken in de border strip. Hieronder is een voorbeeld van een blokkentoren met een border strip (in het rood weergegeven).



Dit verband, in combinatie met de eerdergenoemde wiskundige resultaten, leidt tot nieuwe en verrassende voorspellingen over systemen van dit soort deeltjes die zich over een rij doosjes kunnen verplaatsen. Dit wordt behandeld in hoofdstuk 3. Ook in deze context leiden mijn resultaten tot effectievere manieren om het gedrag van dit soort systemen te berekenen, waarbij wederom een ingewikkeld probleem wordt opgedeeld in kleinere, minder ingewikkelde problemen. Mijn resultaten zijn in natuurkundig opzicht des te interessanter omdat dit soort systemen van rondspringende deeltjes sinds een jaar of 15 in laboratoria gefabriceerd kunnen worden, met behulp van zogenaamde *trapped ions* (gevangen ionen). Verder spelen deze systemen een belangrijke rol bij tal van toepassingen, die nog altijd in aantal en verscheidenheid toenemen. Mijn resultaten kunnen ook in (sommige van) deze contexten worden toegepast en getest.

In hoofdstuk 4 beschouw ik de toepassing van mijn wiskundige resultaten op bepaalde matrixmodellen - zogeheten toevalsmatrices - en chaotische kwantumsystemen. Chao-

tische systemen, zowel in de kwantummechanica als daarbuiten, zijn systemen waarvan het gedrag sterk afhangt van de begincondities. Dit betekent dat een kleine verandering in een eigenschap van een systeem (zoals de temperatuur, magnetisch veld of de beweegrichting van bepaalde deeltjes) grote gevolgen heeft voor het gedrag van het systeem op een later moment. De eerder genoemde matrixintegralen spelen een belangrijke rol in de beschrijving van chaotische *kwantumsystemen*, waarin deeltjes een bepaald golfachtig karakter krijgen en vice versa. Zoals eerder vermeld geven deze integralen een bepaald gemiddelde van een wiskundige functie. Als we integreren over unitaire matrices is dit gemiddelde te interpreteren als een gemiddelde over alle mogelijke kwantumsystemen. Als men op die manier middelt over alle kwantumsystemen, komt men verrassend genoeg uit op eigenschappen die karakteristiek zijn voor chaotische kwantumsystemen. Simpel gezegd is de overgrote meerderheid van alle kwantumsystemen chaotisch, zodat een gemiddelde over alle mogelijke systemen door chaotische gevallen wordt gedomineerd. Dit verband is een van de centrale aspecten van de wiskundige beschrijving van chaotische kwantumsystemen.

In 1993 is tevens een matrixmodel geïntroduceerd om zogenaamde intermediaire systemen te beschrijven, die het midden houden tussen geordend en chaotisch. Deze intermediaire systemen worden minder goed begrepen dan chaotische of geordende systemen. Hetzelfde matrixmodel wordt toegepast in een ander vakgebied: de wiskundige studie van knopen. Dit is een inmiddels bijna 200 jaar oud, maar nog steeds erg levendig vakgebied. Knopentheorie beschouwt de vraag welke knopen, zoals zeilknopen of Keltische knopen, van elkaar verschillen. Knopen verschillen van elkaar als de ene knoop niet door middel van een continue vervorming - dat wil zeggen zonder het geknoopte touw door te knippen - in een andere knoop getransformeerd kan worden.

De oorspronkelijke motivatie van mijn promotieonderzoek was het toepassen van het eerdergenoemde matrixmodel op de beschrijving van intermediaire systemen.

Daarbij vermoedden mijn begeleider en ik dat deze intermediaire systemen in termen van knopen beschreven zouden kunnen worden. Tot onze verbazing leidden mijn berekeningen in dit matrixmodel niet tot intermediair maar alleen tot chaotisch gedrag. Vele eerdere publicaties concludeerden dat dit model wel intermediair gedrag vertoont, zij het met een andere benadering. Momenteel proberen wij met een nieuwe samenwerking en met behulp van numerieke (computer-)berekeningen opheldering te krijgen over deze schijnbare tegenspraak. Ondanks het uitblijven van het verwachte intermediaire gedrag leidden mijn berekeningen in hoofdstuk 4 toch tot een aantal nieuwe resultaten. Mijn berekeningen resulteerden namelijk in bepaalde knoopinvarianten, waarmee men knopen van elkaar kan onderscheiden. In een bepaald geval nemen deze knoopinvarianten de vorm aan van een verzameling van functies met bijzondere eigenschappen die - voor zover wij weten - nog niet eerder in de wiskundige literatuur beschreven zijn.

Lay summary

This lay summary provides a brief overview of the topics which are treated in this thesis. The first topics are Young-diagrams and the role they play in the computation of certain mathematical objects; so-called unitary matrix integrals. These objects have various applications in physics of which we consider two instances, given by long-range random walkers and chaotic quantum systems.

This thesis, in a broad sense, consider random processes, like the throwing of a coin or a die. The type of object considered here, however, are not coins or dice, but so-called Young diagrams. These objects are similar to kids' block towers, of which there is an example on the next page. Imagine that a child is trying to build a block tower in a room where the floor is at an angle, so that the only way to prevent the blocks from sliding off each other is to build the block tower with one side against the left wall of the room. This means that the block tower is built from bottom to top (as is usually the case) and from left to right, so that blocks which are added at a later stage are positioned to the right and/or above blocks that were placed before. For example, this could lead to the block tower indicated on the next page. There are numbers written in the blocks of this block tower. Strictly speaking, the above object is called a Young *tableau* rather than a Young diagram, but this is not important here. One can imagine that the block with the number 1 was placed first, the block with the number 2 was placed second, etc. The number of ways of ways

to build a block tower then equals the number of ways to inscribe the blocks with the numbers $1, 2, \dots$ which increase from left to right and down to up. That is, the number in a block is greater than the numbers in blocks beneath or to the left of the first block. This requirement ensures that the block tower is indeed built from the floor and the left wall of the room.

8					
5	13				
4	6	9	12		
1	2	3	7	10	11

It is understandable if one starts to wonder at this point why mathematicians and physicists busy themselves with the building of block towers. However, these structures play a central role in various applications, some of which are considered in this thesis. Further, many questions in mathematics and physics are of a ‘combinatorial’ nature, such as the one above. This means these problems are essentially concerned with the different ways to construct a certain object, such as a block tower.

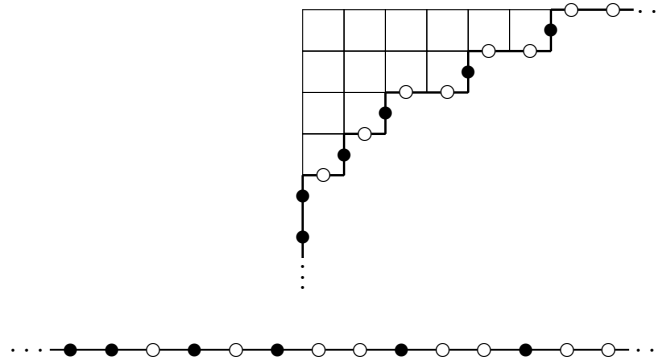
In this thesis, the properties of these block towers are applied to so-called integrals over unitary matrices. Among other things, unitary matrices describe how quantum mechanical systems undergo change, for example as a result of time evolution. Integrals are mathematical objects which, simply put, calculate a certain average of a mathematical function. In the cases considered in this thesis, these functions are characterized by block towers, which is to say that for every block tower there exists a function with certain unique properties. The matrix integrals over these functions have important applications to the aforementioned random processes, as well as the study of prime number, curved spaces, and certain types of particle physics. Chapter 1 treats the necessary background information on Young diagrams and related objects, the role these diagrams play in the computation of matrix integrals, as well

as their applications to problems in physics.

Chapter 2 presents my mathematical results, which provide new ways to compute this type of complicated integral. These results generalize previously found expressions in various ways. The most useful results I found provide a way to split a complicated problem into various, less complicated problems. Solving more of these less complicated problems leads to an answer that is closer to the exact result. This allows one to attain the desired precision with simple calculations without having to solve a difficult problem in its entirety.

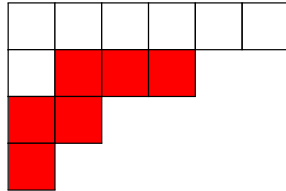
I then apply these calculations to questions in physics. Chapter 3 treats so-called random walks. These are the trajectories of particles which take random steps, where this thesis considers particles which can also move over large distances. One may imagine this type of system as a long row of boxes which may contain a particle. These boxes are small and can therefore contain only a single particle. The particles can be distributed across the boxes in different ways. The study of these types of systems attempts to predict their average behavior. For example, one may wonder what is the probability that a certain particle configuration - a distribution of particles across the boxes - transitions into another configuration by letting particles take random steps.

Interestingly, these types of particle configurations can be described by block towers such as the example given on the first page of this summary. One may do so by following a line which runs along the edge of the block tower and assigning a particle to each vertical side of this edge but no particle to each horizontal side. We also place particles on the (vertical) wall whilst not putting any particles on the (horizontal) floor. If we indicate boxes containing a particle with a black dot, boxes without a particle with a white dot, and we rotate the result by 180 degrees, it may look as the example given on the following page.



If we follow the line along the edge of the diagram from the bottom left to the top right, this results in the sequence of white and black dots given below it. We first encounter two vertical sides with black dots, then a horizontal side with a white dot, then a black dot, etc. By comparing the configuration with the block tower, one may see that the sequences of black and white dots match.

Block towers may also be used to describe particles jumping in between boxes. One may wonder how many ways there are to take a particle and move it one, four, or nineteen boxes to the left or right. These types of processes are described in the language of diagrams by stacking or removing boxes in different ways. One of the central and - as far as we know - new observations in this thesis is the fact that moving particles of greater distances corresponds to the addition or removal of so-called *border strips*. These are sequences of blocks which twist along the side of a block tower like a snake. If we add a border strip to a block tower, this corresponds to moving a particle a number of steps to the right. On the other hand, removing a border strip corresponds to moving a particle to the left. The distance over which we move the particle equals the number of boxes in the border strip. An example of a block tower with a border strip (indicated in red) is given on the following page.



This relation, in combination with the aforementioned mathematical results, leads to novel and surprising predictions for systems of particles which can move along a row of boxes. This is treated in chapter 3. In this context, too, my results lead to more effective ways to compute the behaviour of these types of systems, as they allow one to split up a complicated problem into smaller, less complicated ones. My results are all the more interesting from a physical point of view because these types of systems of particles hopping around a row of boxes can be fabricated in laboratories since roughly 15 years, using so-called *trapped ions*. Further, these systems play a role in various applications, which continue to increase increasing in number and variety. My results may also be checked and applied in (some of) these contexts.

Chapter 4 considers the applications of my mathematical results to certain matrix models - so-called random matrices - and chaotic quantum systems. Chaotic systems, whether quantum-mechanical or not, are systems whose behaviour strongly depends on initial conditions. This means that a small change in a property of a system (such as its temperature, magnetic field, or the direction of motion of certain particles) has a large impact for the behaviour of the system at a later time. The aforementioned matrix integrals play an important role in the description of chaotic *quantum* systems, where particles acquire a wave-like character and vice versa. As mentioned before, the integrals considered here compute a certain average of a mathematical function. If we integrate over unitary matrices, this average can be interpreted as an average over all possible quantum systems. Surprisingly, averaging over all quantum systems in this way leads to properties which are char-

acteristic of chaotic quantum systems. Simply put, the overwhelming majority of all quantum systems are chaotic, so that an average over all systems is dominated by chaotic ones. This relation is one of the central aspects of the mathematical description of chaotic quantum systems.

Almost 30 years ago, a matrix model was introduced to describe so-called intermediate systems, which lie somewhere in between regular (non-chaotic) and chaotic systems. These intermediate systems are less well understood than chaotic or regular systems. The same matrix model is also applied to the mathematical study of knots, which is a by now more than 200 years old but still very active field of research. This field concerns itself with the question which knots, such as sailor's knots or Celtic knots, differ from each other. Knots differ from each other if one knot cannot be transformed into another one through a continuous deformation, that is, without cutting the knotted rope.

The original motivation of my doctoral research was the study of intermediate systems. My supervisor and I suspected that these intermediate systems could be described in terms of knots. To our surprise, my calculations on this matrix model did not lead to intermediate, but only to chaotic behavior. Many previous publications had concluded that this model exhibits intermediate behaviour, albeit with the use of a different approach. We are currently engaged with a new cooperation in an attempt to resolve this apparent contradiction. In spite of the absence of intermediate behaviour, my calculations in chapter 4 did lead to some new results. The result of my calculations are certain knot invariants, which are used to distinguish knots from each other. In a certain limit, these knot invariants take the form of a collection of functions with remarkable properties which - as far as we are aware - have not been described in the mathematical literature before.

Curriculum vitæ

Ik ben op 14 mei 1992 geboren in Nijmegen. Van 2003 tot 2010 volgde ik het Gymnasium aan het Canisius College, eveneens in Nijmegen. Van 2011 tot 2014 volgde ik een bachelor Liberal Arts and Sciences aan het Amsterdam University College met wis- en natuurkunde als specialisatie, dat ik Summa Cum Laude afrondde met het hoogste gemiddelde cijfer van het jaar 2014. Hiervoor schreef ik een scriptie onder begeleiding van Eric Laenen genaamd *On chiral symmetry, Goldstone bosons, and the pion sigma model*. Van 2015 tot 2018 volgde ik de Master Theoretische Fysica aan de Universiteit Utrecht, die ik Cum Laude voltooide. Als onderdeel hiervan schreef ik een masterscriptie onder begeleiding van Gerard 't Hooft, met als titel *On BMS-transformations and the shock wave S-matrix*. Tijdens mijn masteropleiding heb ik een aantal maanden aan de Ludwig-Maximilians-Universität in München gestudeerd als onderdeel van een Erasmusuitwisseling. Op verzoek van Dieter Lüst, professor aldaar, heb ik een dictaat geschreven aan de hand van zijn colleges over zwarte gaten. Nadat we werden benaderd door Springer is dit dictaat in boekvorm gepubliceerd onder de naam *Black Hole Information and Thermodynamics*. In 2018 begon ik aan mijn promotietraject onder begeleiding van Vladimir Gritsev en Cristiane de Morais-Smith, wat uiteindelijk heeft geleid tot het schrijven van dit proefschrift.